ALMA MATER STUDIORUM – UNIVERSITÀ DI BOLOGNA
FACOLTÀ DI SCIENZE MATEMATICHE, FISICHE E NATURALI

DOTTORATO DI RICERCA IN

GEOFISICA

CICLO: XXII

Settore scientifico-disciplinare di afferenza: **GEO-10**

TITOLO TESI

WAVE FIELD MODELING IN HETEROGENEOUS MEDIA USING THE SPECTRAL ELEMENT METHOD: APPLICATION TO THE DAVID GLACIER MICROSEISMICITY

Presentata da
PIERO BASINI

Coordinatore Dottorato
PROF. MICHELE DRAGONI

Relatore
DR. ANDREA MORELLI

Esame finale anno 2010

Contents

List of Figures

List of Tables

Introduction

Even if the Antarctic continent is considered as nearly aseismic seismic events of different nature had been investigated by scientists.
A particular kind of seismic signals, associated with the movement of large glaciers, are the glacial earthquakes recorded in Alaska, Greenland and also in Antarctica [17]. Another kind of event which occur inside glaciers are the icequakes: these events are usually associated with the creation of crevasses in the shallow part of the ice layer [28], but they can actually occur at any depth [12]. Subglacial micro-earthquakes, occurring beneath Ice Streams B and C in West Antarctica, have been widely studied and they are associated with the dynamic of the ice streams themselves [32][33].
Others areas of Antarctica show the presence of similar events: during a seismic campaign carried out in the zone of the Transantarctic Mountains (TAM) in Victoria Land a set of seismic events belonging to the David Glacier area were recorded [35]. To further investigate these phenomena a seismic campaign within Italian and New Zealander Antarctic programs had been carried out during the period November 2003 through February 2004: Italian and New Zealand researchers deployed a temporary broadband seismographic network around the David Glacier area and recorded, among the others, a set of 121 seismic events which are considered as *basal earthquakes*, that is to say they could be caused by the friction produced by the motion of the ice against the bedrock [34].
The work of this thesis deals mainly with these microseismic phenomena because they presents very interesting and peculiar characteristics: their hypocenters show high spatial clusterization, within each clusters the events present very similar waveforms and their spectra contain high surface wave energy at frequencies less than $1\ Hz$.
The presence of this surface wave energy and the spatial clusterization of hypocenters are incompatible with usual tectonics events, this is why they had been located at the interface between ice and bedrock. I have focused my attention on this high contribution of low frequencies to the spectra: it can be related to effects on wave propagation caused by the presence of ice which could act as a wave guide for these low frequencies waves. Thus I have decided to investigate the role played by the ice layer in the propagation of the wave field.
During the last thirty years the scientific community experienced sensible improvements in the quality and quantity of seismic data, thanks to the spreading of instruments like broadband seismometers. In order to exploit all the information provided by these data a lot of numerical methods had been developed which basically solve the equations of motion. Because of computational costs problems these techniques were developed in order to solve

approximations of the equations of motion, nevertheless nowadays a large number of clusters is available thus new numerical methods capable to solve numerically the complete equations of motion had been developed. All of these methods require a representation of the investigation domain made by a mesh, that is to say a set of geometrical elements which could be tetrahedra or hexahedra.
Among all the numerical techniques I have chose to use the spectral element method (SEM): this method was initially developed for the study of the dynamic of fluids [29], then it was applied to the field of seismology [14]. This method is capable to simulate the propagation of seismic waves in a given domain Ω representing analytical functions by mean of polynomial functions. Furthermore it is capable of including in the simulations effects due to the topography, to lateral variations in compressional-wave speed, shear-wave speed and density, as well as they can accommodate full 21-parameter anisotropy and lateral variations in attenuation. A peculiarity of the spectral element method is that the mesh used to represent the domain of investigation has to be made uniquely by hexahedral elements, furthermore the mesh should honor all the discontinuities of the domain Ω otherwise the melting of different physical properties in the same spectral element will introduce numerical errors in the synthetic seismograms.
To perform simulations of seismic waves propagation I have used the open source package SPECFEM [21] in which Jeroen Tromp (Princeton University) and Dimitri Komatitsch (University of Pau) have implemented the SEM.
I have firstly created a three-dimensional representation of the David Glacier using two different data sets: the Radarsat Antarctic Mapping Project Digital Elevation Model Version 2 [24] which describes the topography of the study area and BEDMAP which contains the description of the subglacial morphology. I have then created a three dimensional mesh of this geological model using the mesh generation toolkit developed at Sandia National Laboratories [11]. Because of the complexity of ice layer geometry the mesh I have created does not honor the bedrock interface: information about subglacial morphology are introduced by interpolating the physical properties of ice and rock within the spectral elements located across the interface.
In order to check the effects produced on the synthetic seismograms by the definition of the investigation domain geometry (i.e. the topography and the subglacial morphology) and by the interpolation of different physical properties in the same spectral element I have decided to use two-dimensional meshes: this kind of meshes are easier to be obtained and the computational costs of 2D simulations are lower than the three-dimensional ones. I have produced several meshes starting from a set of profiles of the geological model, each of them including the position of one seismic station and of the seismic event hypocenter.
All the simulations add been performed using the cluster SGI Altix ICE 8200EX (JADE) at *Centre Informatique National de l'Enseignement Suprieur* CINES and the cluster IBM P575 Power 6 (sp6) at *Consorzio Interuniversitario* CINECA.
The results obtained by these simulations are not able to reproduce the complete waveforms of the analyzed events: incoherences between synthetics seismograms and recorded data are probably related to the limited level of knowledge on the David Glacier geology and on the

parameters of the sources events. Nevertheless these synthetics contain very interesting information both on the role played by the ice layer in the propagation of seismic waves and on the capabilities of spectral element method.

Chapter 1

David Glacier

1.1 Introduction

Antarctica is the southernmost continent of the world, centered on the South Pole and extended asymmetrically around it. Its surface (more than 14.0 million km^2) makes it the fifth-larger continent, about 1.3 times larger than Europe (Figure 1.1).

The most part of the continent is covered by ice with an average thickness of about $1.6\ km$

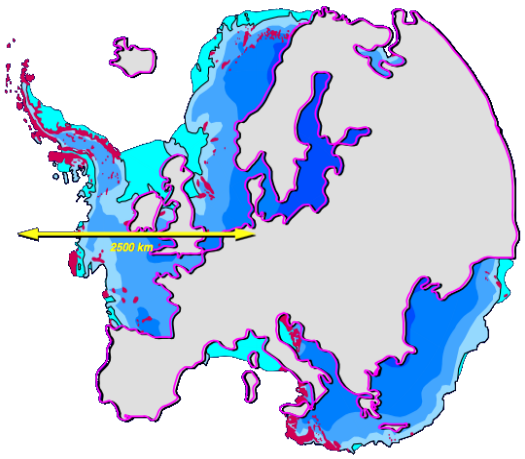

Figure 1.1: Size comparison between Antarctica and Europe. Author: Hannes Grobe.

and maximum thickness of about $4.5\ km$, a peculiarity which makes Antarctica the biggest reservoir of ice and fresh water of the world, in fact the Antarctica ice sheet contains about the 90% of the world's ice.

In addition to that there is the total absence of native human population, so during the first part of the last century some nations claimed sovereignty in certain regions but they had never been recognized universally.

In 1959, in order to regulate international relations with respect to Antarctica, the countries which were active in Antarctica at that period signed the Antarctic Treaty System (ATS). During the years others agreements had been added to the original one but the main aim

remained always the same: to support scientific research and the exchange of information between scientists from different countries; according to that any military activity in Antarctica, such as weapons testing, is prohibited and exploitation of all mineral resources is banned by the Protocol on Environmental Protection to the Antarctic Treaty.
Thanks to ATS, Antarctica nowadays represents the biggest natural laboratory of the Earth with research stations operating seasonal, such as the Mario Zucchelli Station at Terra Nova Bay, or during the whole year as for the Concordia Station. Researches are interested in different scientific areas of study: from the biology to the physics and to the meteorology. For example Antarctic ices are widely studied by biologists because they contain, trapped in their ice crystals, particles belonging to the atmosphere of the past. These particles provide scientists many information about the history of the earth's climate which can fruitfully contribute to the actual debate about *global warming* and its possible impacts on the environment of the planet [36].

1.2 Antarctic glaciers

The ice layer which covers the Antarctic continent can be divided in two main parts, called respectively the East and the West Antarctic Ice Sheet. Generally ice sheets do not present high values of flow speed, nevertheless within them it is possible to identify areas of fast ice flow. These area are called ice streams and can be defined, accordingly to [40], as the "parts of an inland ice sheet in which the ice flows more rapidly than, and not necessarily in the same direction as, the surrounding ice".
Since ice streams control the ice discharge rate of ice sheets a deep knowledge on them is of fundamental importance: speed flow variations may have control on ice sheets stability, this resulting also in possible dramatic environmental changes at global level. I just want to mention here the fact that the global sea level would rise of $4 - 6\ m$ or more, taking into account also the possible partial melting of West Antarctic Ice Sheet [23].
Furthermore, outlet ice streams, which drain the ice directly into the sea, play an important role in controlling the sea salinity and temperature. Since these parameters have the control on the formation and maintenance of water circulation both at local and continental level, it appears clear that the influence of Antarctic glaciers on the global climate does not deals only with the problem of sea level rise.
For example on the global scale one factor controlling the circulation of water between ocean is the density gradient of water. This gradient gives rise to the so called Thermohaline circulation (THC) and depends locally by surface heat and freshwater fluxes. Thus variations in ice discharge rate of Antarctic ice sheets could produce changes in this current with strong influences on global climate and underwater biodiversity.
Thus a good comprehension of the mechanisms controlling the motion of these glaciers is of fundamental importance in order to better understand possible scenarios of climate evolution.

1.3 Microseismicity at David Glacier

The Antarctic continent is considered as nearly aseismic, nevertheless seismic events of low magnitude have been registered mainly in correspondence of some outlet ice streams. The discussion about their origin and source mechanism is still open, alternatively attributed to icequakes caused by ice brittle deformation on glacier or by iceberg calving or by tectonic earthquakes occurring along faults [35].
A seismic campaign was carried out during the 1999-2000 austral summer in the zone of the Transantarctic Mountains (TAM) in Victoria Land, to better understand the seismicity of the region; during the campaign one hundred and sixty seismic events were located, eighty-four of them were identified as belonging to the zone of the David Glacier [35].
According to the researchers who analyzed data collected during this campaign, neither exact location nor source mechanism could be determined uniquely, thus these microseismic events were the target of a further investigation: during the austral summer of 2003-2004 researchers belonging to Italian and New Zealander Antarctic programs carried out a portable seismographic array campaign focused on the area of the David Glacier [34].
David Glacier is the most imposing outlet glacier in Victoria Land, fed by two main flows which drain an area larger than 200,000 square kilometres of the East Antarctic plateau, with an estimated ice discharge rate of $7.8 \pm 0.7\ km^3/year$ [37],[38]. The northern flow drains from Talos Dome to the Ross Sea, but the main branch of the stream is fed by a network of tributaries which drain a common area of the inner plateau around Dome C and converge in a spectacular icefall normally known as the David Cauldron. As the David Glacier flows into the Ross Sea, it forms a floating mass known as the Drygalski Ice Tongue (Figure 1.2).
This area is characterized by reliefs with height ranging from the sea level to up than $2000\ m$ and ground based missions performed with radio echo sounding techniques revealed an extremely irregular bedrock morphology [39],[41]. Despite these observations the description of the geological structure of the David Glacier area is not complete and the knowledge on both the topography and icethickness is still limited, in particular the structure of the ice layer should be investigated thoroughly: the presence of crevasses and cracks and the variation of compactness could lead to variations in the physical properties of ice, which could play an important role in the nucleation of microseismicity.

1.4 Collection and analysis of data

During the period November 2003 through February 2004 Italian and New Zealand researchers deployed a temporary broadband seismographic network around the David Glacier area (Figure 1.2), all the stations were placed onto Nunataks which are small rocks outcropping from the surrounding ice.
The seismographic network was composed by the following sets of instruments:

- Italian stations:
  sensor: Broadband Trillium Nanometrics 40 sec;
  recorder: Reftek 130-01;

- New Zealander stations:
  sensor: Guralp;
  recorder: Orion.

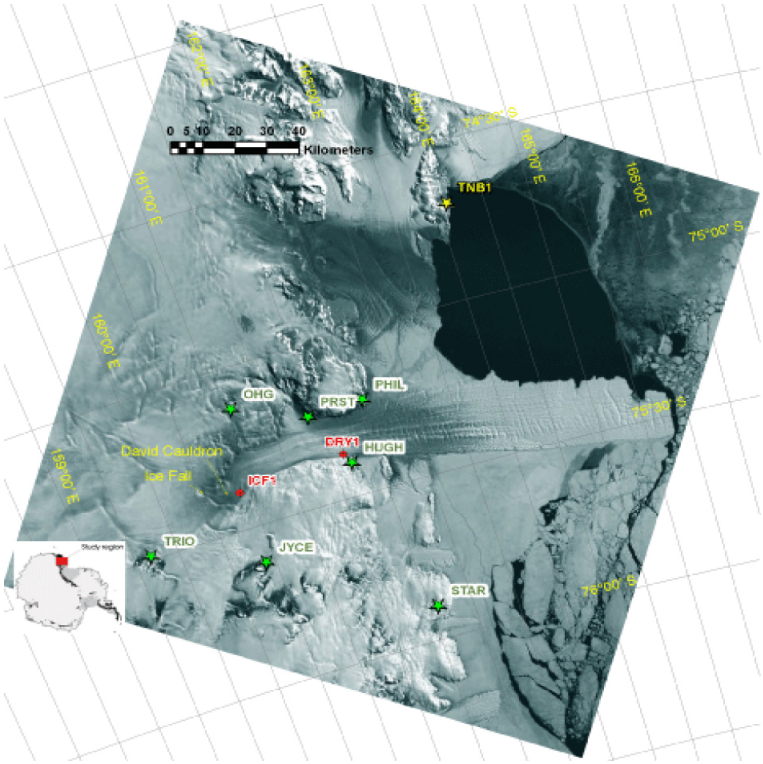

Figure 1.2: View of the study area. Picture had been made collecting together satellite images (ASTER-VNIR), all georeferenced to a South Pole Polar Stereographic projection. Green stars indicate some seismic stations used during the expedition of 2003-2004 austral summer, while red spots indicate two temporary GPS stations. The David Cauldron icefall is located in the lower left part of the image, while the Drygalski Ice Tongue can be seen in the central area on the right. Author: Stefania Danesi.

This set of stations recorded over these months more than 6000 events which can be listed as *icequakes*: these kind of phenomena have origin within the ice layer, have high frequency content and high attenuation ratio with distance. Because of these characteristics each of them was recorded only by a limited number of stations, thus their exact localization was quite impossible as well as the determination of source parameters.
More interestingly, during the same period instruments recorded another set of 121 events; these events were firstly considered as *basal earthquakes*, that is they were supposed to be induced by the movement of the ice layer onto the rock and by the friction generated by this motion. Their local magnitude values were low, M_l ranging between 1.3 and 2.2 but, despite this, these events were recorded also at far, permanent station as Terra Nova Bay (TNV), located at a distance of 200 km from the epicenters.
At first researchers determined the hypocenter localization of these events using the HYPOINVERSE algorithm, then they performed a second and more accurate localization by means of the Double-Difference method of Waldhauser. This analysis allowed to identify three main clusters of epicentres, close to the icefall: the Upstream-South (UP-S), Upstream-North (UP-N), and Downstream (DW) clusters (Figure 1.3(a)).
Events belonging to the DW cluster showed another interesting feature, that is to say that their waveforms presented a high level of similarity (Figure 1.3(b)).
The spectral analysis of the waveforms [34], performed using the Brune model, produced the following mean value for the seismic moment of all the events belonging to the DW cluster: $\overline{M_0} = 3.6N \cdot m$. It has to be noticed that the Brune model could not be applied to the whole signal but only in that region of frequency in which the Brune condition was satisfied, i.e. $\nu > 4\ Hz$: in fact the spectra of the recorded events contain high surface wave energy at frequencies less than $1\ Hz$. (Figure 1.3(c)) The presence of this surface wave energy and the spatial clusterization of hypocenters are incompatible with usual tectonics events: a possible explanation can be found considering the interaction ice-rock as the source mechanism. In particular the spreading of hypocenters belonging to the UP-S and UP-N clusters suggests a combination of ice velocity and topographic effects as triggers of these events. On the other side the hypocenter spatial density shown by the DW can be caused by the presence of a promontory in the basement of the David Cauldron. Furthermore the estimation of source parameters for events belonging to this cluster suggests the rupture of a single asperity under the glacier as the source of these events.
The strong presence of surface waves can be also related to effects on wave propagation caused by the presence of the ice layer which could act as a wave guide for low frequencies waves.
Because the interaction between the glacier and the bedrock appears to be the most probable trigger for these events, a better comprehension of their nucleation process will reflect on a knowledge improvement about the mechanisms driving the motion of David Glacier. Thus I have decided to investigate the role played by the ice layer in the propagation of the wave field. I first have focused my attention on one single event occurred on December 21, 2003 at 8:40 a.m.; the event belongs to the UP-S cluster and has the following coordinates: Latitude = 75,37 S, Longitude = 160,55 E. In particular I have considered the wave field of this event

Station name	Network	Latitude (deg)	Longitude (deg)	Elevation (m)
TRIO	NZ	-75.500	159.690	1145
HUGH	NZ	-75.400	162.200	215
STARR	IT	-75.883	162.583	70
OHG	IT	-75.130	161.130	630
JOYCE	NZ	-75.620	160.890	1230

Table 1.1: List of seismic stations I have used in this study. Their position can be seen in figure 1.2.

recorded at the seismic stations listed in table 1.1.
The study of seismic wave propagation can be performed by means of numerical techniques. Since the topography and the geometry of subglacial interface are supposed to play an important role in the propagation of these particular signals I have decided to use the spectral element method (SEM)[29],[14] because it is capable to deal with complex geological models at reasonable computational costs.

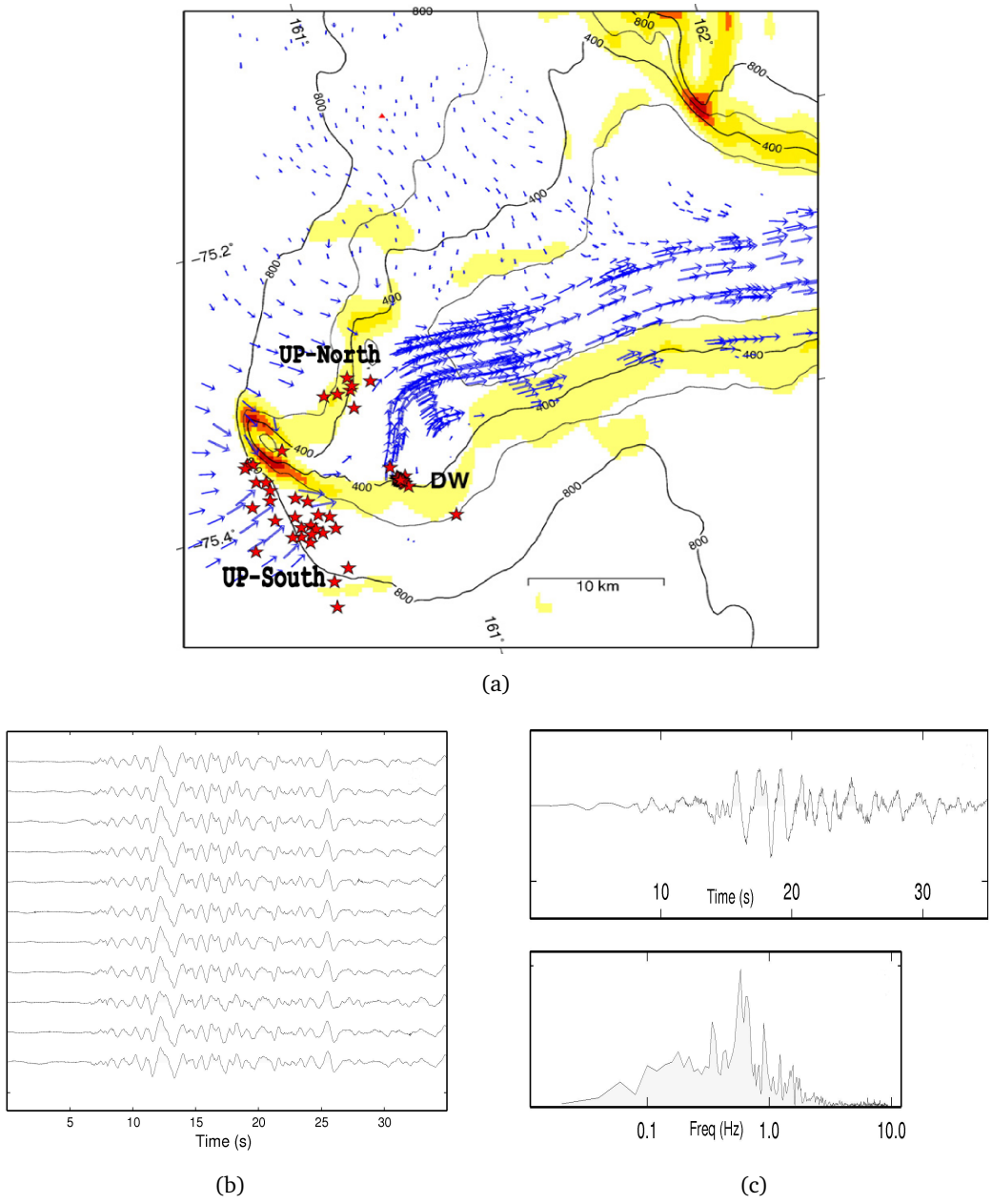

(a)

(b)

(c)

Figure 1.3: Figure 1.3(a): red stars represent events epicentres, their subdivision in three different clusters is unmistakable; blue arrows indicate the velocity field of the glacier [37],[38]; colored areas indicate different slopes, the red being the steepest ones corresponding to the icefall. Figure 1.3(b) shows the impressive similarity between the seismogram vertical components of 11 different events belonging to the DW cluster. Figure 1.3(c): the upper frame shows an event belonging to the UP-S cluster, while the lower frame reproduce its spectral content; it is evident the preponderance of low frequencies. All images modified by [34].

Chapter 2

Spectral Element Method

2.1 Introduction

During the last three decades the quality and quantity of seismic data has been increased considerably thanks to a technological development which introduced instruments such as broadband seismometers which can detect motion over very large ranges of frequencies and amplitudes. Scientists can use these data to study the interior structure of our planet and to improve the knowledge on the propagation of seismic waves in heterogeneous complex media, but numerical methods are needed in order to exploit completely all the information provided by these data.
Simulation of seismic waves propagation implies the use of computer clusters, thus, before their diffusion in the scientific community, scientists were forced to use numerical methods with low computational costs. The approximation of the equations of motion used in these numerical methods, make them useful only in certain regions of the frequency domain. For example the high frequency region is well represented by asymptotic ray theory for an inhomogeneous medium, while the generalized ray theory is more suitable in the case of a vertically stratified medium [31].
Nowadays a large number of clusters is available for the scientific community thus many different numerical techniques had been developed in order to investigate wave propagation phenomena taking into account the complete equations of motion: the finite-difference method (FDM) [26], the finite element method (FEM) [4] and the spectral element method (SEM)[29],[14]. A representation of analytical functions by mean of polynomial functions is used in these methods in order to solve the equation of elastodynamics. Even if all of these methods work well in simple cases problems may arise in more complicated situations: in FD the representation of surface waves is not accurate if there's the need to take into account free-surface boundary conditions; FEM presents high computational costs because of the need to solve linear systems which are very large. For these reasons I have decided to use SEM: it represents a very good choice in terms of accuracy and computational cost [15].
In this chapter I explain the main mathematical characteristics and properties of the SEM and the implications they have onto the construction of the mesh, i.e. the set of polygons used to discretize the domain of investigation; I do not want to treat the problem in an exhaustive

way, for a more detailed description please see [15].

2.2 Equation of elastodynamics and its weak formulation

Basically the aim is to solve, in a given domain Ω (Figure 2.1), the equation of elastodynamics, here written in its differential formulation:

$$\rho \partial_t^2 \mathbf{s} \quad = \quad \nabla \cdot \mathbf{T} + \mathbf{F} \tag{2.1}$$

where **s**(**x**,t) represents the displacement which occurs at position **x** and time t, $\rho(\mathbf{x})$ denotes the density distribution, **F**(**x**,t) is the external body forces tensor and **T** is the stress tensor which is related to the displacement gradient by the Hooke's law: $\mathbf{T} = \mathbf{c} : \nabla \mathbf{s}$, where **c** is the fourth-order elastic tensor which describe the elastic or anelastic properties of the considered media. Associated to this equation there are also the stress-free boundary condition at the

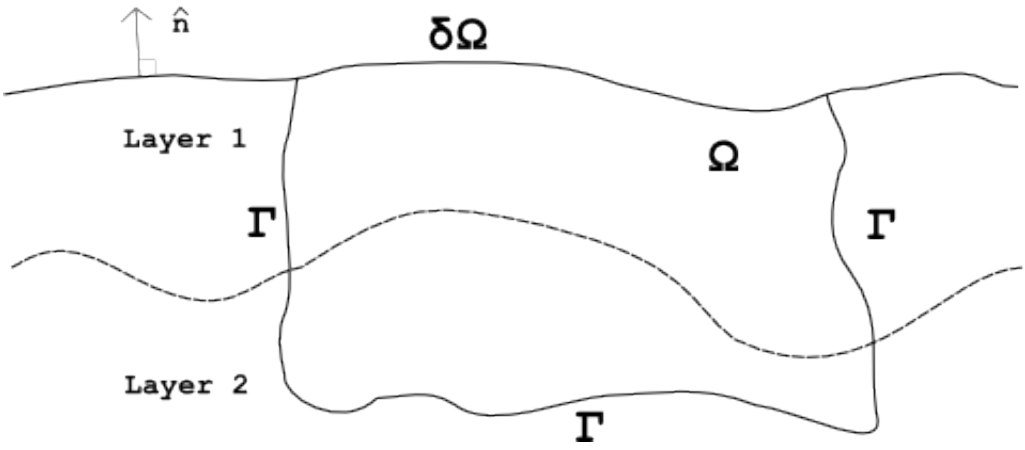

Figure 2.1: A generic geological model containing the domain of investigation Ω, its free surface $\delta\Omega$ and the absorbing boundaries Γ. All the unit outward normal vectors of these surfaces are indicated with $\hat{n}$. The model contains two layers with different physical properties.

free surface $\delta\Omega$ and the absorption of the waves at the internal boundaries of the model Γ; those conditions can be written in the following way according to [15]:

$$\mathbf{T} \cdot \hat{\mathbf{n}} \quad = \quad 0 \tag{2.2}$$

$$\mathbf{T} \cdot \hat{\mathbf{n}} \quad = \quad \rho \left[v_n \left(\hat{\mathbf{n}} \cdot \partial_t s \right) \hat{\mathbf{n}} + v_1 \left(\hat{\mathbf{t}}_1 \cdot \partial_t s \right) \hat{\mathbf{t}}_1 + v_2 \left(\hat{\mathbf{t}}_2 \cdot \partial_t s \right) \hat{\mathbf{t}}_2 \right] \tag{2.3}$$

where: $\hat{\mathbf{n}}$ is the outward versor of the free surface and of the boundaries of the model, $\hat{\mathbf{t}}_1$ and $\hat{\mathbf{t}}_2$ are are orthogonal unit vectors tangential to the absorbing boundary, $v_n$is the quasi-P wave speed of waves traveling in the $\hat{\mathbf{n}}$ direction, v_1 is the quasi-S wave speed of waves polarized in the $\hat{\mathbf{t}}_1$ direction and v_2 is the quasi-S wave speed of waves polarized in the $\hat{\mathbf{t}}_2$ direction. An alternative to this kind of formulation of the elastodynamic problem is its *weak formulation*,

which can be derived considering an arbitrary vector **w**, multiplying both sides of equation (2.1) with it, using the integration by parts rule over the volume Ω and finally imposing the conditions (2.2) and (2.3). The final result is:

$$\int_{\Omega} \rho \mathbf{w} \partial_t^2 \mathbf{s} d^3\mathbf{x} = -\int_{\Omega} \nabla \mathbf{w} : \mathbf{T} d^3\mathbf{x} + \mathbf{M} : \nabla \mathbf{w}\left(\mathbf{x}_s\right) S\left(t\right) + \int_{\Omega} \rho \left[v_n \left(\hat{\mathbf{n}} \cdot \partial_t s\right) \hat{\mathbf{n}} + v_1 \left(\hat{\mathbf{t}}_1 \cdot \partial_t s\right) \hat{\mathbf{t}}_1 + v_2 \left(\hat{\mathbf{t}}_2 \cdot \partial_t s\right) \hat{\mathbf{t}}_2\right] \cdot \mathbf{w} d^2\mathbf{x} \quad . \tag{2.4}$$

where $S(t)$ is the source time function and **M** is a moment tensor.
Because of the fact that the vector **w** is arbitrary the two formulations are equivalent but, in the case of weak formulation, condition (2.2) is automatically included in such a way a topography can be included without mathematical problems and the representation of surface waves results more precise than in FD.

2.3 Discretization of the domain and representation of functions

To solve the weak formulation of the elastodynamic written above the whole model has to be subdivided in several parts, each of them not overlapping with the others and honoring the geological interfaces and the free-surface topography (Figure 2.2). In each element the

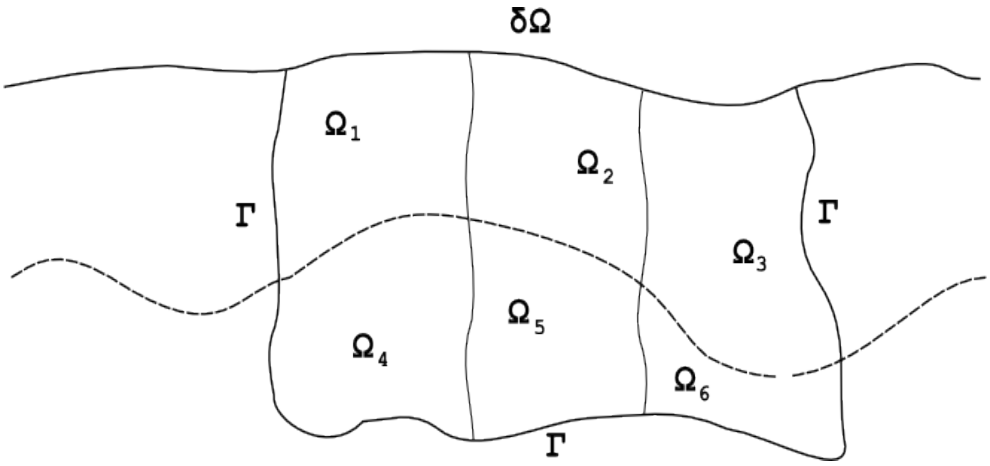

Figure 2.2: Main domain Ω subdivided into six subdomains Ω_i.

functions contained in equation 2.4 can be represented by mean of polynomial functions. In SEM high-degree Lagrange polynomials are used to express functions on the elements; this choice has two important consequences in the whole method: first of all the mass-matrix (i.e. the matrix defined to discretize the concept of mass in the domain of investigation Ω) results exactly diagonal so the numerical accuracy and the efficiency improve a lot, otherwise the elements must be hexahedra. The Lagrange interpolant of degree n_l is defined by $n_l + 1$

Lagrange polynomials by the use of $n_l + 1$ control points ξ_α:

$$l_\alpha^{n_l} = \frac{(\xi - \xi_0)\cdots(\xi - \xi_{\alpha-1})(\xi - \xi_{\alpha+1})\cdots(\xi - \xi_{n_l})}{(\xi_\alpha - \xi_0)\cdots(\xi_\alpha - \xi_{\alpha-1})(\xi_\alpha - \xi_{\alpha+1})\cdots(\xi_\alpha - \xi_{n_l})} \tag{2.5}$$

where $-1 \leq \xi_\alpha \leq 1$ and $\alpha = 1, ..., n_l$.
Because of the fact that hexahedra are isomorphous to the cube, each element can be linked to a reference cube by mean of a mapping function defined as follow:

$$\mathbf{x}(\xi) = \sum_{a=1}^{n_a} N_a(\xi)\,\mathbf{x}_a \tag{2.6}$$

where $\xi = (\xi, \eta, \zeta)$ express the coordinates system in the reference cube, $\mathbf{x}_a(\xi)$ are the reference cube points coordinates, $\mathbf{x}(\xi)$ are the corresponding points in the hexahedral element and they are related by mean of n_a shape functions N_a; these shape functions are expressed in term of the triple product of Lagrange polynomials of degree 1 or 2 depending on the number of control points used to define the hexahedra: eight anchors are enough to parameterize an hexahedra but, to honor the possible deformation of the element, one should add mid-side and center nodes, so the number of control points becomes 27.
By the use of this transformation the reference frame belonging to the reference cube and the one which refers to the hexahedra had been linked together; a very important parameter in the definition of these frames is the Jacobian of the transformation function:

$$J = \left|\frac{\partial(x, y, z)}{\partial(\xi, \eta, \zeta)}\right|. \tag{2.7}$$

The matrix $\left|\frac{\partial(x,y,z)}{\partial(\xi,\eta,\zeta)}\right|$ can be easily found differentiating the mapping equation 2.6:

$$\frac{\partial \mathbf{x}}{\partial \xi} = \sum_{a=1}^{n_a} \frac{\partial N_a}{\partial \xi}\mathbf{x}_a \tag{2.8}$$

The hexahedra should be constructed to avoid the Jacobian to vanish, in such a way that the matrix defined in 2.7 is non-singular and can be inverted, this requirement implies another strict constraint in the design of the mesh but it is of fundamental importance in the representation of functions on the elements.
In these passages I have only considered volume elements but the same process can be easily applied to the boundary elements by simply considering the isomorphism between a quadrilateral element and the square.
Once the model has been subdivided in volume elements the next step is to represent the functions on them; as I have already said in SEM Lagrange interpolants of degree n_l are used to express functions on the elements and the $n_l + 1$ control points needed in the definition 2.5 are chosen to be the Gauss-Lobatto-Legendre points (GLL) which are the root of the following equation:

$$(1 - \xi^2)P'_{n_l}(\xi) = 0 \tag{2.9}$$

where P is the derivative of the Legendre polynomial of degree n_l. A polynomial degree n_l in the range between 5 and 10 is well-suited to represent functions on the hexahedral elements [16]. The integration rule adopted in this SEM in order to approximate both surface and volume integrals is the Gauss-Lobatto-Legendre rule , while for the integration over the time domain a fourth-order Runge-Kutta scheme has been adopted to solve a first order set of equations [15].

2.4 Implications on the construction of the mesh

From the discussion above it appears clear that a good representation of the domain of investigation is a fundamental element in using a SEM. The first thing to be taken into account is the dimension of the hexahedra Δx, which is connected with the degree of the Lagrange interpolant used to represent the functions on the element: for a polynomial of degree n_l each element contains $(n_l + 1)^3$ Gauss-Lobatto-Legendre points, that is to say $n_l + 1$ points in each direction. As I have said in the first part of this chapter the aim of a numerical method like SEM, applied to seismology, is to resolve a wave field to a certain frequency ν_{max} which corresponds to a wavelength λ; a good approximation of this λ implies that it should be sampled by 5 GLL points at least, that is to say a Lagrange interpolant of degree $n_l = 4$ has to be used [7].
This condition can be expressed as follow:

$$\Delta x = \frac{v_{min}}{\nu_{max}} \frac{n_l + 1}{f(n)} \tag{2.10}$$

where v_{min} is the lowest seismic waves velocity in the domain of investigation, ν_{max} is the frequency to be resolved, $f(n)$ is an empirical function depending on the n_l degree of the Lagrange interpolant, basically if $n = 4$, $f(n) = 5$.
The second parameter to be considered is the time step Δt to be used for the time integration scheme in order to have a stable solution of 2.4. The CourantFriedrichsLewy condition (CFL condition) is used [10]: this condition basically defines the Courant stability number $C = \Delta t(v/\Delta h)_{max}$ and states out that it must not be higher than a given upper limit $C_{max} \subseteq [0.3, 0.4]$ which is determined in a heuristic way. The Courant stability upper limit gives the following condition on the time step Δt:

$$\Delta t < C_{max} \frac{v_{min}}{v_{max}} \frac{1}{\nu_{max}} \frac{n + 1}{f(n)} \tag{2.11}$$

where v_{min} and v_{max} are respectively the maximum and minimum wave speed in the element which is considered, and the other variables are defined as in 2.10. The last requirement to be honored in order to construct a good mesh of the domain Ω is that the distortion between each hexahedra and the reference cube has to be as little as possible; this can be translated on a condition about the values of the angles between two connected edge of one element: good angles are near 90 while bad angles are smaller than 30.
A good way to check this is to calculate the maximum value of the equiangle skewness for

each element defined as

$$f_{skew} = \frac{|2\theta - \pi|}{\pi} \tag{2.12}$$

where θ is the angle, measured in radians, between two connected edges of one hexahedron, following this definition an angle of 90 has $f_{skew} = 0$ and an angle of 30 has $f_{skew} = 0.65$.
It is important to keep in mind all the implications of SEM methods discussed above while approaching the creation of the mesh for the domain of investigation. The spectral elements dimension, which is related to the frequency to be resolved (equation 2.10), has to be determined considering the spatial resolution of the model defining the investigation domain Ω. For example a mesh with elements of dimension $10\ m$ can be used to represent a model which has a spatial resolution of $100\ m$. The use of these small elements could be necessary in order to honor the discontinuities of the model but it would not add any information to the initial model. Thus the maximum meaningful frequency which can be resolved by this mesh has to be calculated using the spatial resolution as value for Δx in equation 2.10.

Chapter 3

3D geologic model of David Glacier

3.1 Introduction

In order to create a 3D geologic model of a glacier we need a description of the topography, an ice thickness model and a description of each geological discontinuity below the ice. Data about ice thickness are very difficult to be obtained because they require in-situ measurements such as Ground-penetrating radar or active seismic experiments; perform those kinds of campaigns in the Antarctic region is not easy so, despite of the presence of two scientific stations in the Victoria Land, a model for the David Glacier inner morphology doesn't exist.

3.2 Data sets

I have performed a search throughout the web and I have found out two interesting data sets, one for the description of the free surface of the region and the other regarding the description of subglacial morphology, respectively named Radarsat Antarctic Mapping Project Digital Elevation Model Version 2 (hereinafter RAMPDEM) provided by the National Snow and Ice Data Center - NSIDC, and BEDMAP provided by the British Antarctic Survey - BAS [24][25]. The RAMPDEM was developed by the use of a broad variety of available topographic source data such as satellite radar altimetry, airborne radar surveys, the Antarctic Digital Database (version 2), and large-scale topographic maps from the U.S. Geological Survey (USGS) and the Australian Antarctic Division. Data were collected between the 1940s and present, with most collected during the 1980s and 1990s. All data had been processed in a GIS environment and cover all of Antarctica from 60 S to 90 S **latitude** and from -180 W to 180 E **longitude** and are referred to the WGS84 ellipsoid surface. Developers provide RAMPDEM with three different resolutions, respectively 200 m, 400 m and 1 km but the real horizontal resolution of the RAMPDEM varies from place to place according to the density and scale of the original source data: as stated out by the developers the horizontal resolution of the RAMPDEM is about 200 m in the Transantarctic Mountains and Antarctic Peninsula, and about 400 m in the sloped coastal regions. My interest was focused on an area of David Glacier which belongs to a coastal region, so I have decided to use the RAMPDEM version with the resolution of 400 m.

BEDMAP is a consortium made up of researchers belonging to different institutes of different nations which gathered together all the data concerning the thickness of Antarctic ice sheets collected over the past 50 years in to a single database. This operation led to the creation of a complete model which covers the entire continent, and give useful information about the zones which has to be investigated yet. BEDMAP represents a continental ice thickness model which has a nominal horizontal resolution of 5 km but, due to the difference in data density, this value should be higher depending from the zone which is considered (Figure 3.1). Another feature that has to be taken into account is the fact that while BEDMAP covers also the area of the Antarctic seas providing a model for the bathymetry too, RAMPDEM does not provide any value out of the shore line. Because I was interested in creating a model just for

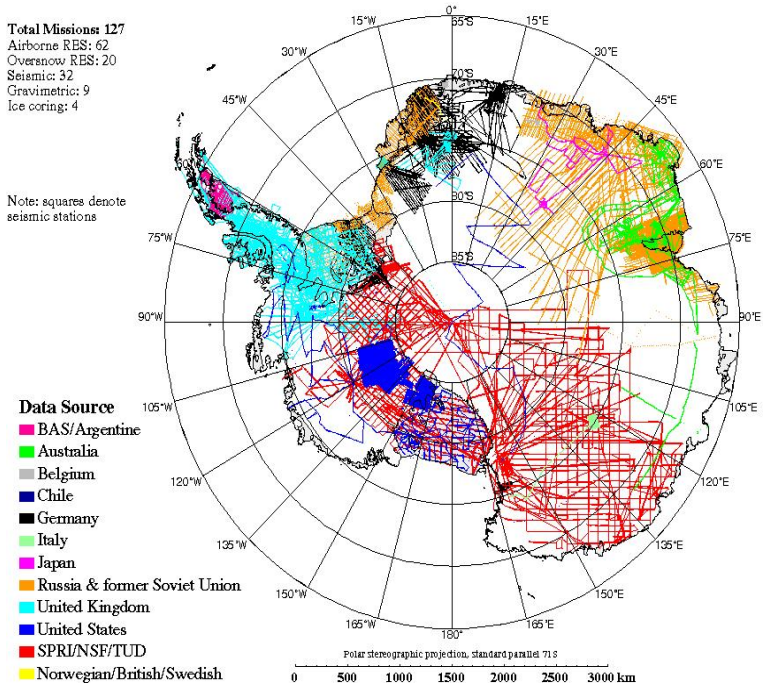

Figure 3.1: Map showing coverage of BEDMAP icethickness data sets [25].

the David Glacier area, and not for the whole Antarctica, I have selected a zone which goes from 158 E to 165 E **longitude** and from 74.5 S to 76.3 S **latitude**: in such a way the borders of the model are far enough from the hypocenters of the micro seismic events and from the locations of the stations (Figure 3.2).

3.3 Rotation of the reference frame

All versions of SPECFEM code use internally the **Universal Transverse Mercator (UTM) projection** to create the mesh from the geological model of the zone you want to investigate about seismic waves propagation. David Glacier belongs to the 58C UTM zone (Figure 3.3). Problems depending on the use of UTM projection in polar regions are notorious: distortion

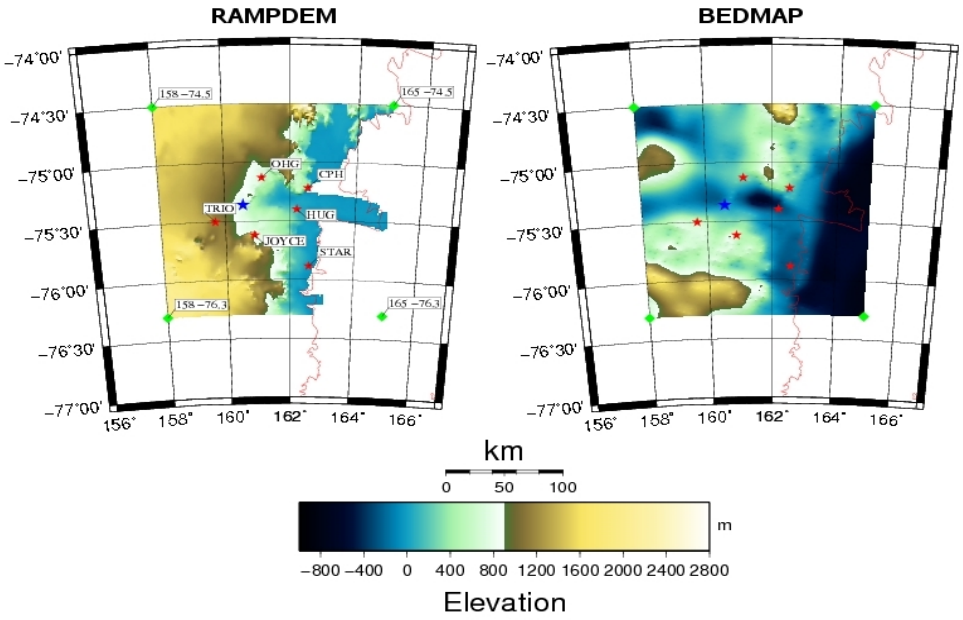

Figure 3.2: RAMPDEM and BEDMAP values showed respectively in the left and in the right frame - Red stars represent seismic stations positions - Blue star represents the hypocenter of a micro-seismic event.

in the distance between two points increases by approaching the North Pole or the South Pole. To avoid these kinds of problems I have decided to rotate RAMPDEM and BEDMAP data in order to have the center of the selected zone coinciding with the intersection between the Equator and the Prime Meridian: at these latitudes using UTM projection will not cause any problem. If we consider two reference frames sharing the same origin, but having different orientations (i.e. xyz and XYZ), we can use Euler angles to describe the rotation needed to pass from one reference system to the other one (Figure 3.4). First of all we have to define the nodal line which is usually obtained by the intersection of two planes ,if we use two homologous planes (i.e. XY and xy are homologous while XY and xz not) then the three Euler angles could be defined in six equivalent ways, all of them identified with a triple combination of the axis (e.g. z-x-z convention, x-y-x convention etc.); I have choose to use the z-y-z convention in which the nodal line is given by the intersection of the xy plane with the XY one, and the three Euler angles are defined as follows:

- Φ the angle between the y axis and the nodal line;
- Θ the angle between the z axis and the Z axis;
- Ψ the angle between the line of nodes and the Y axis.

Following this convention we can rotate the first reference frame on the second one by means of three subsequent rotations (remember that angles are usually defined in such a way that

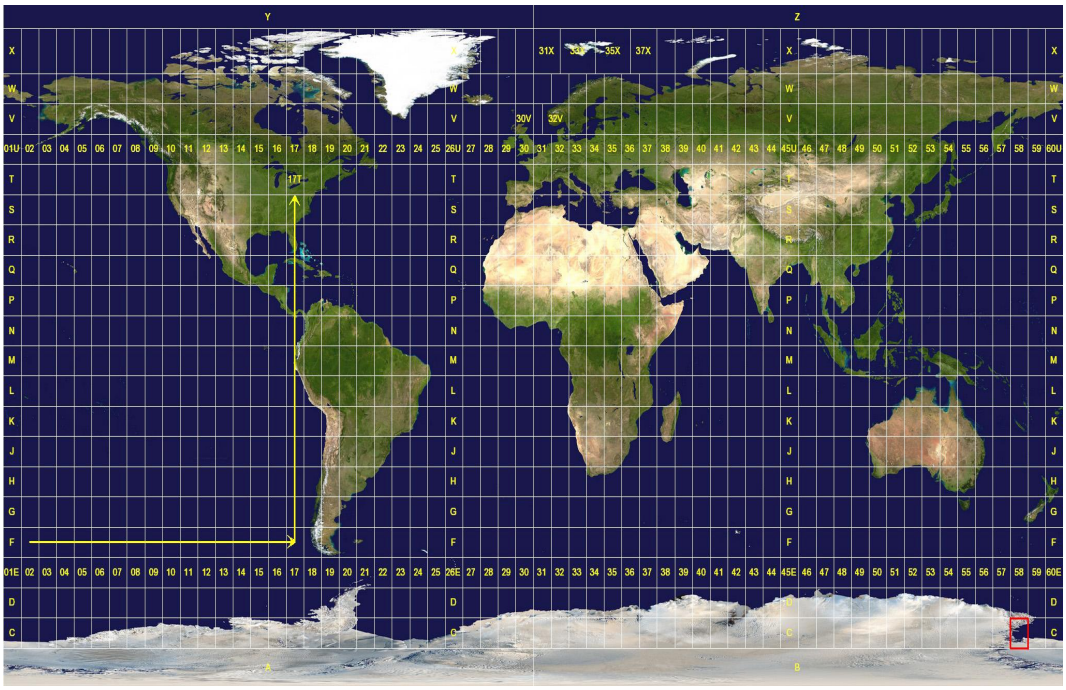

Figure 3.3: UTM Grid zones of the world - David Glacier is located within the red rectangle.

they are positive when they rotate counter-clock-wise):

- rotation of the system about the z-axis by Φ;
- rotation of the system about the y-axis by Θ;
- rotation of the system about the z-axis by Ψ.

The angles Φ and Θ to be used in the Euler rotation are basically the values of **longitude** and **latitude** of the study zone center which are respectively 161.5 E and 75.4 S. The latter rotation about the z-axis concerns only the orientation of the new X Y axes on the plane, this orientation does not deal at all with the propagation of the seismic waves and so there is no need to perform it, for this reason I did not defined Ψ angle. I have written a simple F90 code which takes in input the coordinates of the model points and, by means of the product of three rotation matrixes defined by the angles described above, performs the rotation of the points themselves; in such a way the new study region fills the area which goes from 0.935 W to 0.829 E and from 0.872 N to 0.924 S (Figure 3.5).

3.4 Incoherences between the two data sets

Because of the fact that the two data sets belong to different research groups I have firstly checked if they were consistent by simply superimposing them and as a result I have found out that in certain regions the height of BEDMAP was higher than the RAMPDEM one: I

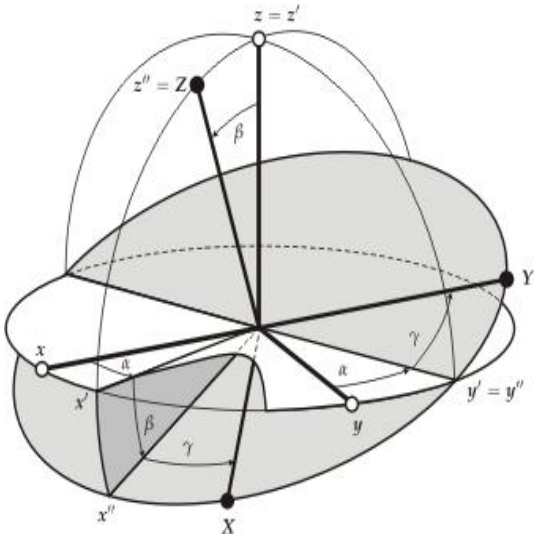

Figure 3.4: Two different reference frames orientations defined by Euler angles.

needed to find out the most reliable in order to correct the other one. I have created a set of benchmark zones using maps provided by the "Museo Nazionale dell'Antartide" (MNA), in which is indicated also the ice thickness [3],[5],[6],[18], and GPS data, obtained by a set of stations located in the David Glacier area [8].
The comparison of these benchmarks height values with the ones given by the two data sets showed up that RAMPDEM is the most reliable one; this result is not surprising: in fact, as I have already said, obtaining ice thickness information is expensive and difficult because are needed data from ground based missions, such as Ground-penetrating radar active seismic experiments and drilling, or airborne radar altimetry. The zones of inconsistency should be divided in two: the ones which belong to a mountain area and the ones which are located in plain (Figure 3.6). I have decided to use different approaches to correct height values of BEDMAP points belonging to these zones: concerning the mountain areas ice thickness values are in the range of 100 meters so the presence of ice should be not important in the propagation of seismic waves, that is why I have decided to make equal BEDMAP height values and the RAMPDEM ones. Regarding the zones in plain I have adopted a little bit more complex criterion: for each point I have calculated the difference between BEDMAP and RAMPDEM data, taking into account this value I have calculated a thickness to be subtracted from BEDMAP heights; in such a way I have created a set of smoothed ice-basins (Figure 3.7). All the operations described above performed by the use of Generic Mapping Tools (GMT) and of some AWK'script and Fortran90 program written myself. The last problem I have encountered in creating a geological model for the David Glacier concerns the height of BEDMAP points corresponding to the seismic stations positions: researchers positioned these stations onto rock outcrops called nunataks, this ensure us that in these points, and in the areas surrounding them, the height of BEDMAP and RAMPDEM models must be equal. A quick search among them showed that BEDMAP values are several meters smaller than the RAMPDEM ones (Fig-

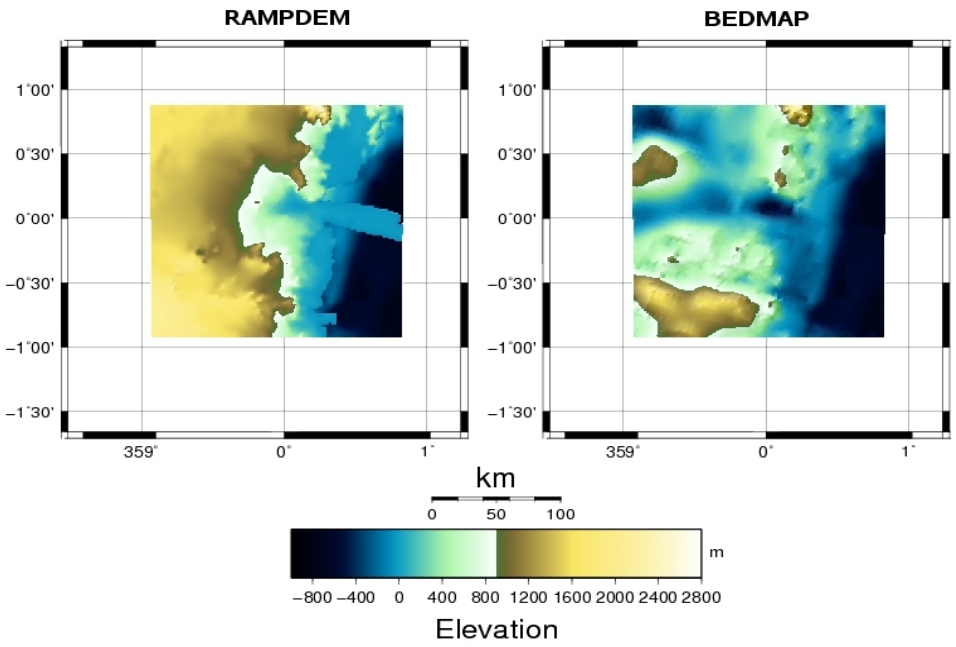

Figure 3.5: RAMPDEM and BEDMAP values showed respectively in the left and in the right frame after the rotation by means of the Euler angles.

ure 3.8(a)) so there is a need to modify the BEDMAP data in order to connect the rock surface with the free surface.
A reasonable way to raise the level of rocks up to the free surface is to insert one hill in correspondence of each stations area. A hill can be parameterized by the use of a very simple geometric shape such as a cone with the following properties: the basal radius value has to be chosen to create a smoothed hill and avoid the creation of a spike while the height is given by the difference of the GPS value and the smallest z value which can be found in the area surrounding the station (Figure 3.8(b)).
I will then check the topographic effect of these artificial features on seismic wave propagation. Although this clearly is an ad hoc modification, not based on specific structural information, it seems the only way to produce seismograms that can resemble the actual situation, I emphasize that otherwise I should have placed the corresponding stations on ice, while they are clearly located on rocky hill-like outcrops known as nunataks.

The software I have used to modify the zone around each seismic station is EarthVision®: thanks to an intuitive graphical user interface it allows to easily manipulate only certain areas of a data set by inserting corrective values, with a weight which is defined by the user itself, and to check the results of such changes in real time. The 3D model can be then exported in several different formats including the *gOcad Group file* (*.gp) in which the three coordinates of all the points of the model are represented by a vertex identifier and these vertexes are used to define a set of triangles representing the surface of the model as shown in Figure 3.9.

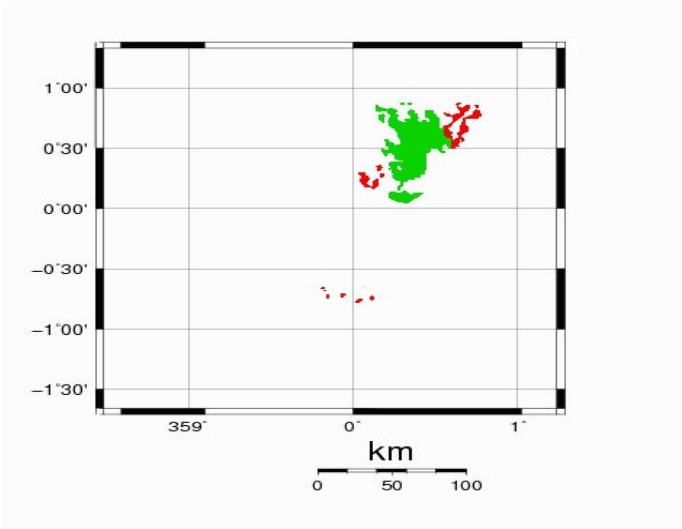

Figure 3.6: Zones of inconsistency: red ones belong to mountain areas, green ones belong to plain areas.

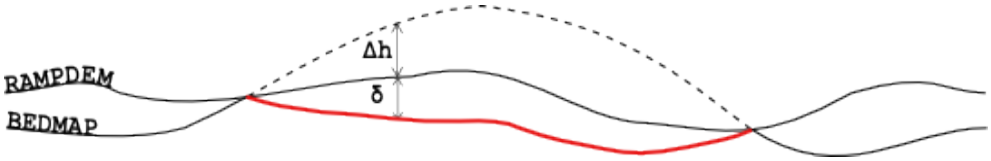

Figure 3.7: Example of inconsistency zone in plain: dotted line represents points with BEDMAP height higher than RAMPDEM one, Δh is the difference of the two models height values and δ is a parameter which depends on the value of Δh. Red line is the final result for BEDMAP and is given by $BEDMAP - (\Delta h + \delta)$.

In all the pictures I made with EarthVision® the axes have different scales, in particular the z one is in meters while the x and y are in geographical degrees and cover an area of about $4 * 10^4 km^2$; I made this choice in order to emphasize the topography and subglacial morphology features, this is why the hills I have introduced appear more as spikes. As a result of these operations I have obtained a reasonable geologic model of David Glacier region shown in Figure 3.10.

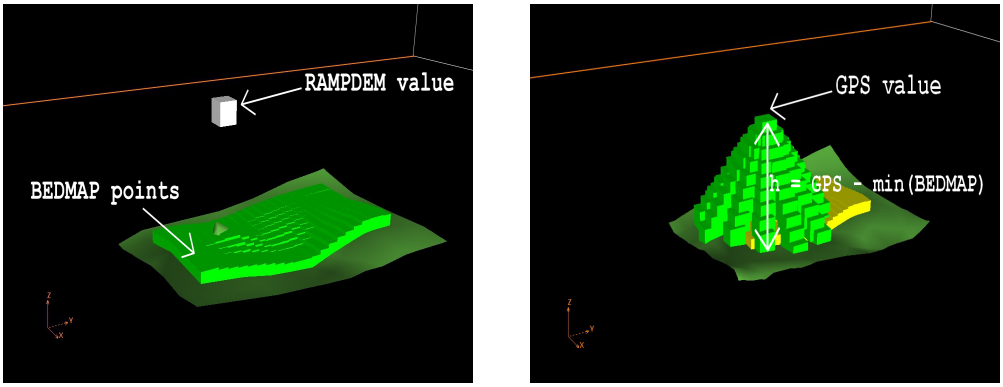

(a) (b)

Figure 3.8: Figure 3.8(a): STARR station - RAMPDEM height value represented by the white cube, BEDMAP height values represented by green cubes. Figure 3.8(b): connection between RAMPDEM and BEDMAP values around STARR station.

```
VRTX 1 862317.538384 96585.607749 2348.884126
VRTX 2 862567.438151 96584.267796 2304.065752
VRTX 3 862521.144873 96585.827122 2304.065752
VRTX 4 862569.017064 96580.159002 2304.065752
VRTX 5 862923.307087 96582.352730 2240.242572
...
...
TRGL 1597 1598 1599
TRGL 1599 1598 66922
TRGL 1538 1537 1525
TRGL 1610 1611 1597
TRGL 1597 1599 1613
TRGL 1599 1612 1613
```

Figure 3.9: Section of a *gp* file. Each vertex (VRTX) is identified by an ID and three coordinates. Each triangle (TRGL) is defined by three vertex IDs.

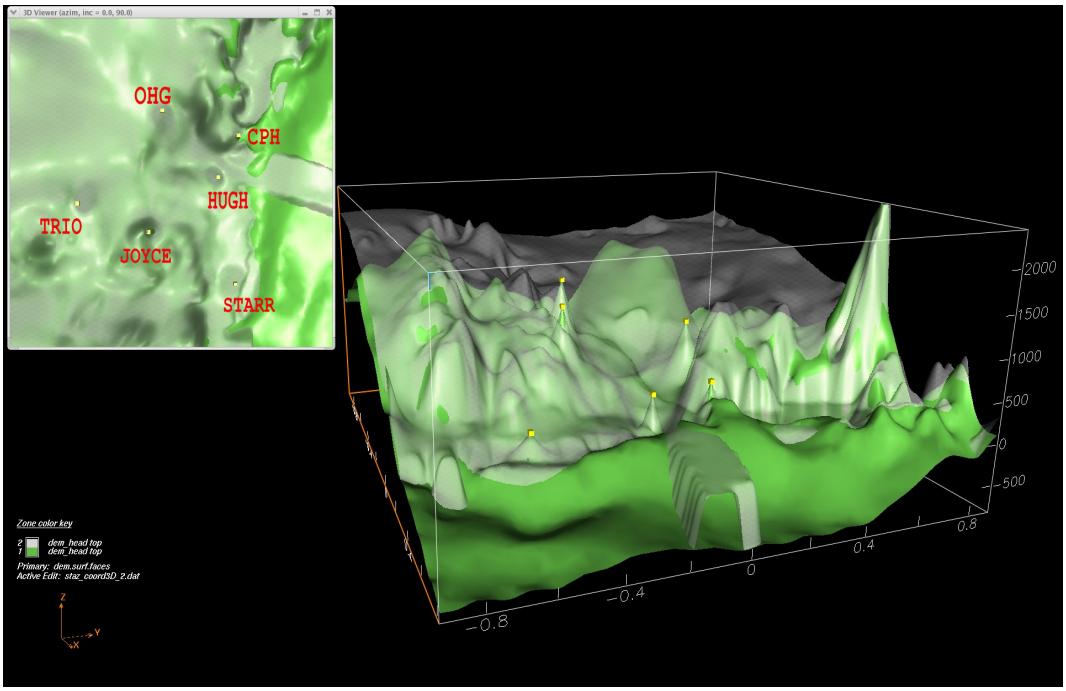

Figure 3.10: David Glacier geologic model: RAMPDEM values represented in white, BEDMAP values represented in green, yellow square represents seismic stations positions. Upper left corner shows a top planar view of the region.

Chapter 4

Creation of the mesh

4.1 Introduction

The term mesh describes a set of geometric shapes which are all connected together, in 3D computer graphics meshes are used to represent the surfaces and the volume of a three dimensional object. The elements which constitute the mesh are usually tetrahedra or hexahedra in order to simplify the rendering operation, but also more complex polygons such as concave polygons or polygons with holes can be used. However each element of a mesh is composed by a certain number of vertices which are connected by mean of a topology and form a set of edges, these delimit the faces of the element which form the volume of the polygon.
In numerical methods two kind of meshes are commonly used: the structured meshes and the unstructured ones. The difference between them can be explained considering the topological dimension of the domain of investigation d, i.e. $d = 2$ or $d = 3$ when dealing respectively with a two-dimensional or three-dimensional problem. A structured mesh must be constructed in a way that every interior vertex has exactly $2d$ neighbors, on the other hand an unstructured mesh does not need to follow this rule.
Using a different approach it can be said that a structured mesh has a regular connectivity between its elements and can be obtained for example by the distortion of the elements of a regular grid. On the contrary an unstructured mesh is characterized by an irregular connectivity which has to be explicity stored.
As seen in Chapter 2 the definition of SEM implies some important restrictions on the creation of the mesh:

- the linear dimension of the elements controls both the frequency resolution of the simulations and the time step to be used,
- the shape deformation of the elements from the reference cube determines the stability of the simulations.

In addition to that there are other elements to be taken into account while creating a mesh: the generic domain of investigation Ω may contain boundaries of regions with different physical properties, because a geological model often contains features such as sedimentary basins

with peculiar geometries it is difficult to find simple discontinuities as in 2.1. As I said in Chapter 2 each element of the mesh contains a set of GLL points used to solve the elastodynamic equations, in these points are stored the physical properties of each material contained in Ω and they can vary inside an element, so there is the possibility to represent an interface even if the mesh is not able to follow it by mean of interpolation.
A mesh should honor all the discontinuities of the domain Ω otherwise the melting of different physical properties in the same spectral element will introduce numerical errors in the synthetic seismograms. Furthermore this kind of interpolation will produce, in the case of an oblique interface, an undesired staircase sampling of the model and non-physical diffractions in the synthetic seismograms. I will check the influence that this kind of approximation has on the synthetic seismograms.
Furthermore the numerical resolution of the mesh should be constant in the whole model, that is to say that the number of the GLL points used to represent the desired wavelength λ should be the same in each zone of the domain Ω. Because of the fact that normally wave speeds increases with depth the mesh should have an higher number of elements near the free surface and in regions with low wave speed according to 2.10.
The last thing to be considered while approaching the creation of the mesh is the computational cost of seismic wave propagation simulations: the number of elements in a mesh varies from hundreds of thousands, for local-scale simulation with low-frequency content, to hundreds of millions, for regional-scale simulations.
In order to create the mesh of the David Glacier geological model I have decided to used the CUBIT mesh generation toolkit developed at Sandia National Laboratories [11]. CUBIT is a two- and three-dimensional element mesh generator which can handle both tetrahedra and hexahedra elements, it provides the user with a large variety of tools and algorithms to modify and decompose the geometry and to control the meshing process, it also includes a very useful Python Interface.
The creation of a 3D mesh is not an easy task and three dimensional simulations have high computational costs, so I have decided to create also a set of meshes in two dimensions, which are easier to be constructed, to be able to test the influence on the numerical simulations of different parameters such as the description of the geometry of the model, the approximation of the interfaces by mean of physical properties interpolation or the source time function used in the simulations.

4.2 3D mesh

Softwares for 3D imaging make use of different 3D modeling kernels which provide different features to create three-dimensional geometries and modify them characteristics. Among these kernels, or engines, there are also the 3D ACIS modeler (hereinafter ACIS) and the Facet geometry engine (hereinafter FACET). The main difference between these two engines is that while ACIS makes use of B-spline to create and manipulate curves, surfaces and volumes, FACET represents the geometry by mean of a collection of polygons, basically planar

triangles or quadrilateral.
The first step to be accomplished, in order to create the mesh, is to import in CUBIT the geometry description of the investigation domain: the software can accept in input files belonging to both the ACIS modeler and the FACET engine.
As pointed out in the previous chapter, EarthVision® exports the surfaces created for the David Glacier geological model in *gOcad Group file* (*.gp) format file described in 3.9; unfortunately this format is not directly supported by CUBIT so I have written a brief AWK script which converts a *gp* file into a FACET one: in such a way importing the RAMPDEM and BEDMAP surfaces in CUBIT is almost automatic. Because the CUBIT package offers a wider variety of tools and algorithms to be used in the ACIS environment than in the FACET one it should be useful to switch the geometry engine from the second one to the first. This can be accomplished easily using a tool provided directly by CUBIT: starting from a surface meshed with a *map* or *submap* scheme it is possible to create a new surface belonging to the ACIS geometry engine without information loss. The result of this operation is shown in Figure 4.1.
It appears clear that the layer between the two surfaces is really thin and near the stations

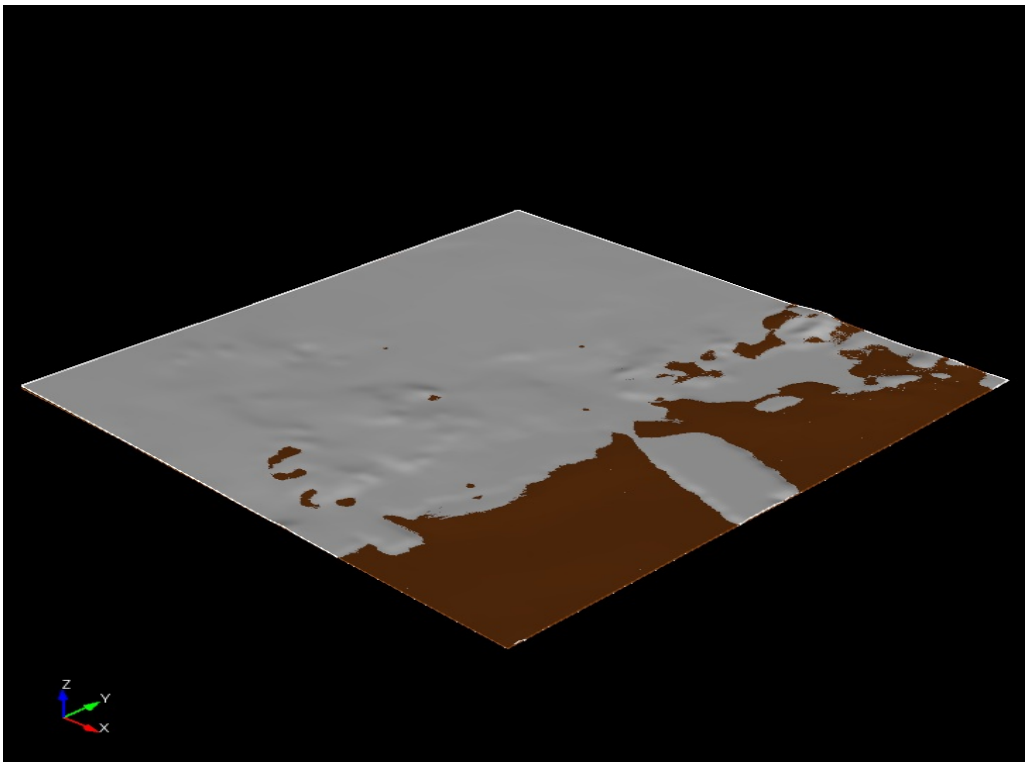

Figure 4.1: Surfaces of RAMPDEM and BEDMAP models imported in CUBIT and represented respectively with white and brown colors. In all the picture made with CUBIT, unlike for the ones obtained with EarthVision®, there is no exaggeration on the vertical axis.

areas, the zones in which I have introduced the cones to connect BEDMAP with RAMPDEM, the situation get worse in such a way that the meshing operation would become really hard if not impossible: even the use of small elements would not avoid the rise of a bad skewness

factor (Figure 4.2).

Taking into account the fact that the knowledge about the subglacial morphology model is

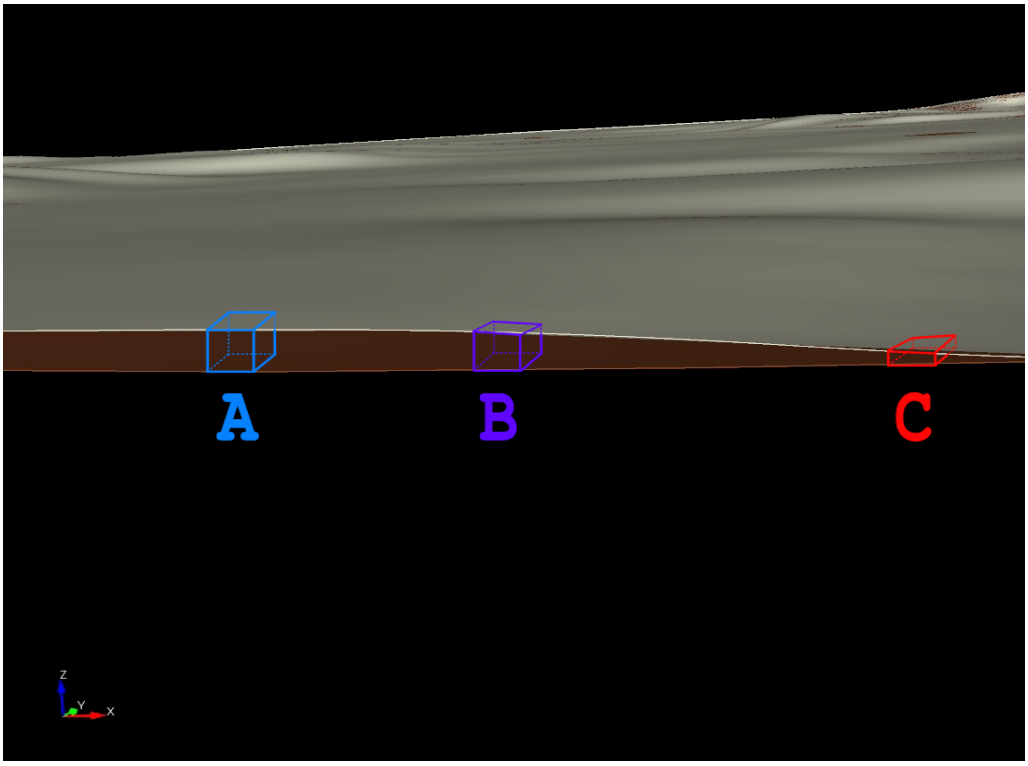

Figure 4.2: Example of three hexahedral elements used to mesh the connection zone between bedrock and topographic surfaces: it can be noted easily that while element A is a cube and element B shows only some distortion, element C, in order to honor the zone in which icethickness goes zero, almost collapse.

poor I have thought that creating a mesh following the interface ice-rock would probably be a waste of time, so I have decided to generate the mesh using only the free surface of the model and to insert the BEDMAP surface by mean of the GLL points interpolation I have described in the previous paragraph.

When I started creating the mesh for the David Glacier, the package SPECFEM3D_BASIN was not yet completely ready to accept a mesh created with CUBIT: in fact some features were not usable in the simulations, for example the *absorbing conditions* of the bottom layer were not yet tested and this could cause the presence of undesirable reflected waves into the synthetic seismograms.

I have calculated the value of the depth at which the bottom layer of the mesh has to be placed in order to avoid the presence of this unfair noise in the following way: I have took $t = 80\ sec$ as the length of synthetic seismograms, $z_{crust} = 24\ km$ as the thickness of the crust layer with a mean speed of P-waves equal to $\bar{v}_{crust} = 6.3\ km/sec$, $v_{mantle} = 8.1\ km/sec$ as the P-waves speed in the mantle layer (all values obtained by CRUST 2.0), therefore the mantle

layer depth z_{mantle} can be obtained using the formula

$$z_{mantle} = \frac{v_{mantle}}{2}\left(t - \frac{2 \cdot z_{crust}}{\bar{v}_{crust}}\right) = \frac{8.1}{2}\left(80 - \frac{2 \cdot 24}{6.4}\right) \simeq 300\ km. \tag{4.1}$$

So the depth of the mesh bottom layer is given by the sum $z_{crust} + z_{mantle} = 324\ km$. The final result is shown in Figure 4.3.

To determine the dimension of the elements to be used in the construction of the mesh I have

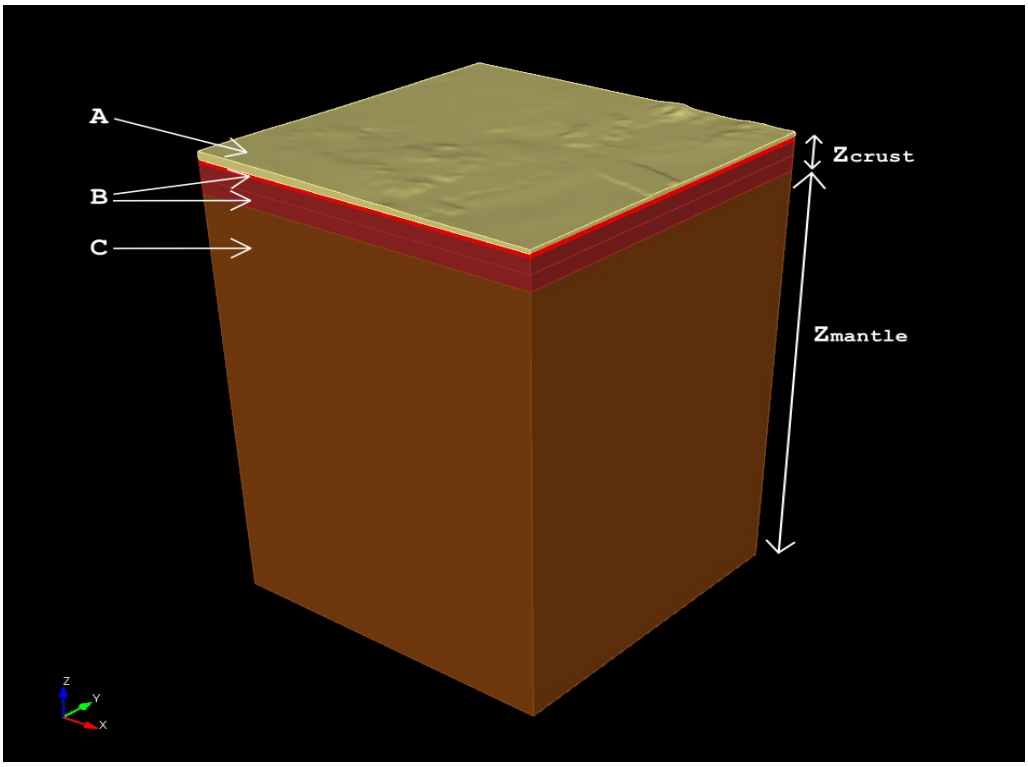

Figure 4.3: Image of the volume obtained for the David Glacier geological model using CUBIT. On the top surface of the volume it is possible to distinguish the features of RAMPDEM topographic model (light yellow color). Zone **A** contains both the *ice* layer and the first part of the *bedrock* layer; zone **B** represents the *upper* and *lower crust* layer; zone **C** describes the *mantle* area. The value z_{mantle} is obtained following equation 4.1.

used equation 2.10, where in this case the seismic wave speed minimum value is the value of Rayleigh waves speed propagation in ice $v_{min} = 0.89 \cdot v_s^{ice} = 1.7\ km/sec$, the maximum frequency to be solved is $\nu_{max} = 3\ Hz$ and the degree of Lagrange interpolant is $n_l = 4$, the resulting upper limit of the element linear dimension is $\Delta x_{max} = 550\ m$; in order to avoid loss of information in the neighborhood of $3Hz$ I have chosen a value of $500m$ for Δx.
This value is well suited for the elements contained within the ice but, because of the fact that

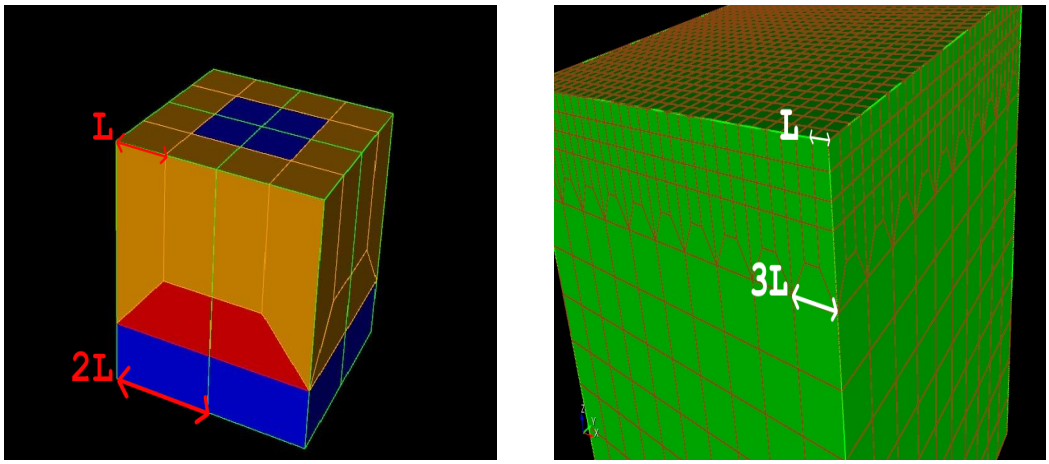

(a) (b)

Figure 4.4: Figure 4.4(a): example of doubling refinement obtained with a Fortran90 code written by Dimitri Komatitsch. Figure 4.4(b): example of CUBIT native refinement algorithm; linear dimension of element edges increases from L to $3L$ producing a transition between 1 to 27 hexahedra.

wave speed increases with depth, the same equation leads to another value while considering the physical properties of bedrock region: here the minimum wave speed value is $v_{min} = 3.2\ km/sec$, so in order to solve the same frequency $\nu = 3\ Hz$, elements with edges length of $900\ m$ are enough.
A good improvement in term of computational cost lies in the possibility of enlarging element dimension from the value in the ice layer to the one in the bedrock layer; the ratio between the edge length is almost $1:2$ so a *doubling* algorithm is required (Figure 4.4(a)). Unfortunately the CUBIT package provides another algorithm called *refinement* which produces a transition between 1 to 27 hexahedra, with a resulting tripling in the linear dimension of the elements as shown in Figure 4.4(b).

That notwithstanding CUBIT provides a wide variety of tools to mesh lines, surfaces and volumes, by combining some of them it is possible to create a sort of *home-made doubling*.
Here it is a brief description of the schemes and algorithms I have used to create a refinement with a transition ratio of $1:2$:

- scheme *equal*: it meshes a curve using producing a set of equidistant nodes, the number of nodes has to be set in advance;
- scheme *map*: this scheme produces the mesh of a surface or of a volume using quadrilateral or hexahedral elements, it requires that each side and the corresponding obverse contains the same number of elements;
- scheme *pave*: it meshes a surface in an unstructured way using quadrilateral elements;
- *sweep* command: given a source surface, which has to be already meshed, and a target

surface not yet meshed, this command produces an extruded (i.e. with a fixed cross-sectional profile) hexahedral mesh of the volume between the two surfaces.

First of all I have divided the whole volume into 3 parts, in order to honor the major discontinuities of the geological model: the transition between upper and lower crust and between the lower crust and the mantle. After that I have inserted two additional surfaces into the upper part of the volume creating two transitional layers to be used to perform the *doubling*. I have meshed the free surface with elements of $500\ m$ using the scheme *map*, this scheme often changes the length of elements edges producing wrong results mainly on the boundaries of the surface. To avoid this problem I have firstly meshed the boundaries of the free surface with edges of $500\ m$, in such a way the mesh process is more constrained to honor the dimension of elements (volume A in figures 4.5(a) and 4.5(b)). I have then propagated using the *sweep* command the mesh till the first layer in which I have previously divided the volume.
The layer has got four lateral surfaces which can be divided in two different couples formed by one lateral surface and its opposite: I have meshed the lower sides of one couple (Figure 4.5(a): line C and its opposite) using the scheme *equal* taking a value of $500\ m$ for the distance between nodes, while I have meshed the lower sides of the other couple (Figure 4.5(a):line D and its opposite) with elements of dimension $900m$; I have then used the scheme *pave* to mesh one of these surfaces (same figure, surface B) and, taking its opposite as the target surface, I have meshed the whole volume of this first layer using the command *sweep* (Figure 4.5(b)).
Using the same passages described above I have meshed the second transitional layer, obtaining as final result the passage from element with linear dimension of about $500\ m$ to hexahedra with edges of $900\ m$. Finally I have simply used the command *sweep* to mesh all the remaining parts of the volume (Figure 4.5(c)). Figure 4.5(d) shows two slices of hexahedral elements obtained following these passages.
As stated out in the chapter on the Spectral Element Method, the quality of the mesh has to be checked in order to avoid numerical problems during the simulation: the two parameters to be controlled are the Jacobian of equation 2.7 and the skewness factor defined in equation 2.12, in particular the first one should always be positive and should never vanish while the second one must be lower than 0.65.
CUBIT provides useful tools to check the quality of the mesh and both the Jacobian and the skewness are taken into account, but the definition of skewness used is slightly different from the one given in equation 2.12, so I have checked the values of the Jacobian directly with CUBIT algorithm while I have used a Python script by Emanuele Casarotti (personal communication) to check the skewness of the elements, the results are shown in figures 4.6(a),4.6(b) and 4.6(c). It appears clear that the mesh I have obtained has a very good quality level, in particular the values of skewness are quite impressive: this is a direct consequence of the fact that I have not honored the ice-rock interface.

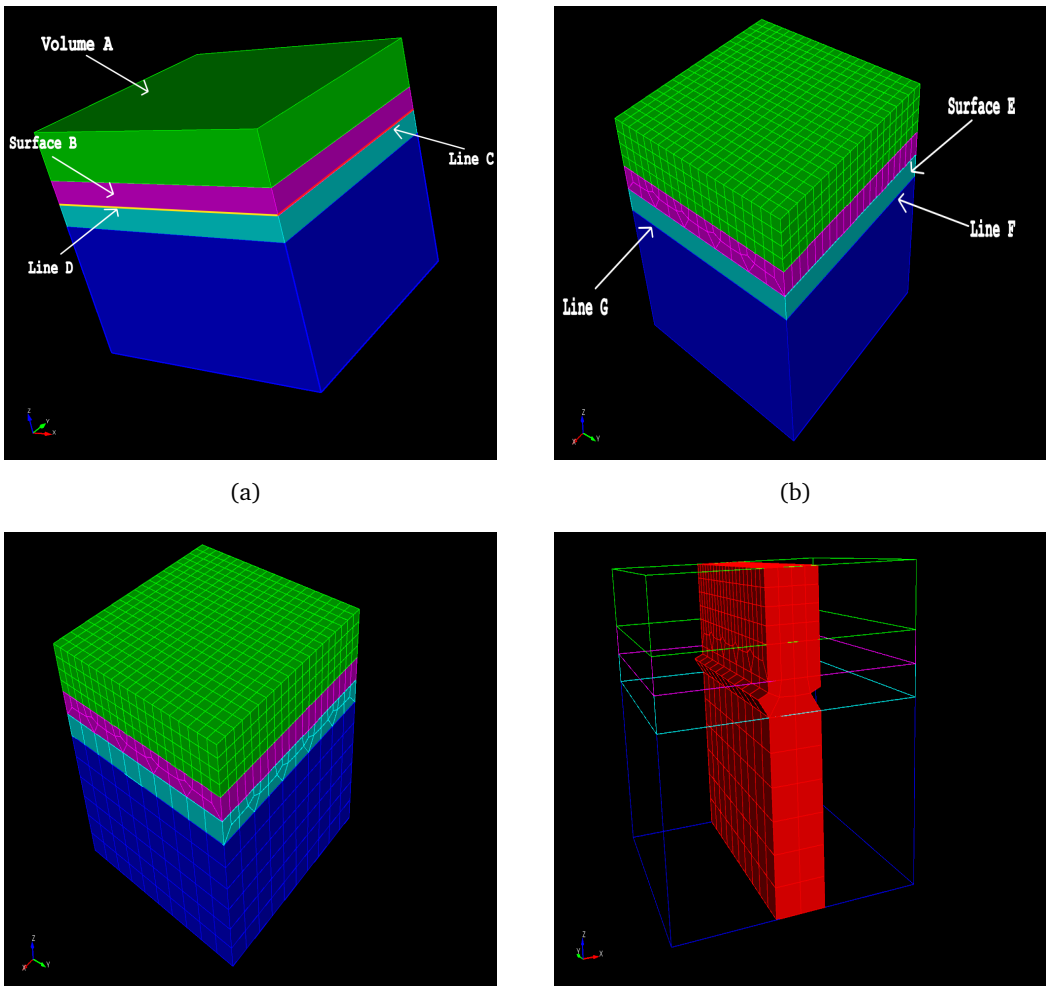

(a) (b)

(c) (d)

Figure 4.5: These pictures represent the passages I have done to perform the doubling.

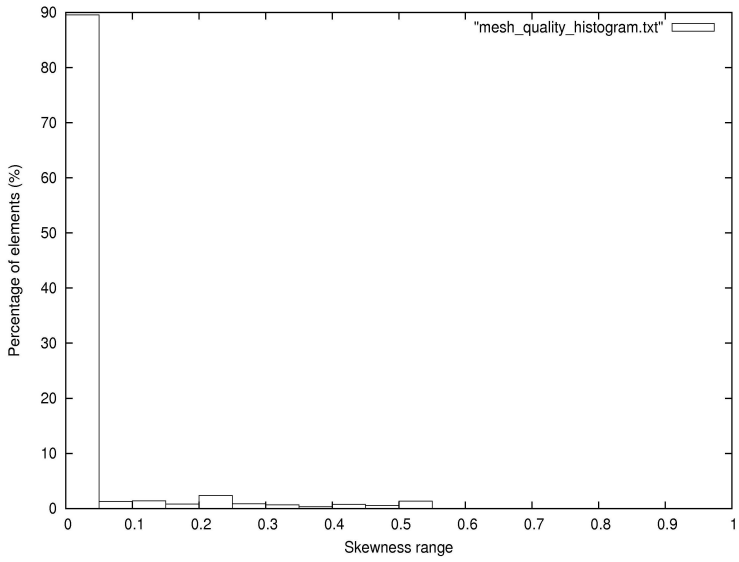

(a)

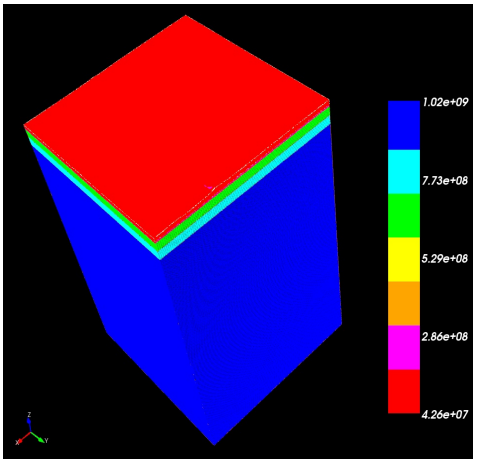

(b)

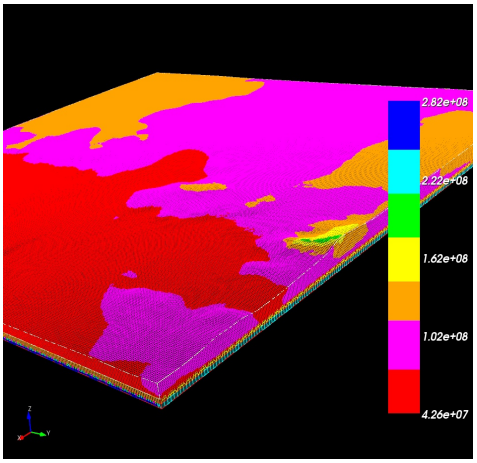

(c)

Figure 4.6: Figure 4.6(a): histogram showing the distribution of *equiangle skewness* values in terms of elements percentage. Figure 4.6(b): Jacobian values for all the elements of David Glacier mesh obtained using the quality check tools provided by CUBIT. Figure 4.6(c): CUBIT is capable to show also only certain ranges of values for the Jacobian, in this way it is possible to check the worst elements of the mesh and to decide how improve their quality.

4.3 2D meshes

A two dimensional mesh represents a good laboratory to test the influence on the wave propagation of different parameters, in fact the creation of a mesh in two dimensions is easier and faster than in three dimensions, and also the numerical simulations have a lower computational cost because of the reduction of the number of elements.
Using GMT I have extracted from the digital elevation model RAMPDEM and the bedrock topographic model BEDMAP a set of five profiles each of them including the position of one seismic station and of the seismic event hypocenter.
I have produced three different sets of meshes in order to analyze the effect that have onto the synthetics seismograms both the interpolation of different physical properties onto the GLL points of the spectral elements, and the changes of RAMPDEM and BEDMAP models.

4.3.1 Complete meshes

In this set of meshes I have explicitly represented the discontinuity into the model also the interface between ice and rock, honoring this discontinuity causes some problems mainly in the neighborhood of the stations, where the icethickness goes zero: this produces at least one element with a high skewness in correspondence of the connection between bedrock and free surface even if elements with small dimensions are used as shown in Figure 4.7.
Even if the creation of a mesh strongly depends on the geometry of the model, I have found

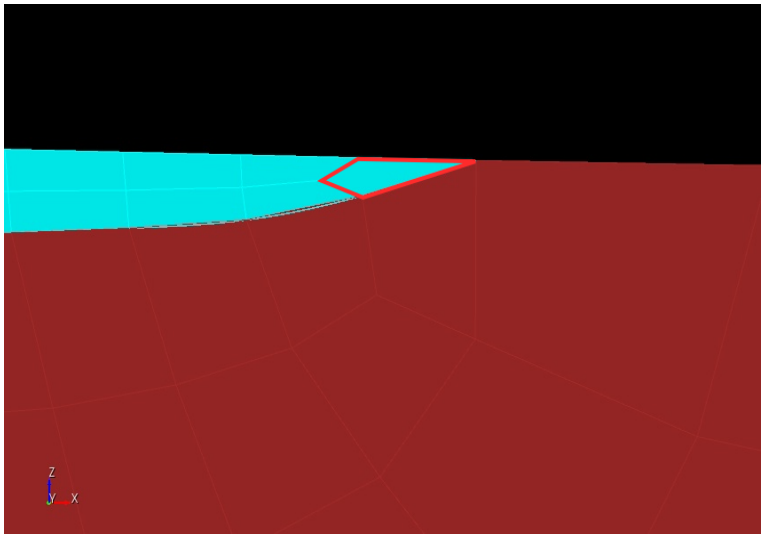

Figure 4.7: In this picture we possible to see the problems related to the zones of connection between bedrock and earth surface models: elements used to mesh the ice layer have linear dimension of $50m$, nevertheless at least one element - in figure the one with red edges - with a bad *equiangle skewness* is created.

a good outline which can be used in two dimensional meshing processes; in addition to the

CUBIT tools used to create the 3D mesh there are the following ones:

- command *sweep*: it can be applied also to a basic geometric element in order to create another object with an additional dimension, e.g. applied to a curve the command creates a surface;
- command *project*: according to its name this command projects a curve onto a surface;
- command *imprint*: this command let the user to divide a surface *imprinting* it with a set of curves;
- command *Collapse Angle*: by mean of this command it is possible to collapse small angles at vertices using virtual geometry.

The outline mentioned above can be described as follow: the first thing to be done is to import all the curves needed to define the model, i.e. all the geological discontinuities, such as ice-rock and topographic surfaces; after that the linear dimension for the quadrangular elements of the mesh must be set. In this case in order to create a mesh honoring the ice-bedrock interface I have chosen an element size of $50\ m$.
It is important to emphasize that this element dimension does not produce an improvement of the simulation frequency resolution which can be obtained only by mean of an improvement of the spatial resolution of the geological model: according to equation (2.10) the resulting theoretical resolution in frequency is $\nu_{max} = 30\ Hz$.
As for the 3D case the linear dimension of mesh elements can widen with the depth, so in rock region a dimension of $800\ m$ is suitable; to do so I have created an additional set of curves defining a transition region in which the *home-made doubling* can be performed.
All of these curves are created using the ACIS geometry engine, thus they are all defined using B-spline, it has to be noticed that often these curves, as created through CUBIT, do not result coplanars presumably because of some approximations, please note that even if differences in coordinates are not dramatic they could lead to serious problems during the creation of the mesh. I have solved this problem as follow: I have applied the *sweep* command to the digital elevation curve in order to create a generic surface, and I have *projected* and *imprinted* all the curves onto this surface, the final result is shown in Figure 4.8.

As mentioned before there is one last problem to be solved: all the zones where the ice thickness approaches zero produces elements with a bad skew factor; in order to avoid this I have used the command *Collapse Angle* described above, this produces a little step in correspondence of the link between the elevation and bedrock curves, anyway this step of about $50m$ should not introduce impurities into the simulations.
I have then meshed the ice thickness layer using the scheme *pave* with elements of $50m$, I have used the same scheme also to mesh the transition zones just below the BEDMAP discontinuity increasing the element dimension from $50m$ to $800m$ by mean of the so called *home-made doubling* (Figure 4.9(a),4.9(b),4.10(a)).
As for the three dimensional mesh I have checked the quality using another Python script due to E. Casarotti (personal communication) and I have found out, in certain cases elements with a skewness factor higher than the upper limit of 0.65: this is normal considering the fact

that the mesh honors perfectly all the discontinuities of the geological model.
A possible way to correct this kind of problem is to smooth the mesh using one of the scheme provided by CUBIT, but when the problem is related only to a small set of elements a better solution is to change directly the position of the nodes of the elements by hand.
The quality check script is also able to find the smallest edge contained in the mesh in order to determine the time step resolution to be used in the simulations according to equation 2.11: the value of $50\ m$ that I have fixed for the dimension of the elements, is considered by CUBIT as an upper limit and the use of *pave* scheme to produce a mesh honoring the discontinuities leads to the creation of elements with smaller edges (Figure 4.10(b)).

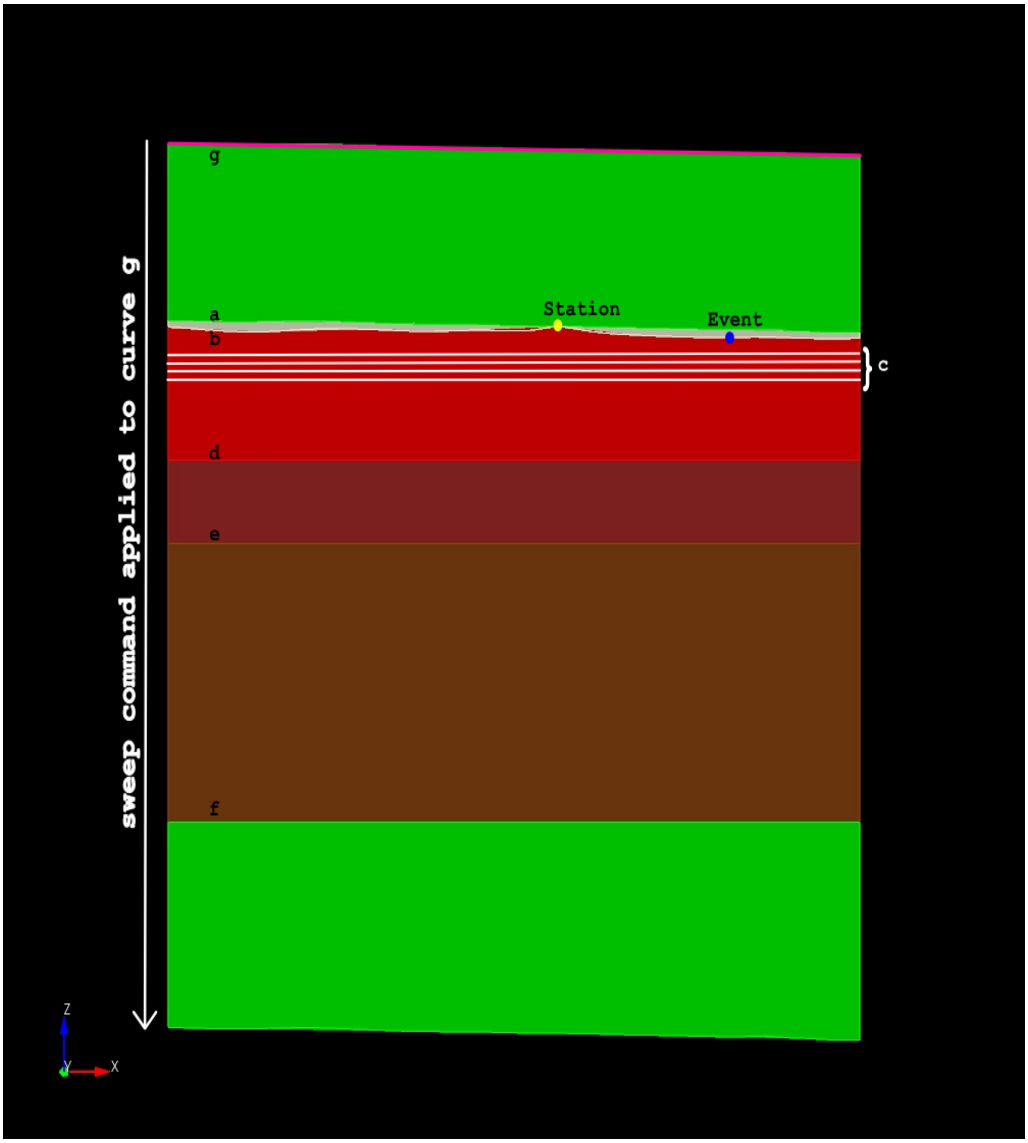

Figure 4.8: Example of the outline I have used to create the 2D meshes set. Curves *a,b* represent elevation and bedrock profiles while curves *d,e,f* represent respectively the interface between upper and lower crust, lower crust and mantle and the bottom layer. The set of white curves named *c* defines the region in which the *home made doubling* can be performed. The curve *g* is the one on which the *sweep* command is applied. Green surfaces are artefact that I have created in order to avoid problems while imprinting all the curves, thus they will not be meshed.

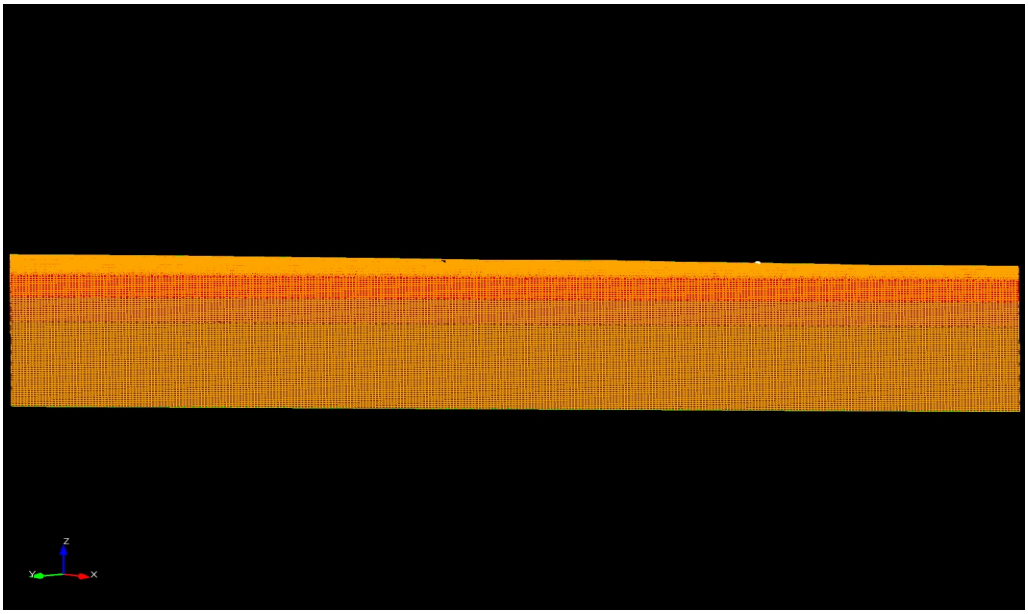

(a)

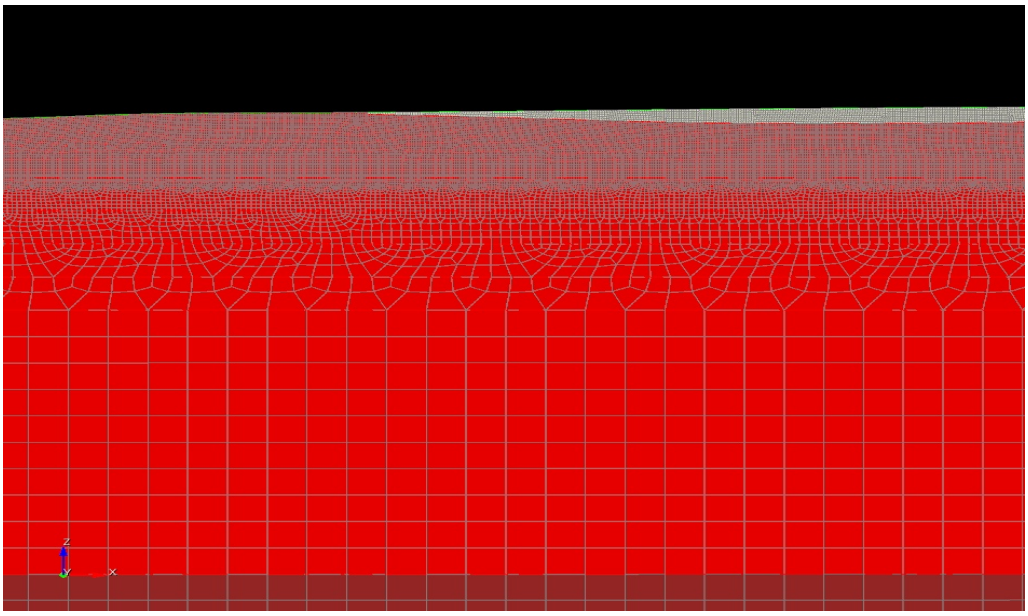

(b)

Figure 4.9: Figure 4.9(a): complete view of the mesh obtained for the profile containing the seismic event and the station STARR. Because of their linear dimension, $50m$, elements of the first layer are not clearly distinguishable. Figure 4.9(b): this picture shows the progressive enlargement of elements linear dimension. The lower part contains elements with edges of $800m$.

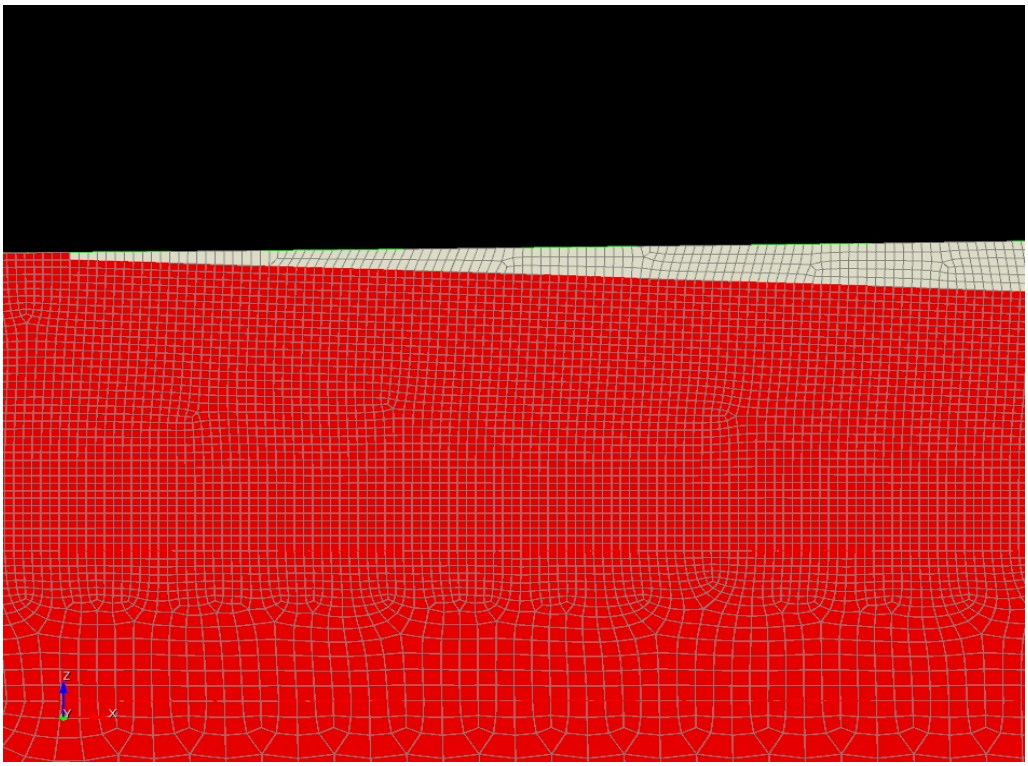

(a)

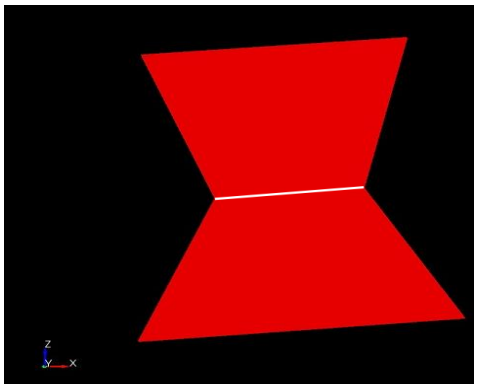

(b)

Figure 4.10: Figure 4.10(a): detail of the mesh showing the area in which icethickness goes zero. The lower part of the picture reproduces the first *home made doubling* layer. Figure 4.10(b): using the scheme *pave* to honor the geological discontinuities of the model, often leads to the creation of elements with edges smaller than the value required.

4.3.2 Meshes not honoring BEDMAP model

As mentioned in the first part of this chapter the GLL points contained into one spectral element can store physical properties belonging to different materials. This possibility is useful to represent interfaces and discontinuities within the model which should be difficult to honor explicity by the mesh. However this approximation leads to a staircase sampling of the model and introduces undesired alterations in synthetic seismograms.
The point to be clarified is about the size of the error committed in this way: in order to better understand this feature I have created a set of two dimensional meshes starting from the same profiles used to create the complete ones but without honoring the bedrock interface.
The meshes which contain also the ice-rock interface should be taken as benchmark for any kind of consideration.
In this case the use of elements with edges of $50\ m$ in the upper layer of the model would not be necessary but, in order to compare in a systematic way results belonging to similar meshes, I have decided to use, even in the creation of these meshes, the same dimension of the elements used before (Figure 4.11(a)).

4.3.3 Perturbation of the two models

I have created one last set of two dimensional meshes in order to understand which changes should be introduced onto the synthetic seismograms by an hypothetical improvement on the knowledge of both elevation and bedrock models.
As for the case described in the previous paragraph I have considered the meshes which honor also the ice-rock interface as the benchmark for any comparison of synthetic seismograms.
In other words the question I have tried to answer is: in which way the spatial resolution of the two data sets used to define the geological model acts onto the simulations in the range of frequencies I want to solve (i.e. $\nu \leq 3\ Hz$)?
I have created for each profile an additional one of total length equal to the distance between the selected seismic event and the seismic station, and with a distance between points defined as $\Delta x = 100\ m$; I have assigned to each of these points a height value by mean of a random number generation process with amplitude spreading between $-50\ m$ and $+50\ m$ then I have superimposed these new profiles on the original ones, both for RAMPDEM and BEDMAP model. The final result is a modification in the height of the points, belonging to the path *station-event*, of maximum amplitude equal to $\Delta z = 100\ m$.
To perform the meshing process I have followed the same passages described before and the final result can be seen in Figure 4.11(b).

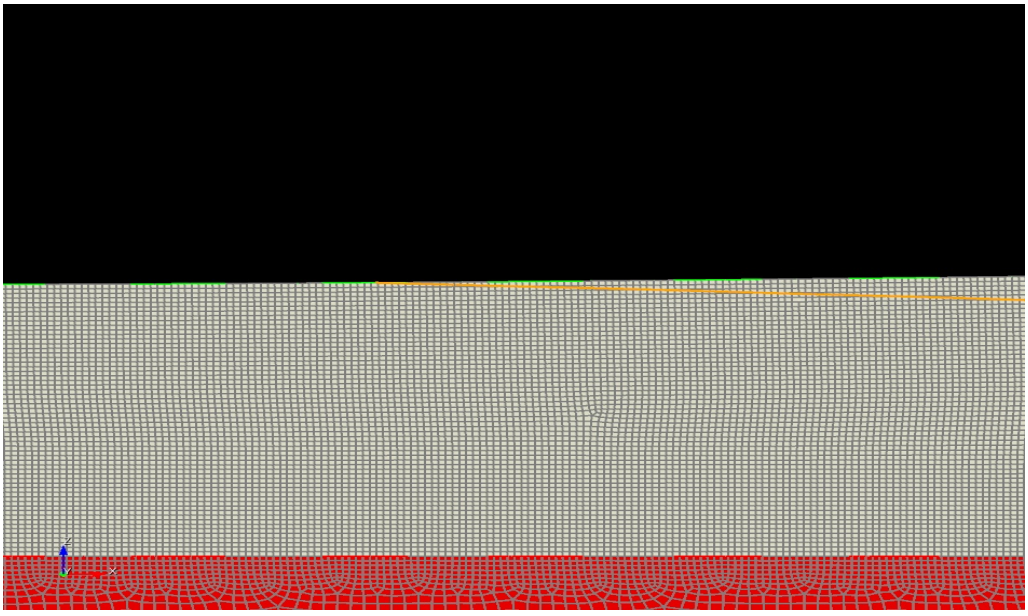

(a)

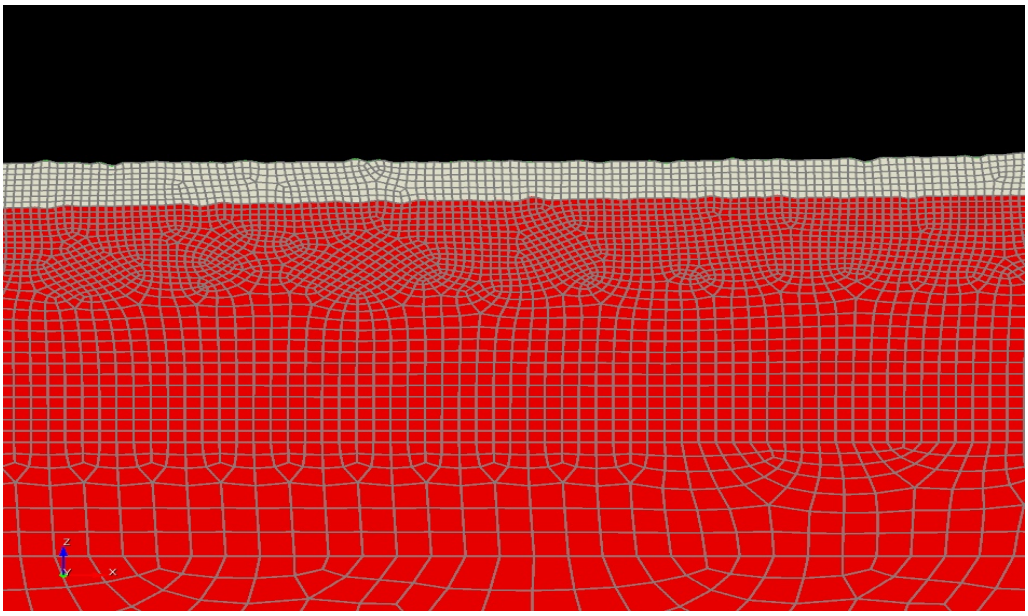

(b)

Figure 4.11: Figure 4.11(a): particular of the mesh for the profile containing station STARR in which the mesh does not honor the BEDMAP model. The interface ice-bedrock is represented by the orange line. Figure 4.11(b): particular of the mesh I have obtained perturbing both RAMPDEM and BEDMAP models.

Chapter 5

Simulations

5.1 Introduction

The Spectral Element Method described in Chapter 2 is well implemented in the open source package SPECFEM: the main developers of this code are professor Jeroen Tromp (Princeton University), professor Dimitri Komatitsch (University of Pau) and their colleagues.
I have chosen to use two different releases of the code to perform my simulations:
SPECFEM3D_BASIN and SPECFEM2D. There is also another version of the code, that is to say the
SPECFEM3D_GLOBE which is more suited to perform wave propagation simulations at a global scale [13],[16],[21].
Both SPECFEM3D_BASIN and SPECFEM2D are completely written in *Fortran 90*, they are capable of including in the simulations effects due to the topography, to lateral variations in compressional-wave speed, shear-wave speed and density, as well as they can accommodate full 21-parameter anisotropy and lateral variations in attenuation. Because of the fact that a typical seismic wave propagation simulation requires an enormous number of elements, depending on the scale of the simulation and on the frequency content also tens of millions of elements can be required, the need of a parallel computational approach is unmistakable: the computational domain represented by the mesh is decomposed using the incorporated SCOTCH software library [19], while the Message Passing Interface (MPI) is used to parallelize the code.
The code had been tested on a wide variety of clusters and it is provided with a *Makefile* containing a number of suggested entries for various compilers, thus the compilation of the whole code is not too hard even for a user without deep knowledge in parallel computing and programming.

5.2 SPECFEM3D_BASIN

The package SPECFEM3D_BASIN is composed of two main parts, that is to say the *mesher* and the *solver*; they receive input parameters from the *Par_file* where all the information needed for the simulation have to be stored. It is important to notice that the *mesher* and the *solver* can be run separately: this feature is of fundamental importance since it allows the use of a mesh created with an external software such as CUBIT.
Both *mesher* and *solver* use internally the **UTM coordinates** thus the zone number to be used to perform the projection must be defined: because of the problems related to the distortion caused by performing UTM projection in the of the poles I have decided to rotate the entire model of David Glacier using the Euler angles obtaining a resulting UTM zone number equal to 31.

5.2.1 The mesher

The *mesher* is a portion of the code which is capable to create a mesh of the investigation domain to be used in the seismic wave propagation simulations. In the *Par_file* the user has to define the size of the mesh and the number of the elements to be used for its creation, in addition to that there are other two important files needed in input by the *mesher*: the first one is the *Model* file containing the values of seismic wave speed contained in the different areas of the geological model, the other one is the *Topography* file which contains the description of the investigation domain free surface, in case it could include also the *bathymetry*.
Other important parameters that have to be defined in the *Par_file* are the total record length and the number of processors to be used to perform the simulation: because of the fact that the model has three dimensions the total number of processors must be divided along the two horizontal axes of the reference frame in which the computational domain is defined; the *mesher* performs the partition of the whole mesh in several slices according to the division defined above. For a complete description of all the parameters that have to be set in the *Par_file* please see the manual of SPECFEM3D_BASIN available online at [21].
It has to be noticed that the package SPECFEM3D_BASIN was originally created to simulate southern California seismic waves propagation thus the *mesher* was originally thought to describe the Los Angeles Basin [13]. Even if the code can be changed and adapted in order to represent other geological models, every modification is complex and the general nature of the SEM approach to the problem of seismic waves propagation can be lost, thus the capability of the code to accept meshes created with external softwares like CUBIT represents a great opportunity.
It is possible to create all the files needed by the SPECFEM3D_BASIN partitioner directly using CUBIT and its Python interface, in particular I have used a script due to Emanuele Casarotti (personal communication); before running this exporting script the mesh should be prepared as follows:

- the elements of the mesh has to be divided into several blocks; each block must contain elements belonging to a single geological formations of the model,

- each block has to be identified by a numerical ID and the physical properties of the material contained in it, that is to say v_p, v_s and ρ,
- the faces which form the surface of the topography have to be gathered together into a single block which must be identified by the name *face_topo*,
- the faces which form the absorbing boundaries of the model have to be gathered together firstly into a single block, secondly into a set of blocks corresponding to the various absorbing surfaces of the model (i.e. the one defined by the plane $x = Xmax$, the one define by the plane $x = Xmin$ and so on).

All the operations described above can be easily performed in CUBIT. After this preparation the script can be run and it gives in output the set of ASCII files described in Table 5.1. Once the mesh is exported it can be inserted into the code and partitioned using the SCOTCH software library.

5.2.2 The solver

The *solver* is the part of the code which actually performs the simulation; it needs in input three different files: the *Par_file* which was discussed in the previous paragraph, a file containing the list of the seismic stations located within the model and a file which contains the description of the earthquake source.
For each entry in the *STATION* file the user must specify the name of the station and other information, such as latitude and longitude (which should be expressed in geographical coordinates), elevation and burial depth if the station is placed in a borehole. The code is able to calculate and write seismograms at any number of stations without dramatic increase in terms of numerical cost.
I have reported in Table 5.2 the file *STATION* I have used to perform the simulations: it should be noticed that values of latitude and longitude are referred to the reference frame obtained by rotating the whole model using Euler angles as described in Chapter 3. Latitude, longitude and elevation values, taken from [9], are used by *solver* to localize the GLL point nearest to the station and then they are replaced by GLL point coordinates.
The *CMTSOLUTION* file is used to represent the earthquake source and its format is based on the one of the Harvard Centroid-Moment Tensor catalog. An example of *CMTSOLUTION* file is shown in Table 5.3. An important parameter to be defined in *CMTSOLUTION* file is the source half-duration (*half_duration*): a value of zero for this parameters corresponds to simulate a step source-time function, while non-zero values correspond to a Gaussian source-time function with half-width equal to *half_duration*. The authors of SPECFEM3D_BASIN suggest to use *half_duration* $= 0$ and to convolve the resulting seismograms with the desired source-time function using a software such as Seismic Analysis Code SAC2000 [22].
As I have said in Chapter 1 the origin of events belonging to the UP-S cluster probably lies in the friction generated by stick-slip motion of the glacier against the bedrock; because of the fact that the parametrization of this kind of source is a no-trivial task I have decided to make

Output files of CUBIT mesh exporting process				
mesh file	it contains the connectivity between all the elements of the mesh			
format:	Element ID	ID node1	...	ID node8
nodes coords file	it contains the coordinates of the nodes of all the elements of the mesh			
format	node ID	x coordinate	y coordinate	z coordinate
nummaterial velocity file	it is a table with the physical properties of the elements contained in the geological model, each material is associated to a number (flag)			
format	flag	$\rho\ (kg/m^3)$	$v_p\ (km/s)$	$v_s\ (km/s)$
free surface file	here are stored the ID of the hexahedra containing one face belonging to the free surface of the model and the four nodes which identify this face			
format	Element ID	ID node1	...	ID node4
absorbing surface file	here are stored the ID of the hexahedra containing at least one face belonging to one of the absorbing surfaces of the model, that is to say the lateral ones and the bottom layer, moreover it contains also the four nodes which identify each face			
format	Element ID	ID node1	...	ID node4
surface file absorbing	Xmin Xmax Ymin Ymax bottom	these five files contains the faces of hexahedra belonging to each individual absorbing boundary of the model. The format is equal to the *absorbing surface file* one		

Table 5.1: Description of the files obtained exporting a three dimensional mesh from CUBIT.

a first approximation of the problem representing the source by means of a classical moment tensor.
FPSPACK is a set of FORTRAN77 routines developed by Gasperini and Vannucci [20]; it performs the computation of earthquakes fault plane solutions in different parameters and reference systems.
I have identified the hypothetical fault plane with the slope of David Glacier's icefall and, by means of geometrical considerations, I have found the following three parameters which describe the fault plane:

- *strike* $= 135°$
- *dip* $= 35°$
- *rake* $= -90°$

Station name	Network	Latitude (deg)	Longitude (deg)	Elevation (m)	Burial (m)
TRIO	NZ	-0.10692	-0.4531	1145	0.00
HUGH	NZ	-0.00103	0.17644	215	0.00
STARR	IT	-0.48541	0.26414	70	0.00
OHG	IT	0.26971	-0.09495	630	0.00
JOYCE	NZ	-0.22077	-0.15150	1230	0.00

Table 5.2: *STATION* I have used in my simulations. Station latitude and longitude should be provided in geographical coordinates.

I have used these three values and the mean value for the seismic moment $\overline{M_0} = 3.6N \cdot m$ as input parameters of the FPSPACK and I have obtained the moment tensor of equation 5.1.

	yyyy/mm/dd	hh/mm/sec	lat	lon	depth	mb	Ms	name
PDE	2001 9 9	23 59 17.78	34.0745	-118.3792	6.4	4.2	4.2	HOLLYWOOD

event name: 9703873

time shift: 0.0000

half duration: 0.0000

latitude: 34.0745

longitude: -118.3792

depth: 5.4000

Mrr: -0.002000e+23

Mtt: -0.064000e+23

Mpp: 0.066000e+23

Mrt: -0.090000e+23

Mrp: -0.002000e+23

Mtp: 0.188000e+23

Table 5.3: Example of *CMTSOLUTION* file format.

$$\mathbf{M} = \begin{bmatrix} M_{rr} & M_{r\theta} & M_{r\phi} \\ M_{\theta r} & M_{\theta\theta} & M_{\theta\phi} \\ M_{\phi r} & M_{\phi\theta} & M_{\phi\phi} \end{bmatrix} =$$

$$= \begin{bmatrix} 1.785415919186654 & -1.785415919186653 & 0.9190100670206053 \\ -1.785415919186653 & 1.785415919186653 & -0.9190100670206049 \\ 0.9190100670206053 & -0.9190100670206049 & -3.570831838373307 \end{bmatrix} \cdot E + 18 \quad (5.1)$$

5.3 Results of 3D simulation

I have performed a first simulation using a mesh of the David Glacier created by means of the internal mesher of the code. Unfortunately at present the version of SPECFEM3D able to accept meshes created with CUBIT is not available, thus I was forced to use the internal *mesher* of SPECFEM3D_BASIN to perform the simulation.
I have used the same linear dimension of $500\ m$ and $900\ m$, used for the 3D mesh created with CUBIT, to create respectively the elements within the ice layer and the ones beyond the bedrock interface. Differences between this mesh and the one I have created with CUBIT are slight and depend on the fact that the SPECFEM3D_BASIN *mesher* contains a routine which is capable to perform a *doubling refinement* as described in Figure 4.4(a), thus this mesh contains fewer spectral elements than the one create with CUBIT. This mesh incorporates the definition of the topography and, as the one obtained with CUBIT, does not honor the discontinuity ice-bedrock, I have then used a modification of the solver, that verifies the position of GLL points, determining if they are above or below the bedrock interface and consequently assigning them the ice or rock physical properties.
I have performed this simulation using the cluster SGI Altix ICE 8200EX (JADE) at *Centre Informatique National de l'Enseignement Suprieur* CINES. The rank of this cluster in the TOP500 project [42] is 26, according to the list of December 2009.
In order to compare the synthetics seismograms obtained from this simulations and the data recorded at the seismic stations I have processed both sets of data. I have removed the instrumental effect from the recorded signals, then I have differentiated them and I have applied a four-pole Butterworth filter with corners frequencies at 0.4 Hz and 3 Hz, in such a way I have obtained the data velocity components. I did not need to remove the instrumental effects from the synthetics seismograms thus I have just differentiated them and I have applied the same Butterworth filter.
Comparison between these two data sets is shown in figures from 5.1 to 5.15.Because of differences in amplitudes and phases between synthetic seismograms and recorded data I have not superimposed the two sets. In order to be able to compare the signals I have amplified the synthetics ones using an amplification factor h_{mul} which I have calculated for each of them. I have also removed the *Y axis* because it was meaningless. Thus the comparison between these two data sets is more qualitative than quantitative, nevertheless some interesting remarks can be done.
First of all consider the factors I have used to amplify the synthetic seismograms: their values range between 20 and 160. The differences in amplitude between the two sets of signals can be explained as follows: I have used in the simulation the mean value of scalar moment determined for the events of DW cluster but the event I have tried to reproduce belongs to the UP-S cluster. Events of this cluster present usually higher magnitude values than the ones of DW cluster. I have made this choice because reliable scalar moments have not been determined for the UP-S cluster events, while events belonging to DW cluster had been widely analyzed ([34]) and their characteristics are well known, thus I have preferred to use their scalar moment mean value as a first approximation.
Another interesting feature can be noticed from the spectral analysis of the signal: most of the

synthetics spectra show larger amplitudes for frequencies $\nu > 1Hz$ than the one of recorded data. The presence of these high frequencies can be caused by the fact that I have not directly inserted the bedrock surface into the mesh but I have represented it by means of interpolation of physical properties of ice and rocks on the GLL points; as pointed out in paragraph 4.1 this could produce the presence of imprecisions in the synthetics seismograms. There is another factor which has to be taken into account in order to explain this feature: I have considered the ice layer as an homogeneous medium with constant physical properties while in reality they can easily vary. For example changes in the chemical composition of ice can lead to the creation of areas with different density values, or variation in environmental parameters such as the temperature can produce the partial melting of some zones of the glacier. Even if the code SPECFEM3D_BASIN is capable to deal with lateral variations in compressional-wave speed, shear-wave speed and density, these kind of properties are very difficult to be modeled and require a deep geological knowledge of the study area.
Waveforms of the signals are influenced mainly by the definition of the geologic model, in particular, as I have said in paragraph 1.4, the ice layer could act as a guide for low frequencies waves and its shape could control the form of the final part of the seismograms. Thus the quality of the data sets used to define the 3D model of David Glacier is of fundamental importance. Uncertainties on these data sets, especially the ones on the BEDMAP model, can be considered as the main cause for the differences between the recorded waveforms and the synthetics ones.
For this reason I have also decided to use the same value for the scalar moment in the following simulations: since the main differences between synthetics seismograms and real data deal with the a priori knowledge of the geologic model I thought that it should be useless spending time in investigating the source representation.
It has to be noticed that during the period of data acquisition the GPS set at the seismic station JOYCE experienced a malfunctioning which can justify the difference in time between the first arrivals of the recorded data and the ones of the synthetic seismograms.

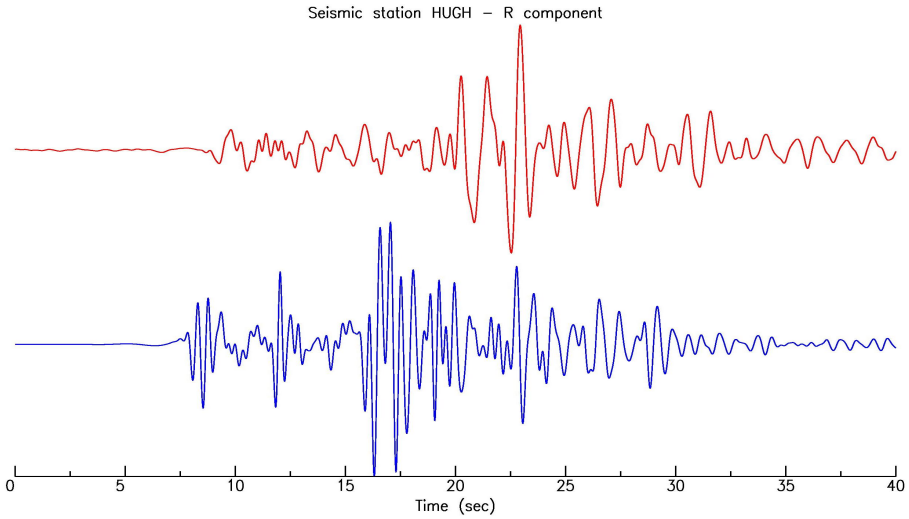

(a)

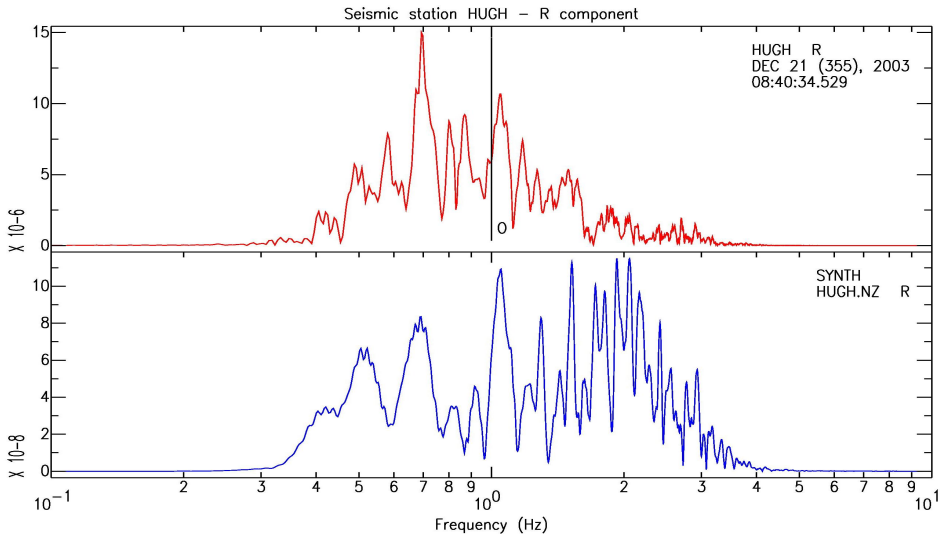

(b)

Figure 5.1: Comparison between data recorded at seismic station HUGH (red line) and the results of 3D (blue line) simulation. Radial components are shown in Figure 5.1(a), synthetics amplified by a factor $h_{mul}^{BLUE} = 80$. In Figure 5.1(b) are shown the result of signals spectral analysis.

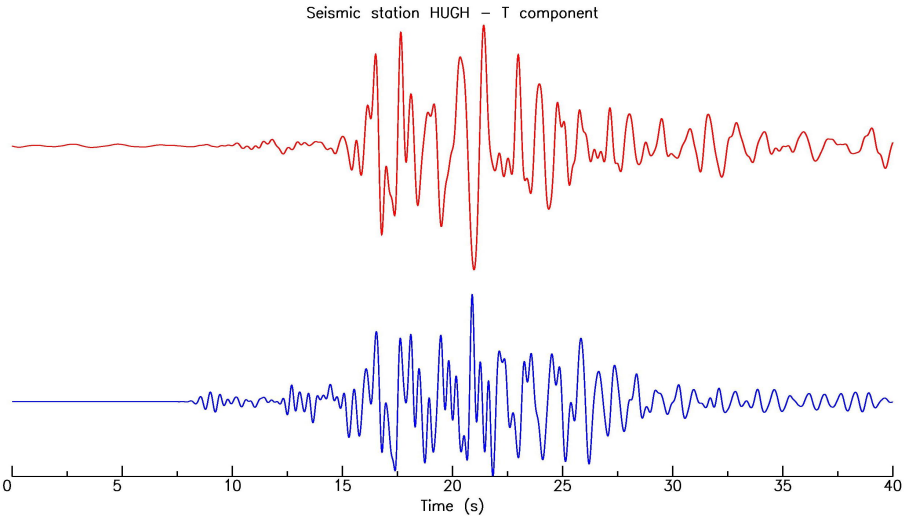

(a)

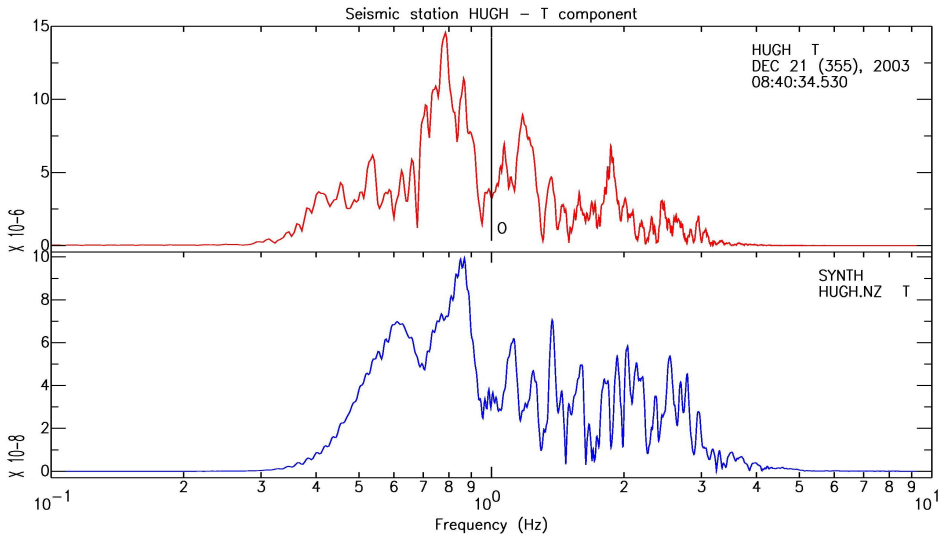

(b)

Figure 5.2: Comparison between data recorded at seismic station HUGH (red line) and the results of 3D (blue line) simulation. Transverse components are shown in Figure 5.2(a), synthetics amplified by a factor $h_{mul}^{BLUE} = 80$. In Figure 5.2(b) are shown the result of signals spectral analysis.

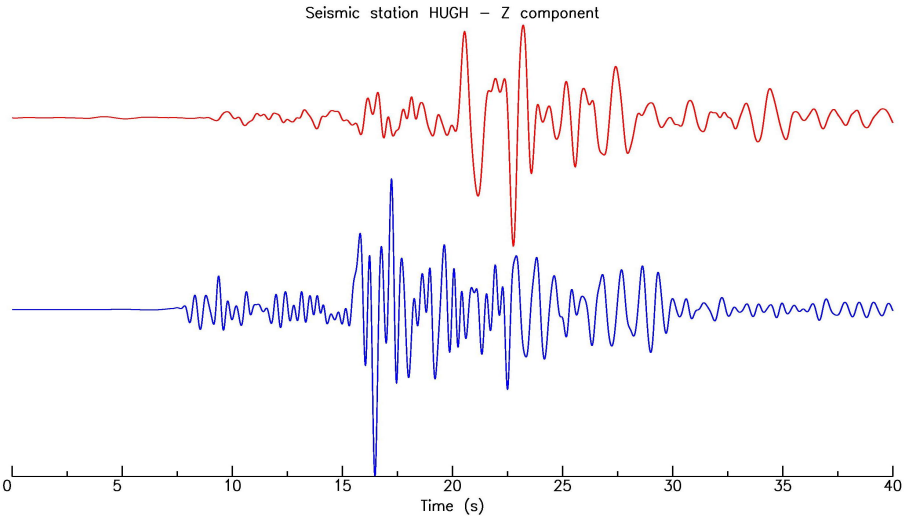

(a)

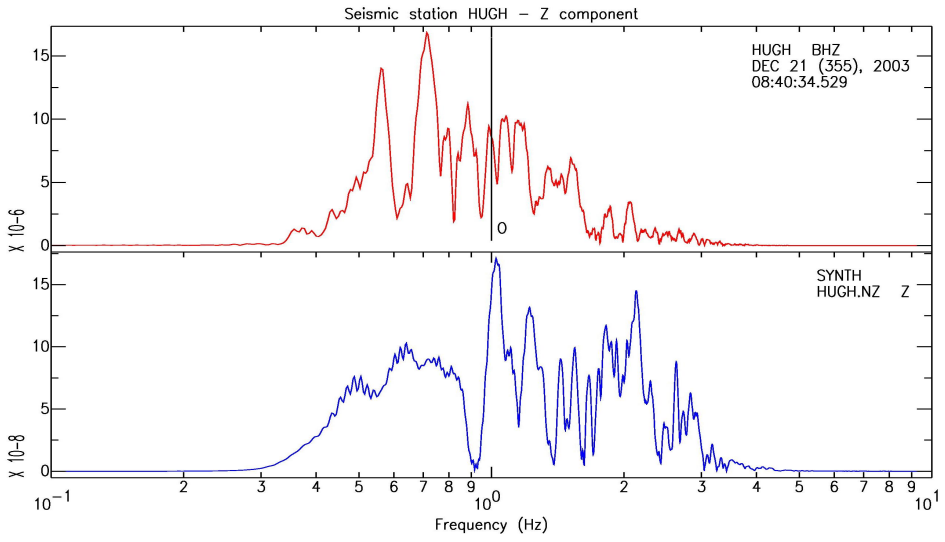

(b)

Figure 5.3: Comparison between data recorded at seismic station HUGH (red line) and the results of 3D (blue line) simulation. Vertical components are shown in Figure 5.3(a), synthetics amplified by a factor $h_{mul}^{BLUE} = 80$. In Figure 5.3(b) are shown the result of signals spectral analysis.

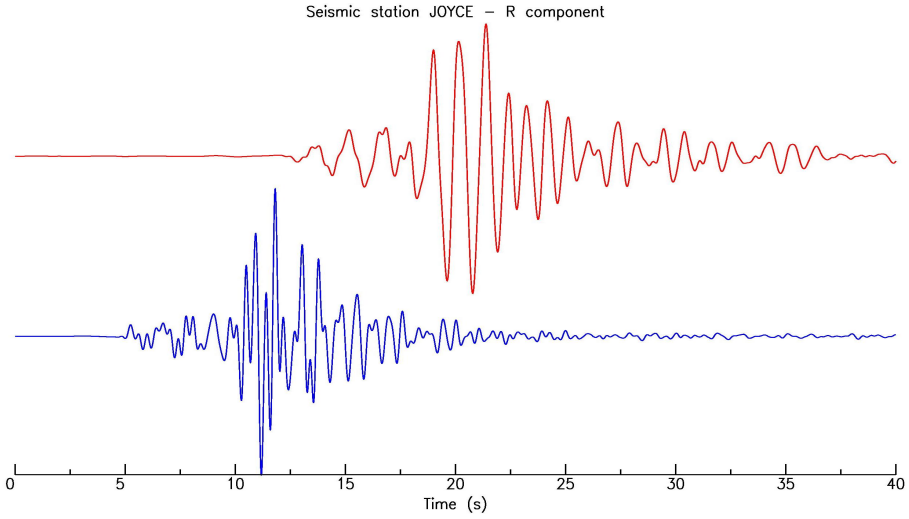

(a)

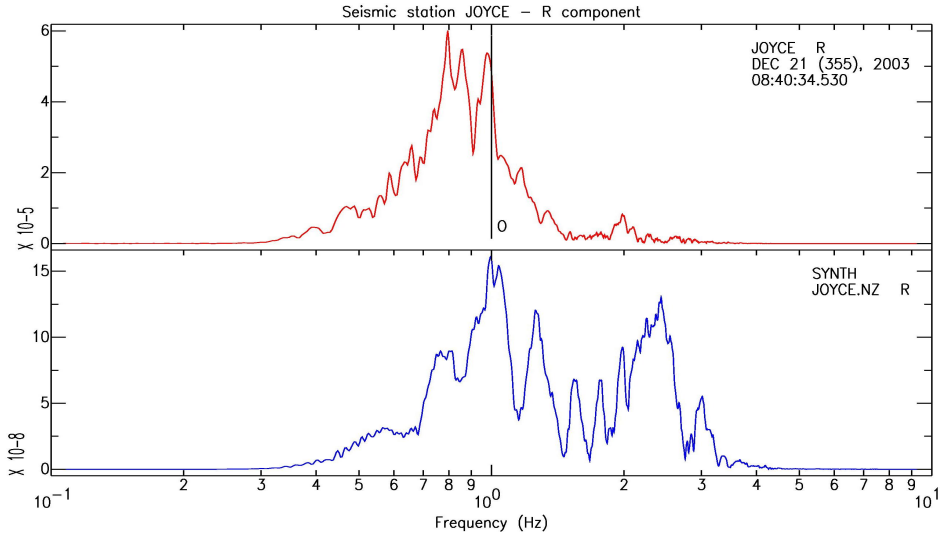

(b)

Figure 5.4: Comparison between data recorded at seismic station JOYCE (red line) and the results of 3D (blue line) simulation. Radial components are shown in Figure 5.4(a), synthetics amplified by a factor $h_{mul}^{BLUE} = 160$. In Figure 5.4(b) are shown the result of signals spectral analysis. Note that the time reference for the data stream is not reliable because of failure of the GPS clock.

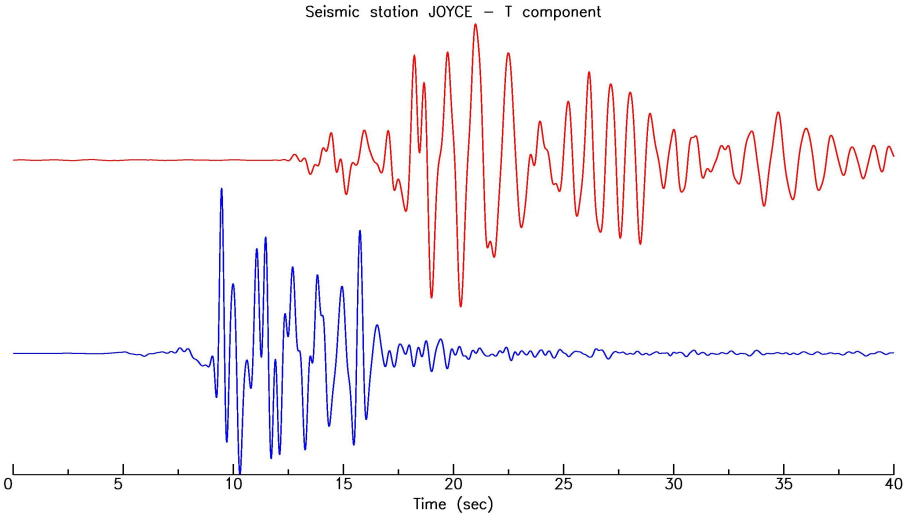

(a)

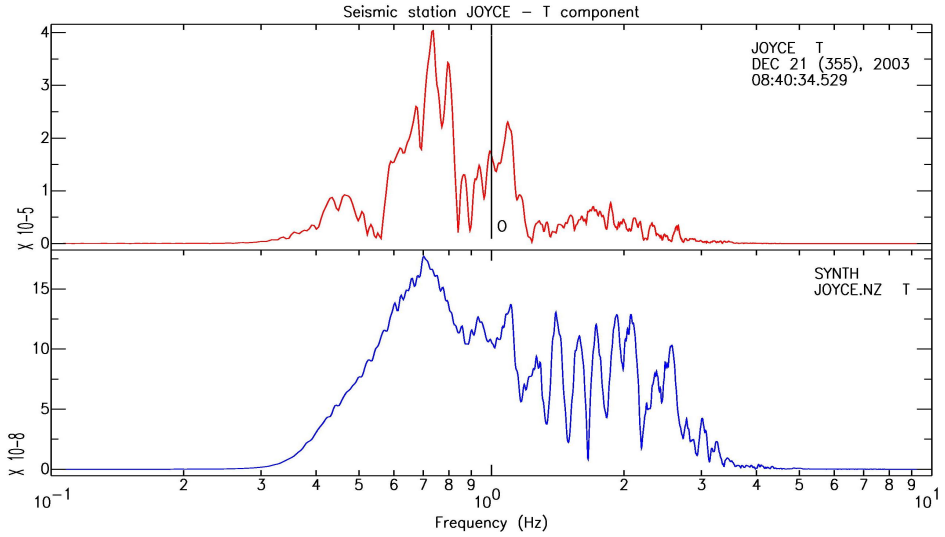

(b)

Figure 5.5: Comparison between data recorded at seismic station JOYCE (red line) and the results of 3D (blue line) simulation. Transverse components are shown in Figure 5.5(a), synthetics amplified by a factor $h_{mul}^{BLUE} = 80$. In Figure 5.5(b) are shown the result of signals spectral analysis. Note that the time reference for the data stream is not reliable because of failure of the GPS clock.

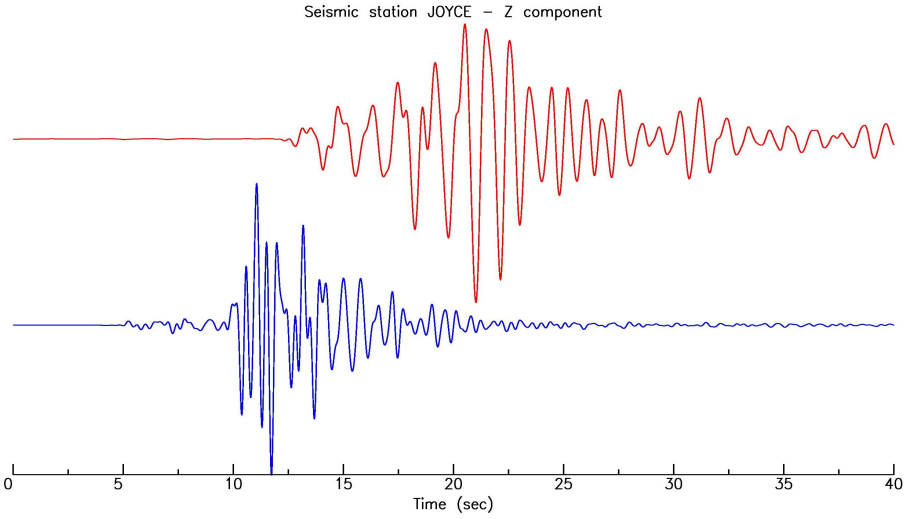

(a)

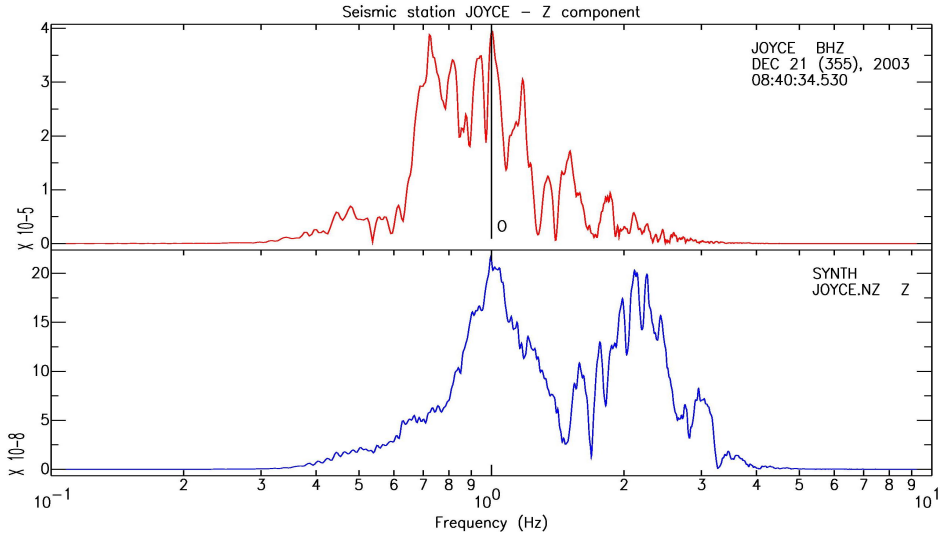

(b)

Figure 5.6: Comparison between data recorded at seismic station JOYCE (red line) and the results of 3D (blue line) simulation. Vertical components are shown in Figure 5.6(a), synthetics amplified by a factor $h_{mul}^{BLUE} = 80$. In Figure 5.6(b) are shown the result of signals spectral analysis. Note that the time reference for the data stream is not reliable because of failure of the GPS clock.

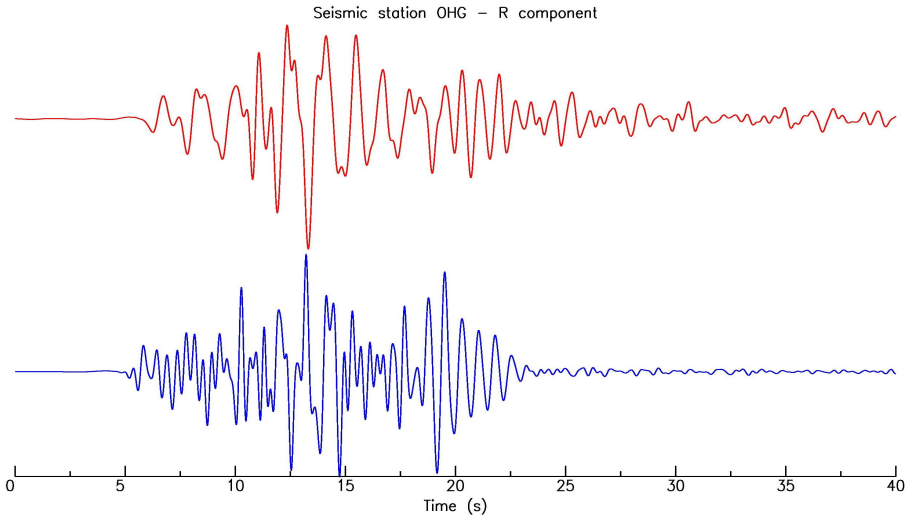

(a)

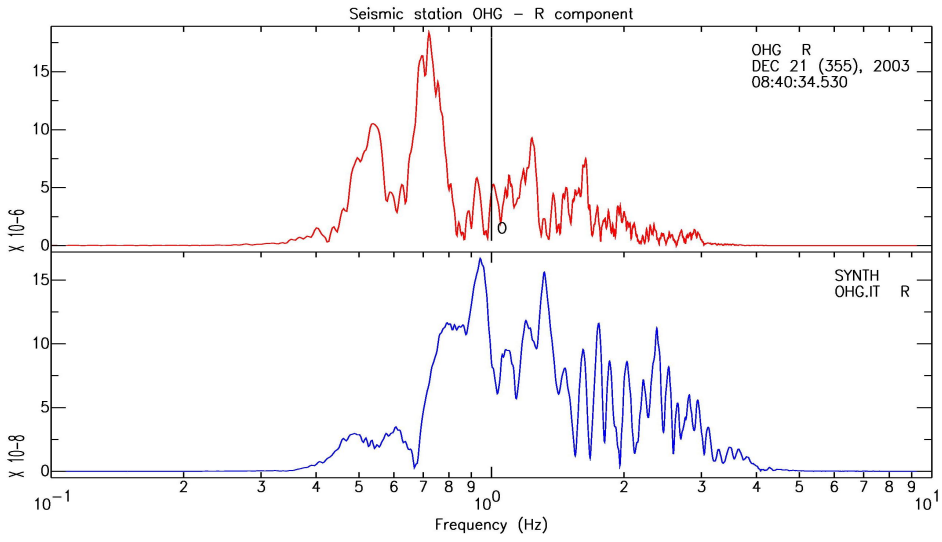

(b)

Figure 5.7: Comparison between data recorded at seismic station OHG (red line) and the results of 3D (blue line) simulation. Radial components are shown in Figure 5.7(a), synthetics amplified by a factor $h_{mul}^{BLUE} = 60$. In Figure 5.7(b) are shown the result of signals spectral analysis.

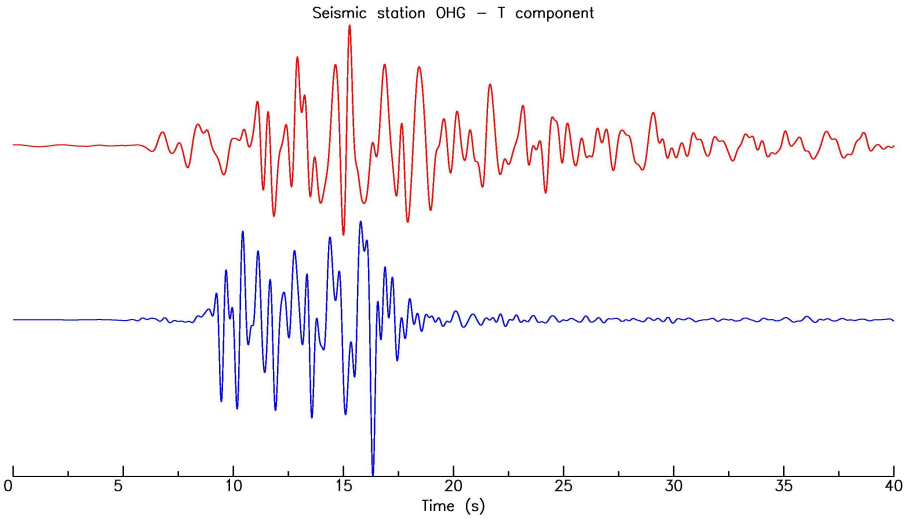

(a)

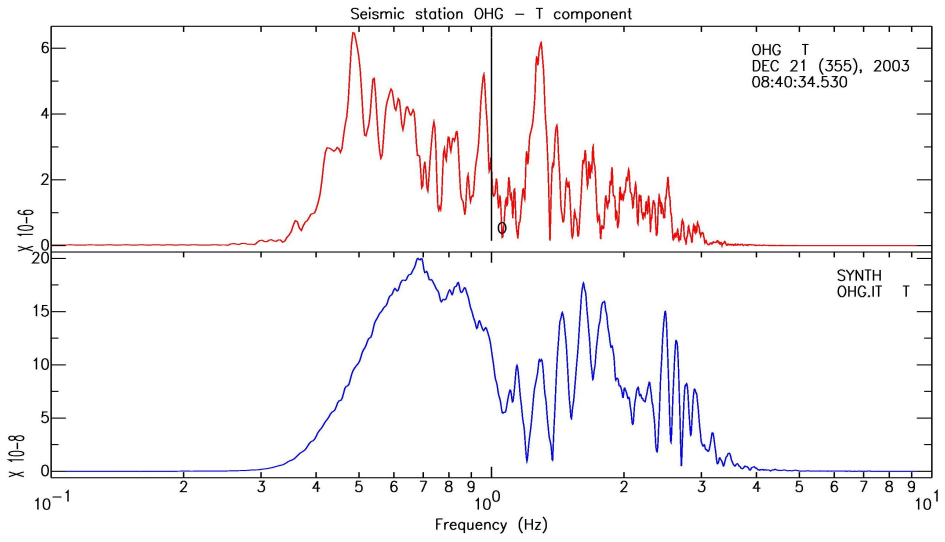

(b)

Figure 5.8: Comparison between data recorded at seismic station OHG (red line) and the results of 3D (blue line) simulation. Transverse components are shown in Figure 5.8(a), synthetics amplified by a factor $h_{mul}^{BLUE} = 20$. In Figure 5.8(b) are shown the result of signals spectral analysis.

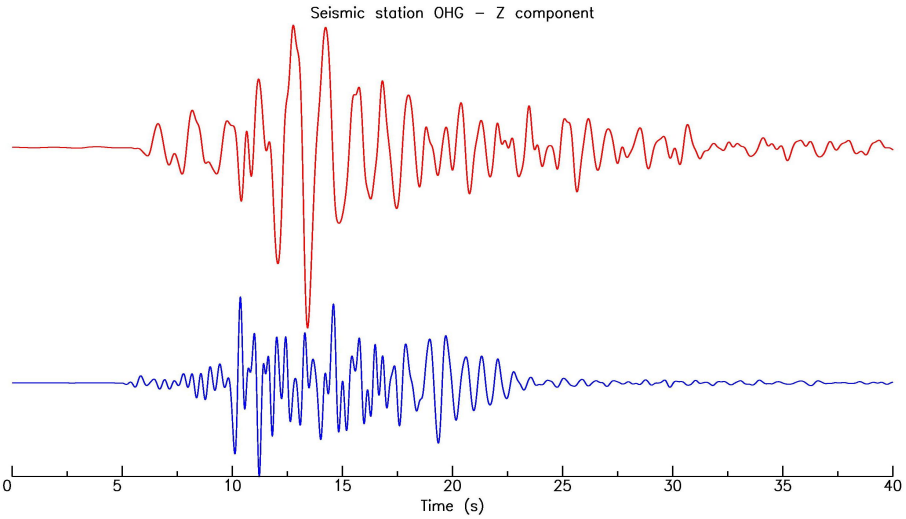

(a)

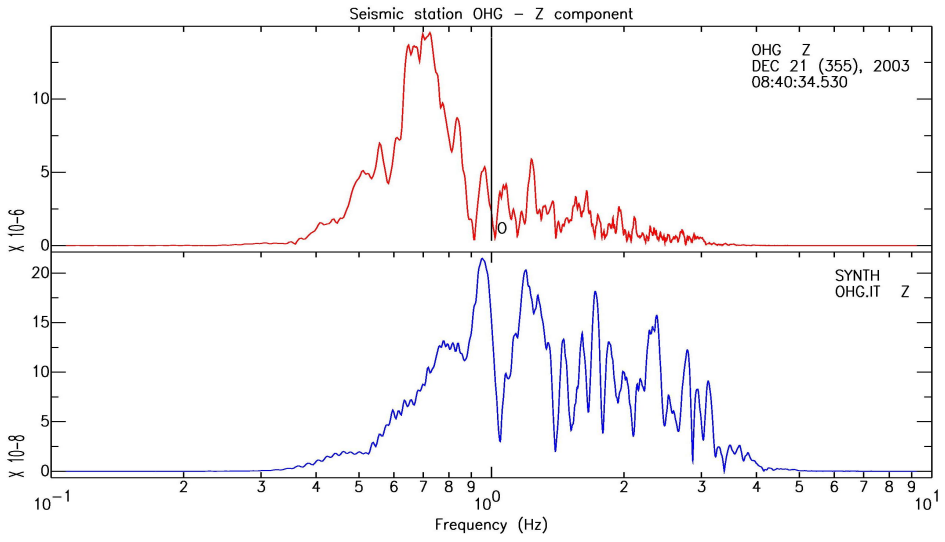

(b)

Figure 5.9: Comparison between data recorded at seismic station OHG (red line) and the results of 3D (blue line) simulation. Vertical components are shown in Figure 5.9(a), synthetics amplified by a factor $h_{mul}^{BLUE} = 20$. In Figure 5.9(b) are shown the result of signals spectral analysis.

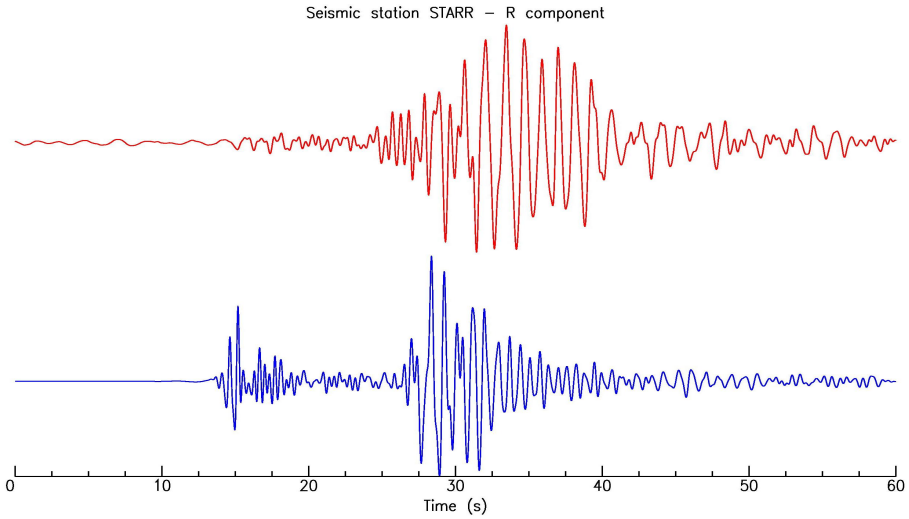

(a)

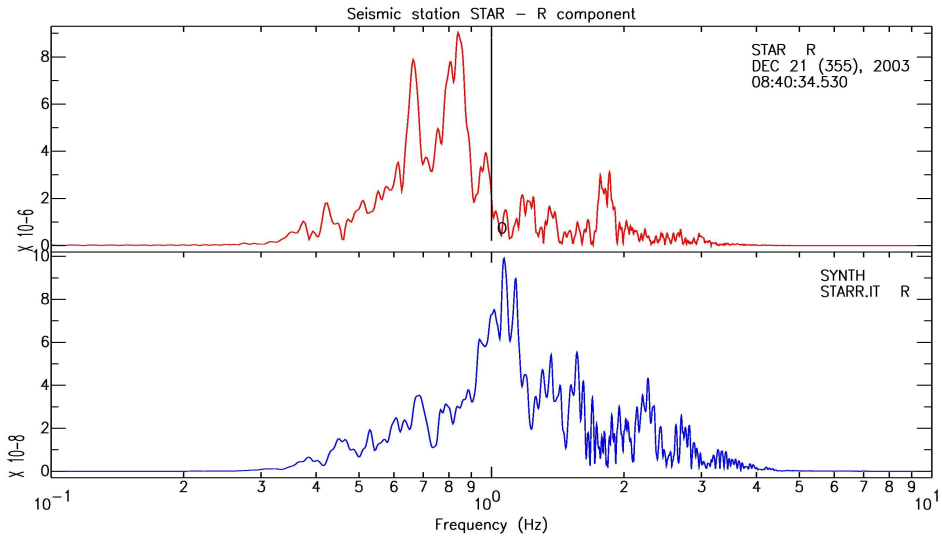

(b)

Figure 5.10: Comparison between data recorded at seismic station STARR (red line) and the results of 3D (blue line) simulation. Radial components are shown in Figure 5.10(a), synthetics amplified by a factor $h_{mul}^{BLUE} = 50$. In Figure 5.10(b) are shown the result of signals spectral analysis.

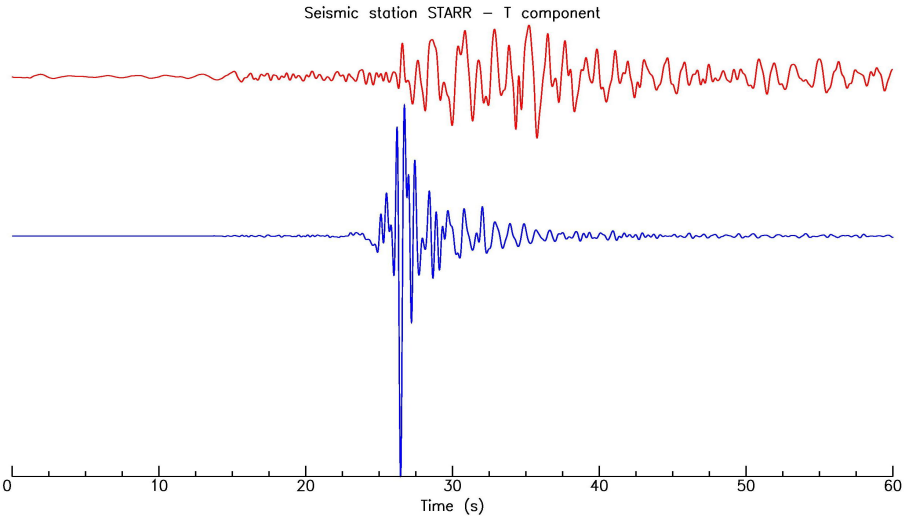

(a)

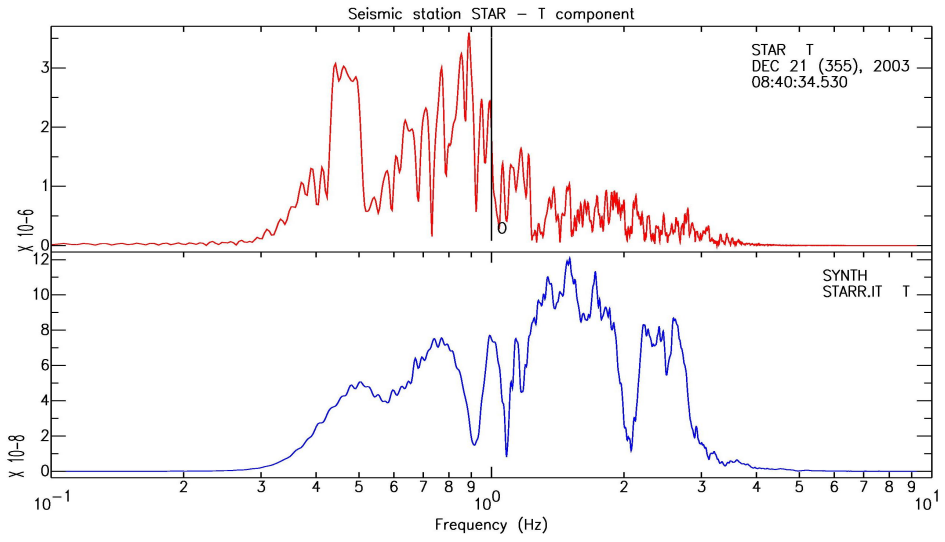

(b)

Figure 5.11: Comparison between data recorded at seismic station STARR (red line) and the results of 3D (blue line) simulation. Transverse components are shown in Figure 5.11(a), synthetics amplified by a factor $h_{mul}^{BLUE} = 20$. In Figure 5.11(b) are shown the result of signals spectral analysis.

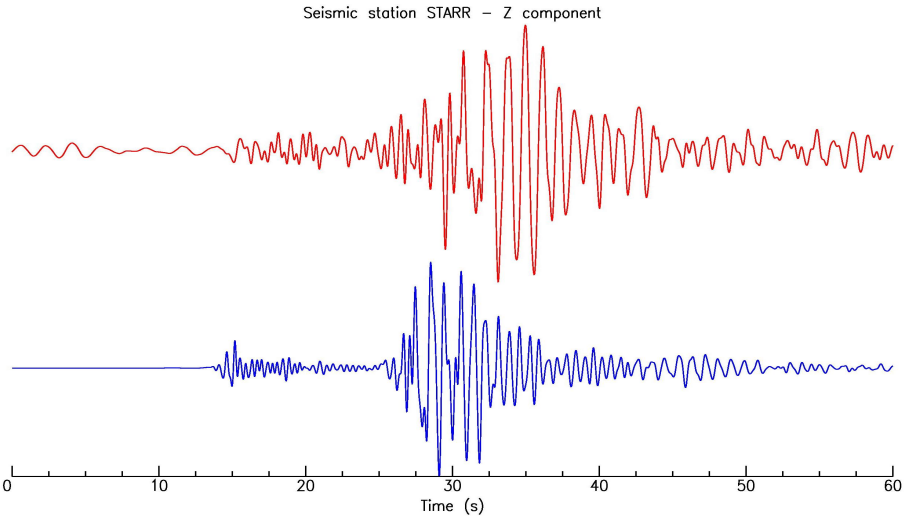

(a)

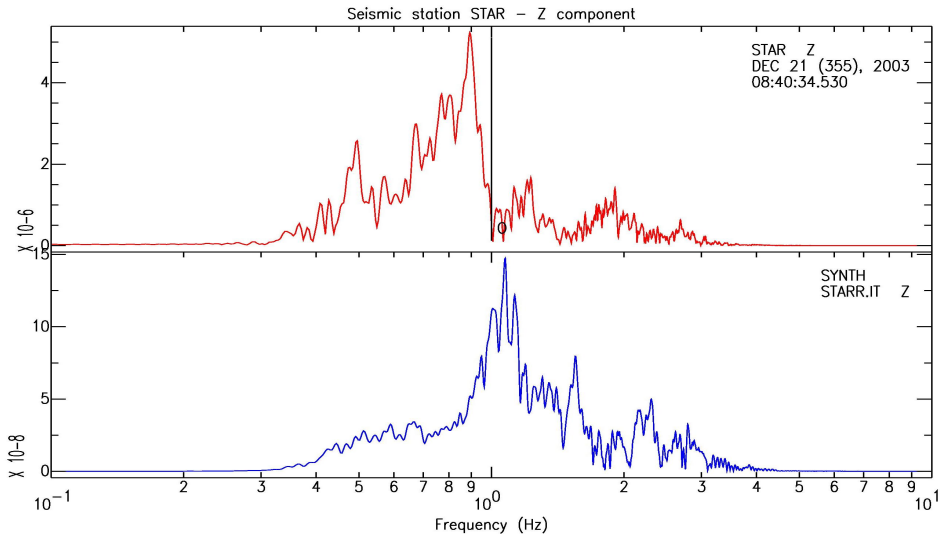

(b)

Figure 5.12: Comparison between data recorded at seismic station STARR (red line) and the results of 3D (blue line) simulation. Vertical components are shown in Figure 5.12(a), synthetics amplified by a factor $h_{mul}^{BLUE} = 20$. In Figure 5.12(b) are shown the result of signals spectral analysis.

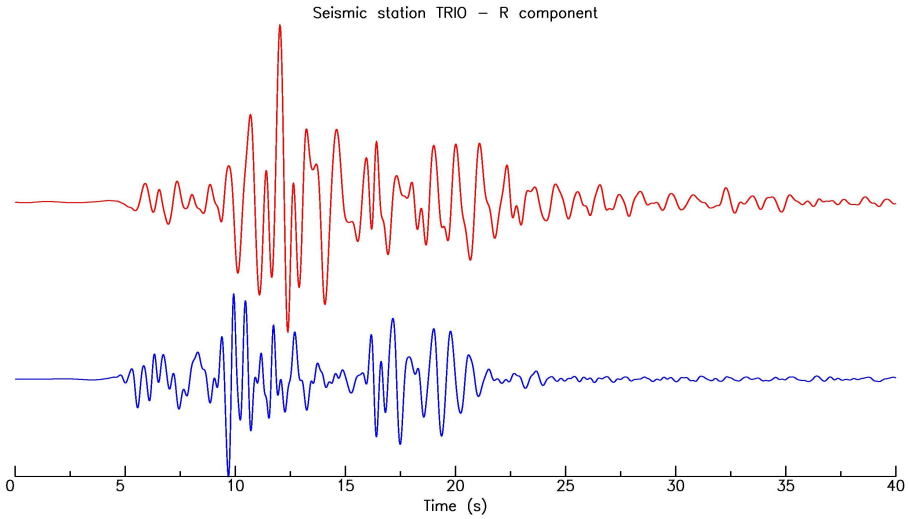

(a)

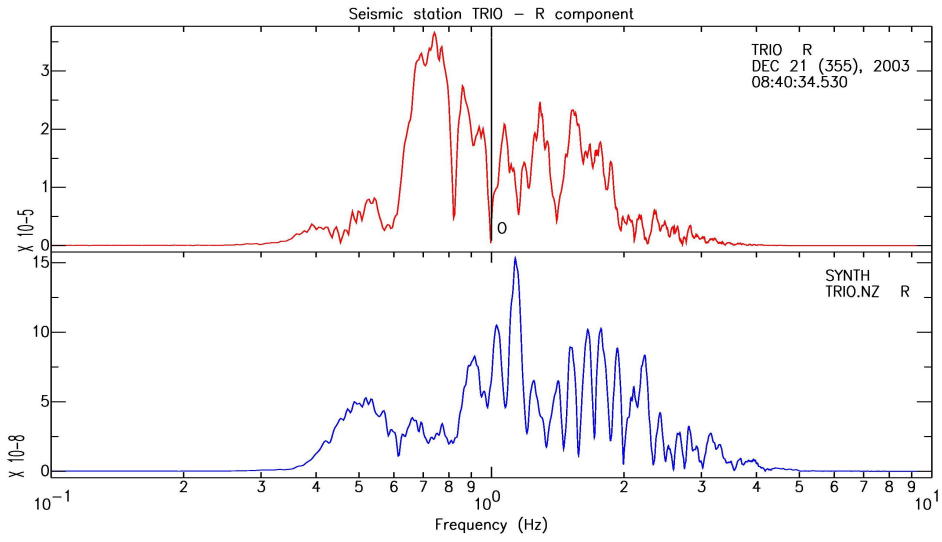

(b)

Figure 5.13: Comparison between data recorded at seismic station TRIO (red line) and the results of 3D (blue line) simulation. Radial components are shown in Figure 5.13(a), synthetics amplified by a factor $h_{mul}^{BLUE} = 150$. In Figure 5.13(b) are shown the result of signals spectral analysis.

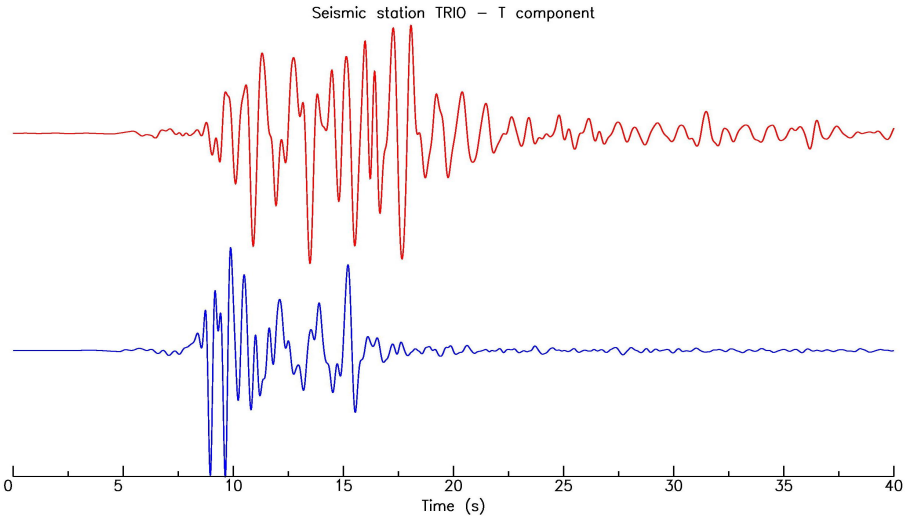

(a)

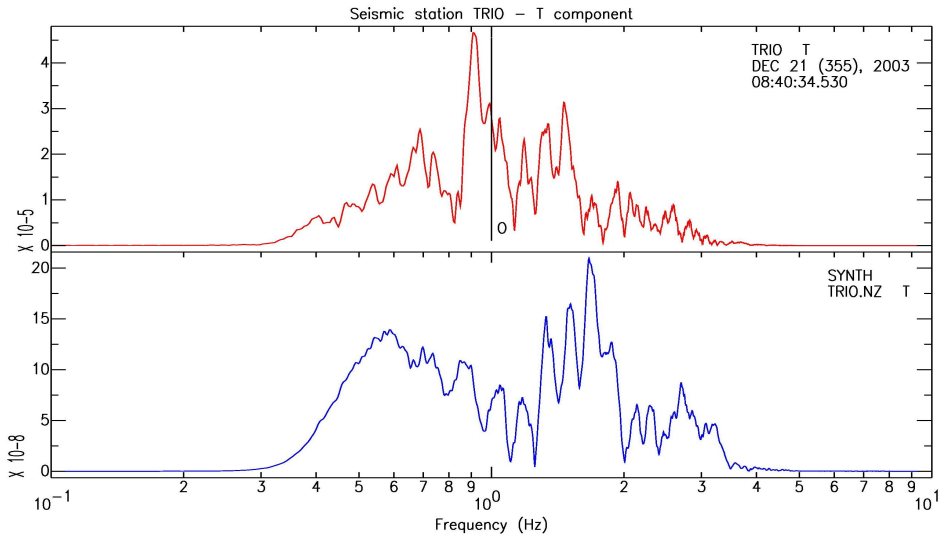

(b)

Figure 5.14: Comparison between data recorded at seismic station TRIO (red line) and the results of 3D (blue line) simulation. Transverse components are shown in Figure 5.14(a), synthetics amplified by a factor $h_{mul}^{BLUE} = 100$. In Figure 5.14(b) are shown the result of signals spectral analysis.

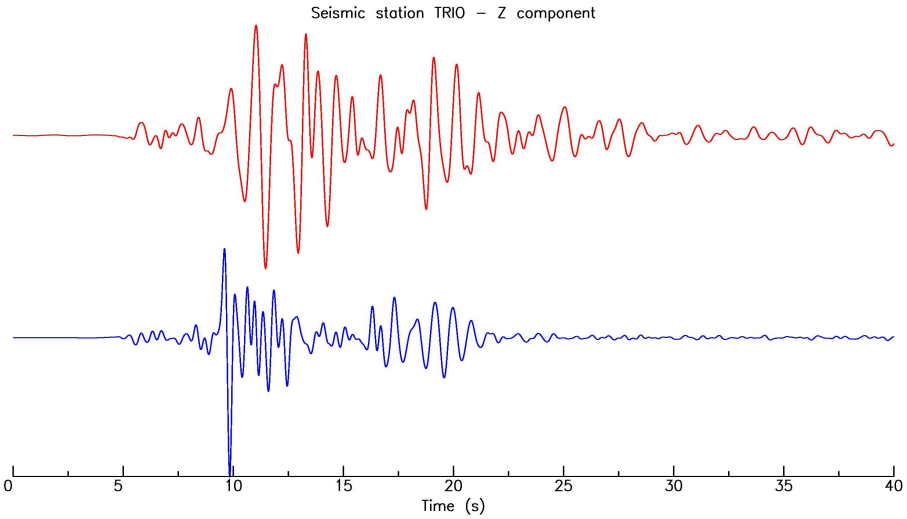

(a)

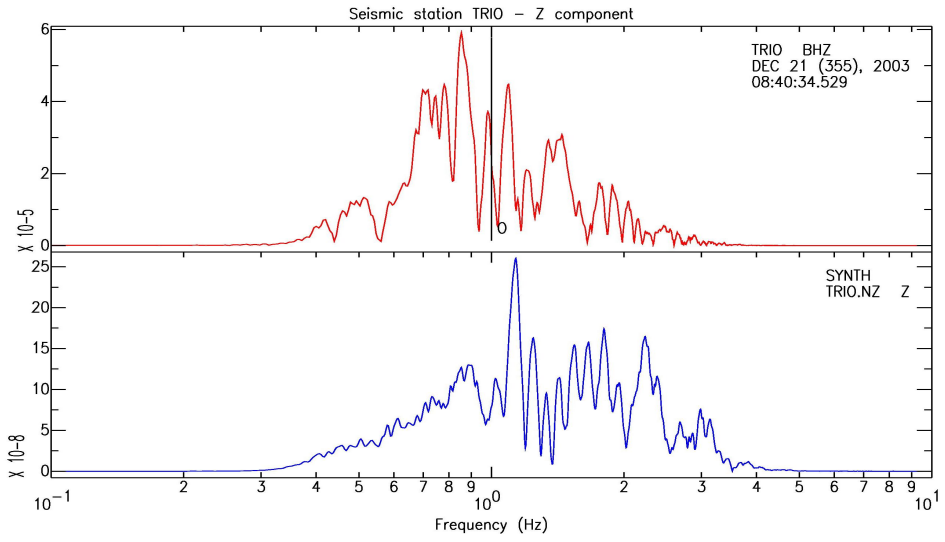

(b)

Figure 5.15: Comparison between data recorded at seismic station TRIO (red line) and the results of 3D (blue line) simulation. Vertical components are shown in Figure 5.15(a), synthetics amplified by a factor $h_{mul}^{BLUE} = 100$. In Figure 5.15(b) are shown the result of signals spectral analysis.

5.4 SPECFEM2D

SPECFEM2D package can perform seismic wave propagation simulations in acoustic, elastic, anelastic and poroelastic media. As for SPECFEM3D_BASIN this version of the code is composed by the *mesher* and the *solver*: their structure is very similar to the one of the three dimensional version thus I will not describe it again.
The latest release of the software (version 6.0) can easily use meshes generated with CUBIT; the exporting process is nearly the same as for the 3D case and it can be accomplished using the Python interface of CUBIT: the mesh should be divided in several blocks each of them characterized by the physical properties of the material to which it belongs, the edges representing the free surface of the model should be gathered together into a single block as well as the edges which form the absorbing sides of the model (the subdivision of the absorbing boundaries is no more needed). To perform the exporting of the meshes I have used a special script (E, Casarotti personal communication), the final result is a set of file (the same obtained for the 3D case) which can be directly inserted in the partitioner of SPECFEM2D.
The *Par_file* and *CMTSOLUTION* files contain the following parameters which are of fundamental importance in the simulations:

- *deltat*: represents the duration of the time step used by the *solver* to compute the wave field during the simulation. It could be determined during the quality check of the mesh as described in Chapter 4;
- *nt*: determines the total number of time steps to be used for the simulation;
- *assign_external_model*: if this option is set **true** the *solver* would replace the information contained in the *nummaterial velocity file* with others given directly by the user; a direct consequence is the possibility to store on the GLL points of one spectral element physical properties belonging to different materials, thus information about discontinuities which can not be honored by the mesh can be taken into account;
- *turn_attenuation_on*: determines if in a simulation the attenuation for solid medium should be used or not. It should be noticed that at present if an external model is used the attenuation can not be used;
- *time_function_type*: determines which kind of function will be used to represent the source of the earthquake; among the possibility there are the Gaussian function and the Heaviside function;
- *moment tensor components*: in the 2D case the moment tensor is represented by a 2×2 matrix and its components are expressed in $N \cdot m$.

I want to emphasize the importance of the possibility of performing an interpolation of physical properties among the GLL points of a single spectral element: as I have pointed out in Chapter 4 geological models often contain features which are really hard to be meshed and can be represented only using this kind of interpolation, which on the other side produce a staircase representation of the model introducing undesirable reflections into the synthetic

seismograms. It appears clear that SPECFEM2D represents an important possibility to quantify the error made using this kind of approximation.
Let consider the two dimensional meshes in which the BEDMAP model is not honored: the upper block of elements of these meshes contain GLL points belonging to both ice and rock; I have created a Fortran90 routine which controls the position of these GLL points determining if they are above or below the BEDMAP interface and consequently assigning them the ice or rock physical properties. I have then introduced this routine in the *solver* and I have performed a set of simulations, the results of which will be shown in the next paragraphs.

5.5 Results of 2D simulations

I have performed all the two dimensional simulations using the cluster IBM P575 Power 6 (sp6) at *Consorzio Interuniversitario* CINECA, this cluster is the most powerful available at present in Italy and its rank among all the supercomputer of the world is 61 (according to the *TOP500 list* of December 2009).
All the two dimensional meshes contained almost the same number of spectral elements, that is to say 250000; according to the result of quality check the time step to be used was $10^{-4}s$, I have set the total length for the synthetic seismograms to $70s$ and I have divided each simulations in 500 processes, thereby each simulations required approximately 2 hr.
For all the 2D simulations I have used the *Heaviside function* to represent the source and I have then filtered the resulting synthetic seismograms using a four-pole Butterworth filter with corners frequencies at 0.4 Hz and 3 Hz.

5.5.1 Simulations with complete meshes

I have performed a first set of simulations using the meshes which honor the interface between ice and rock. In these simulations I have considered the David Glacier profiles containing the following seismic stations: HUGH, JOYCE, OHG, STARR, and TRIO (Figure 3.2).
Figures from 5.16 to 5.25 show these simulations results compared with the three dimensional ones and with the data recorded at the seismic stations. Amplitudes of the three signals present strong differences, in particular the 2D synthetics exceed the others also of three orders of magnitude. Thus a direct comparison made by superimposition of the three signals was not possible: to avoid this problem I have amplified both 3D synthetics and recorded data using a multiplying factor h_{mul}. I have calculated this factor for each station according to the differences in amplitudes of the signals. Finally I have removed from the pictures frames the scale of *Y axis* because it was unimportant, as for the results of the 3D simulation.
An explanation of differences in amplitude between the 2D and 3D synthetics can be found in the definition of the source: in three dimension the source is represented as a point while in two dimension there is geometrical invariance along the third direction, that is to say in the 2D case the source is represented by a line thus in this case the geometrical spreading of

seismic waves is lower than in the 3D case.
Furthermore the 2D Green function is based on a Hankel transform while the 3D Green function is a distribution of Dirac so it is normal to obtain as results of 2D simulations different waveforms with respect to the ones obtained in 3D simulations. These arguments are treated more extensively in [1],[30].
The major improvements in representation of the signal obtained with these 2D simulations can be found considering the spectra of the signals: in particular the contribution given by the high frequency area ($\nu > 1\ Hz$) is lower than in the 3D case. Furthermore in some cases, for example the central part of the OHG radial component (Figure 5.20(a) time interval from $10\ s$ to $20\ s$), the shape of the signal is better reproduced.
According to the fact that for these 2D simulations I have used a mesh honoring the bedrock surface, while in the 3D simulation it was introduce by interpolation, the fact that the changes described above do not involve all the stations indicates that some areas of the geological models are better described than others.
Nevertheless other features does not disappear; consider for example the synthetics obtained for the station STARR: P-waves arrivals are impulsive both in the 3D simulation and in the 2D ones, thus this feature can not be related to the representation bedrock surface into the mesh. A possible explanation for this can be found in the fact that I have created a geological model considering the ice layer as a continuous medium and I have not considered the presence of crevasses; these empty spaces can affect the propagation of seismic waves and in particular can reduce the contribution to the signal of compressional waves. It as to be noticed that crevasses are really hard to be meshed because of their small dimensions.

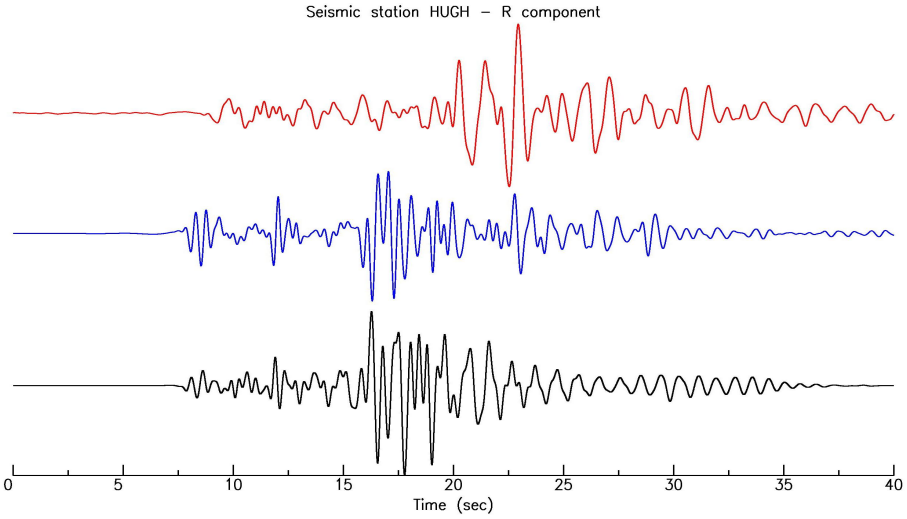

(a)

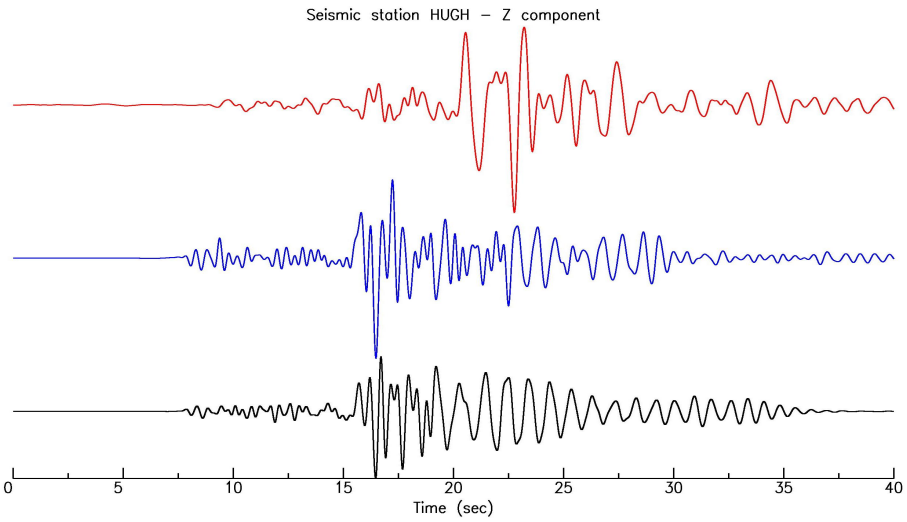

(b)

Figure 5.16: Comparison between data recorded at seismic station HUGH (red line) and the results of both 3D (blue line) and 2D (black line) simulations. Radial components are shown in Figure 5.16(a), vertical components are shown in Figure 5.16(b). I have used the following amplification factors: $h_{mul}^{RED} = 70$, $h_{mul}^{BLUE} = 4 \cdot 10^4$ for both radial and vertical components.

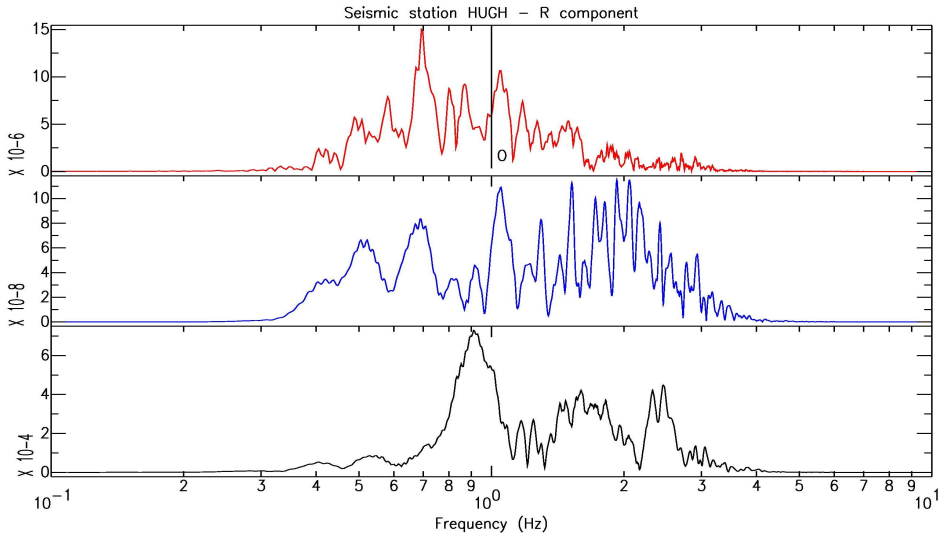

(a)

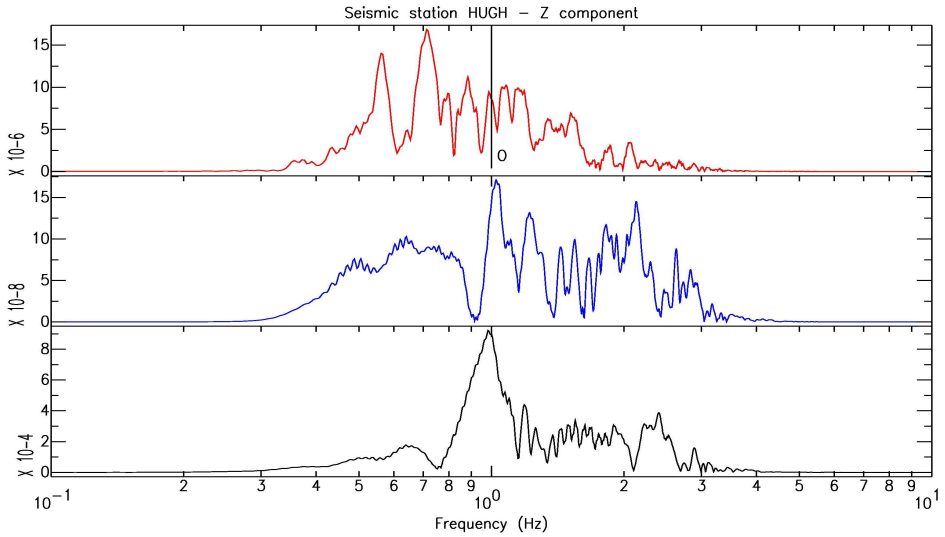

(b)

Figure 5.17: Result of spectral analysis for the signals in Figure 5.16.

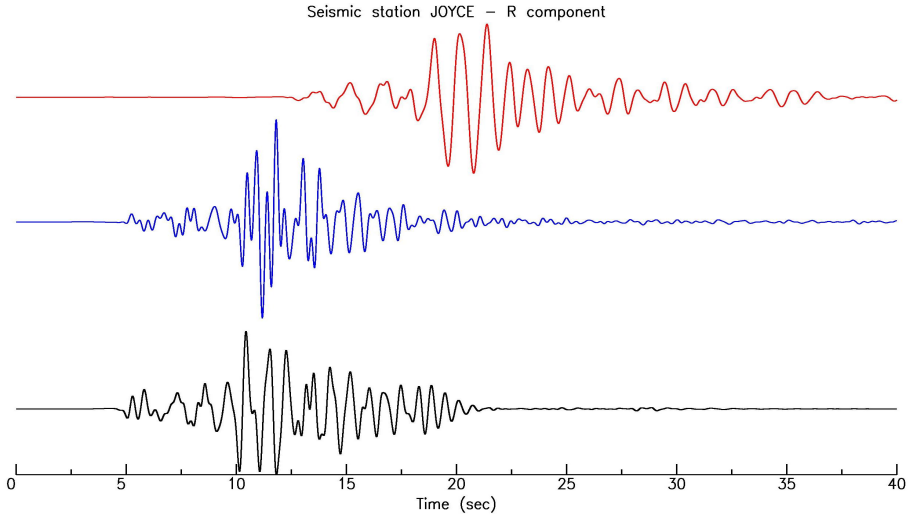

(a)

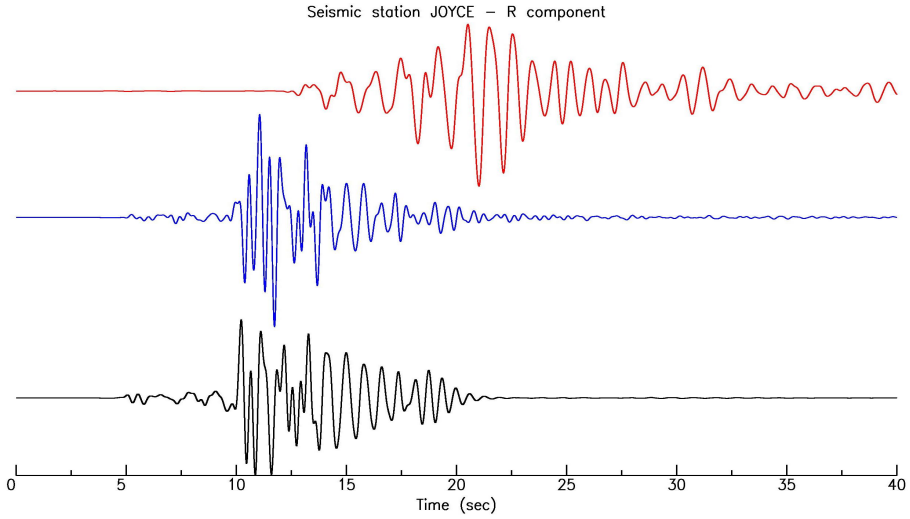

(b)

Figure 5.18: Comparison between data recorded at seismic station JOYCE (red line) and the results of both 3D (blue line) and 2D (black line) simulations. Radial components are shown in Figure 5.18(a), vertical components are shown in Figure 5.18(b). I have used the following amplification factors: $h_{mul}^{RED} = 20$, $h_{mul}^{BLUE} = 4 \cdot 10^4$ for radial components and $h_{mul}^{RED} = 40$, $h_{mul}^{BLUE} = 4 \cdot 10^4$ for vertical components. Note that the time reference for the data stream is not reliable because of failure of the GPS clock.

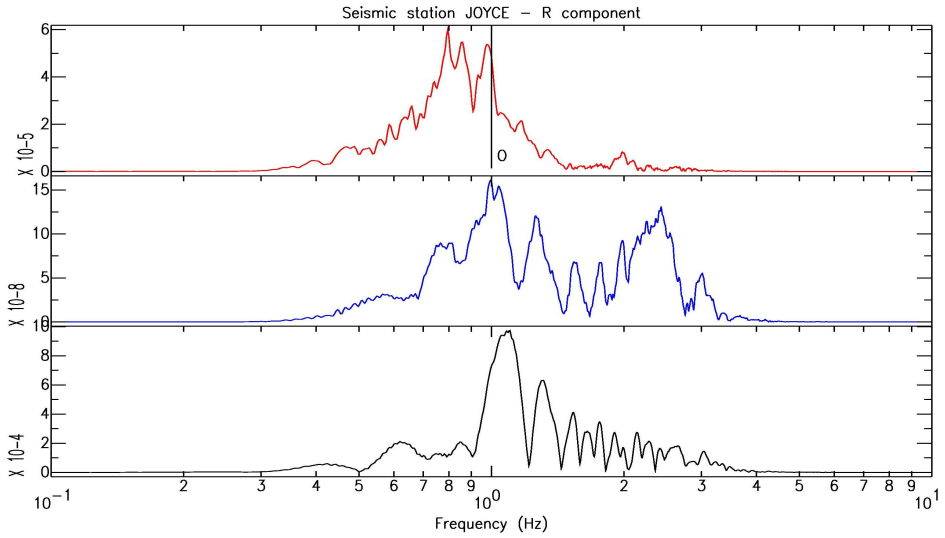

(a)

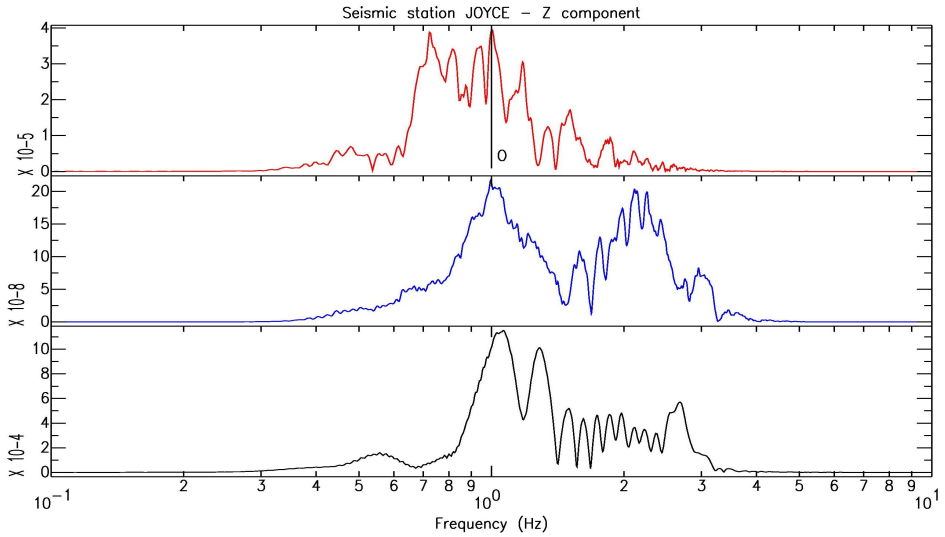

(b)

Figure 5.19: Result of spectral analysis for the signals in Figure 5.18

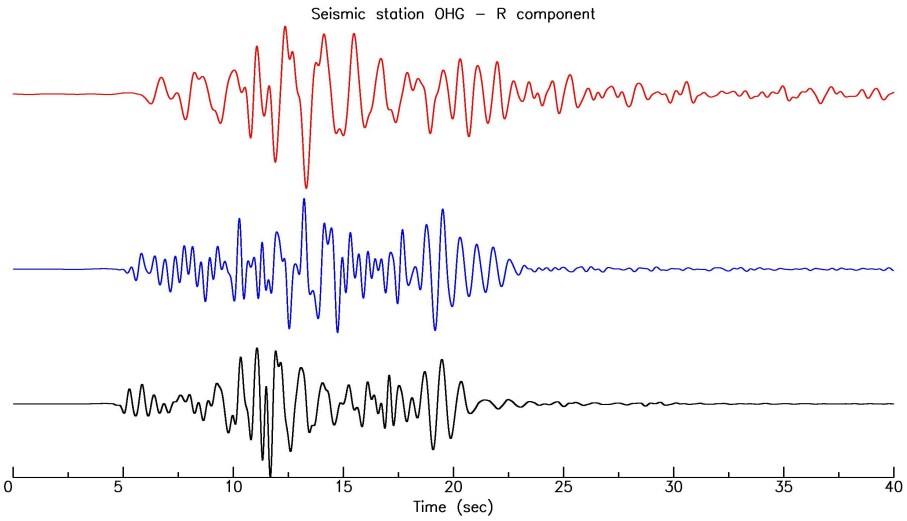

(a)

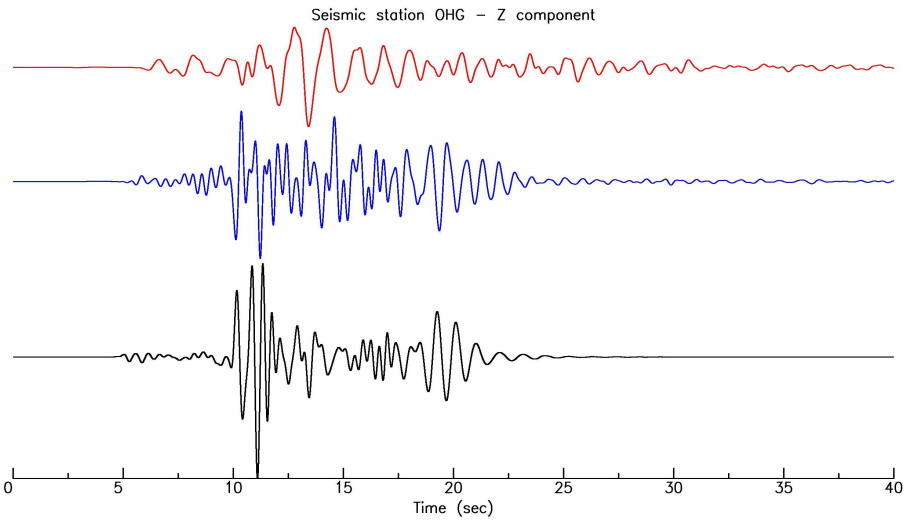

(b)

Figure 5.20: Comparison between data recorded at seismic station OHG (red line) and the results of both 3D (blue line) and 2D (black line) simulations. Radial components are shown in Figure 5.20(a), vertical components are shown in Figure 5.20(b). I have used the following amplification factors: $h_{mul}^{RED} = 80$, $h_{mul}^{BLUE} = 4 \cdot 10^4$ for both radial and vertical components.

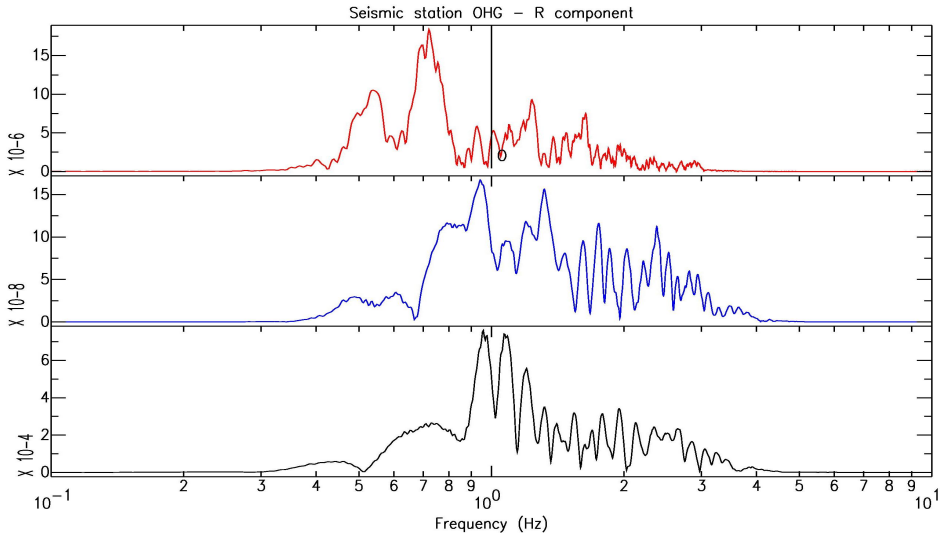

(a)

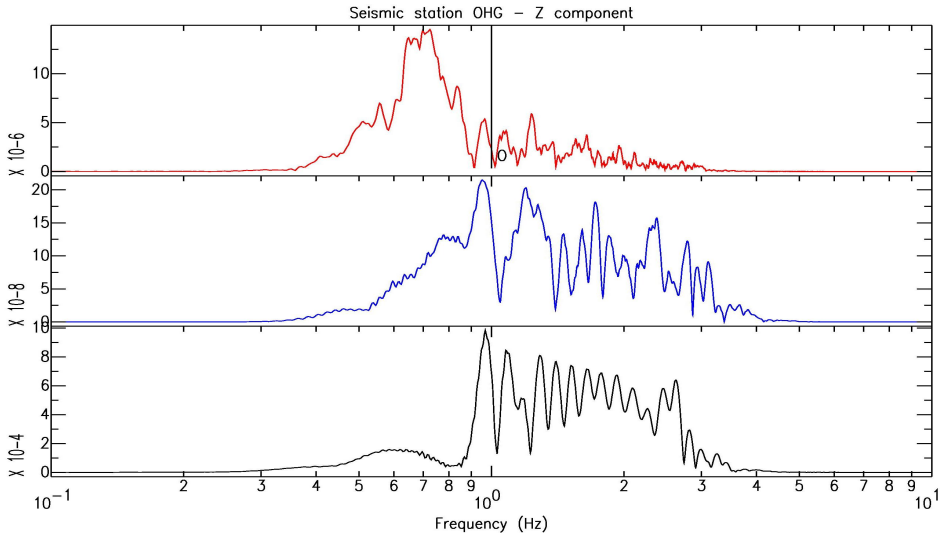

(b)

Figure 5.21: Result of spectral analysis for the signals in Figure 5.20

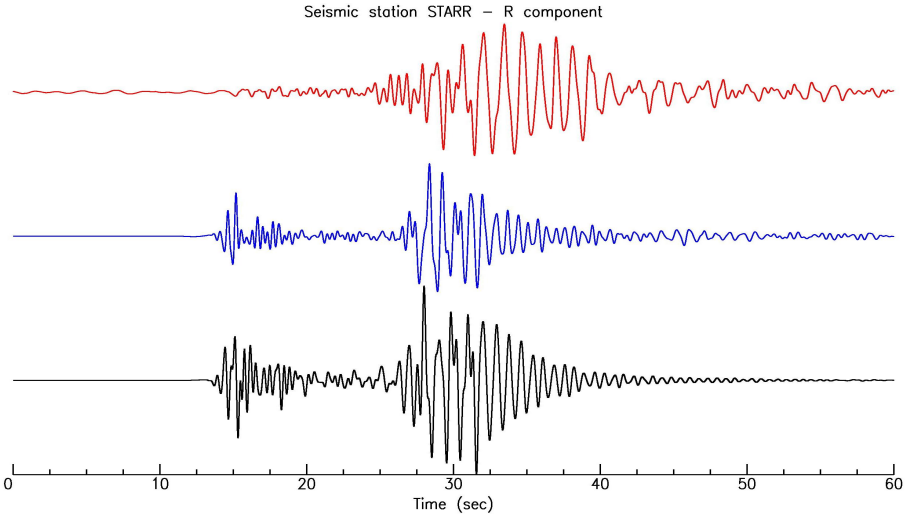

(a)

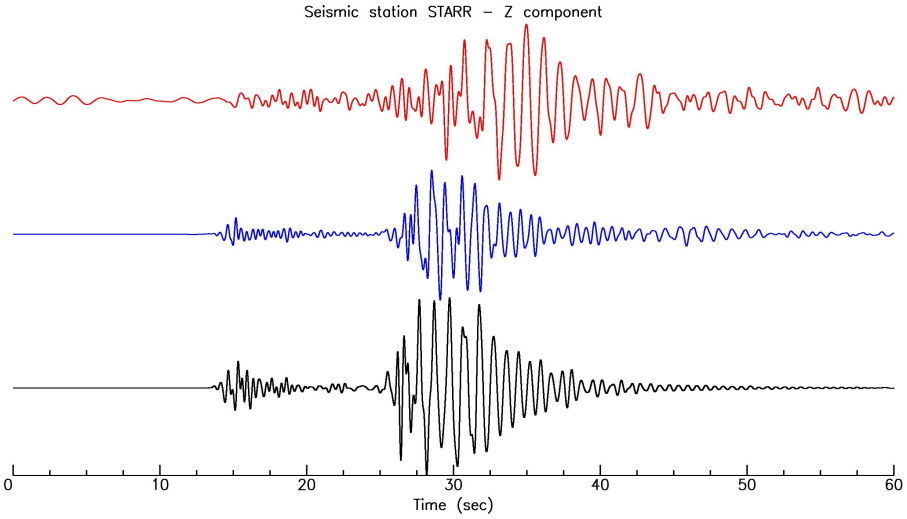

(b)

Figure 5.22: Comparison between data recorded at seismic station STARR (red line) and the results of both 3D (blue line) and 2D (black line) simulations. Radial components are shown in Figure 5.22(a), vertical components are shown in Figure 5.22(b). I have used the following amplification factors: $h_{mul}^{RED} = 80$, $h_{mul}^{BLUE} = 4 \cdot 10^4$ for radial components and $h_{mul}^{RED} = 200$, $h_{mul}^{BLUE} = 4 \cdot 10^4$ for vertical components.

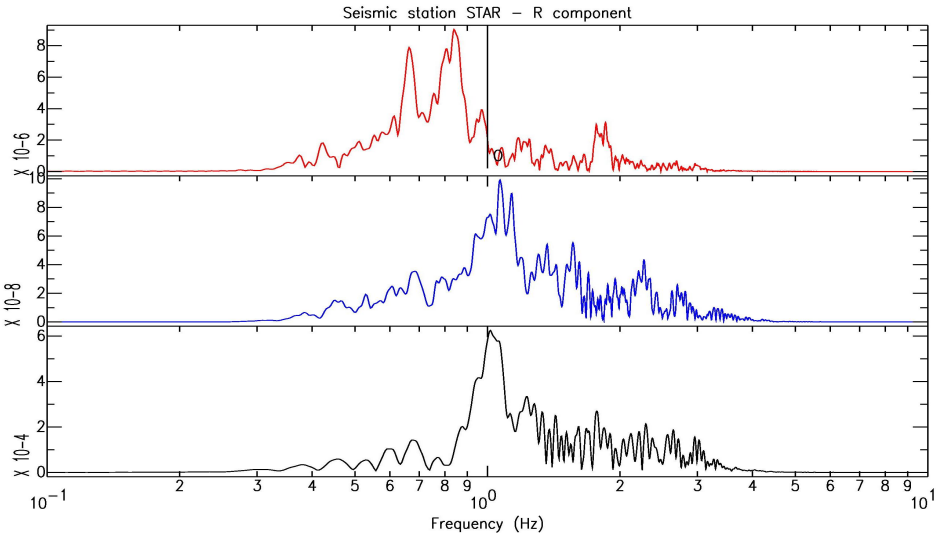

(a)

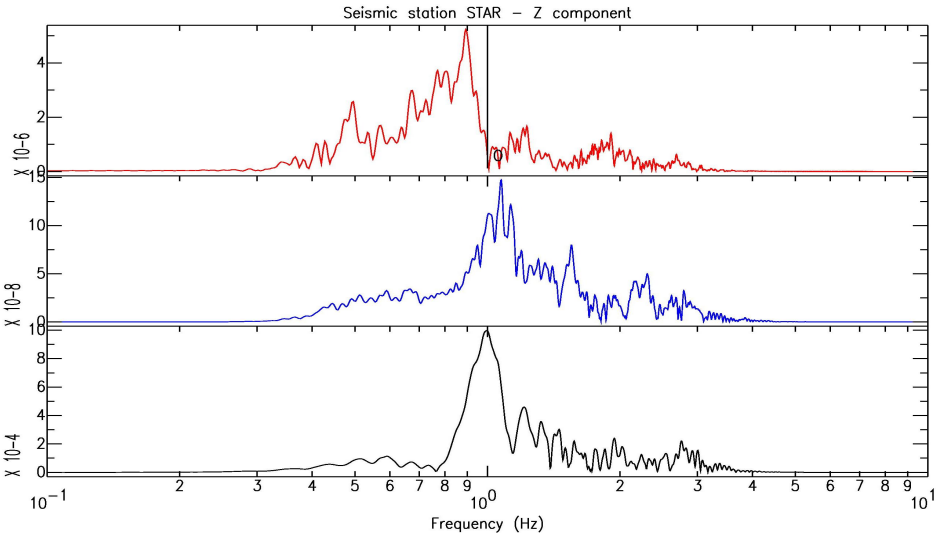

(b)

Figure 5.23: Result of spectral analysis for the signals in Figure 5.22

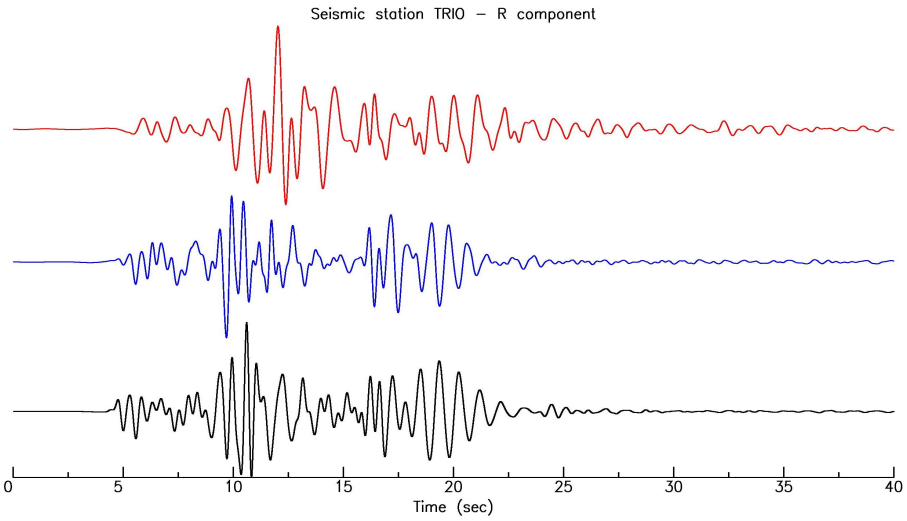

(a)

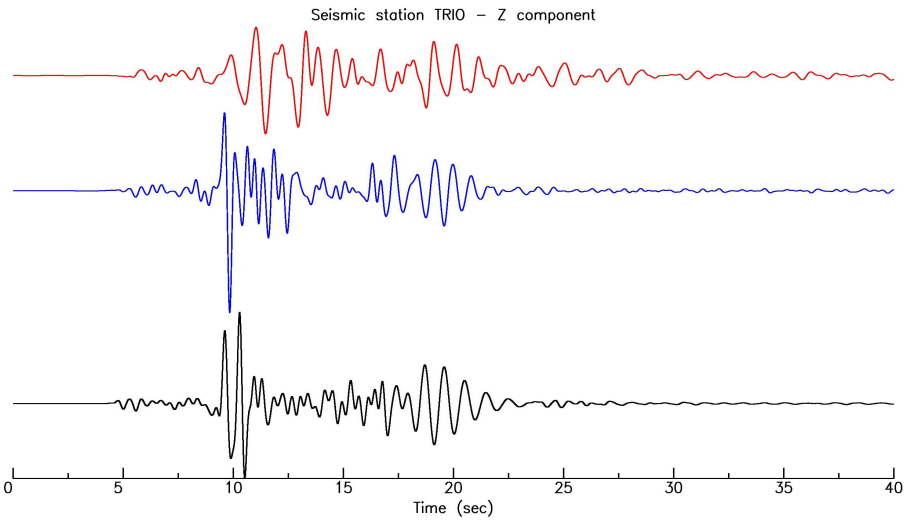

(b)

Figure 5.24: Comparison between data recorded at seismic station TRIO (red line) and the results of both 3D (blue line) and 2D (black line) simulations. Radial components are shown in Figure 5.24(a), vertical components are shown in Figure 5.24(b). I have used the following amplification factors: $h_{mul}^{RED} = 20$, $h_{mul}^{BLUE} = 4 \cdot 10^4$ for both radial and vertical components.

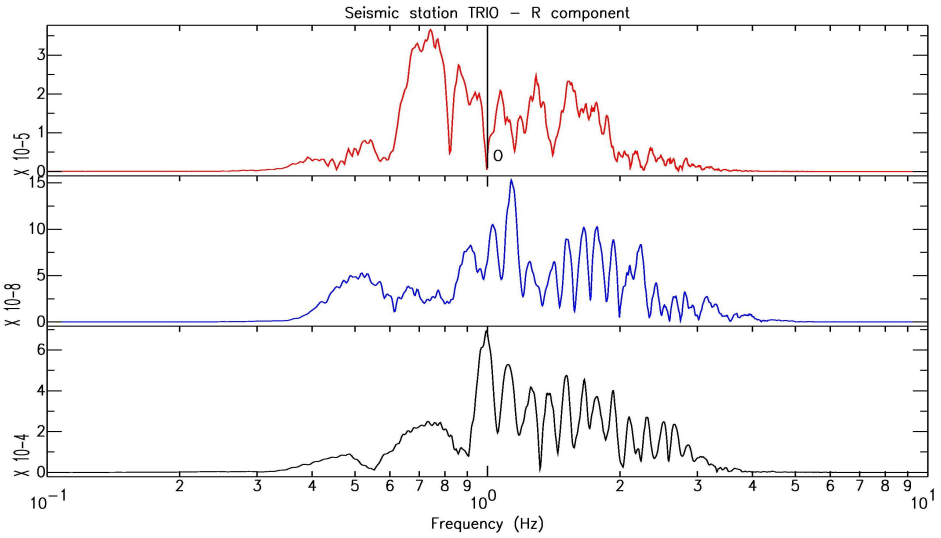

(a)

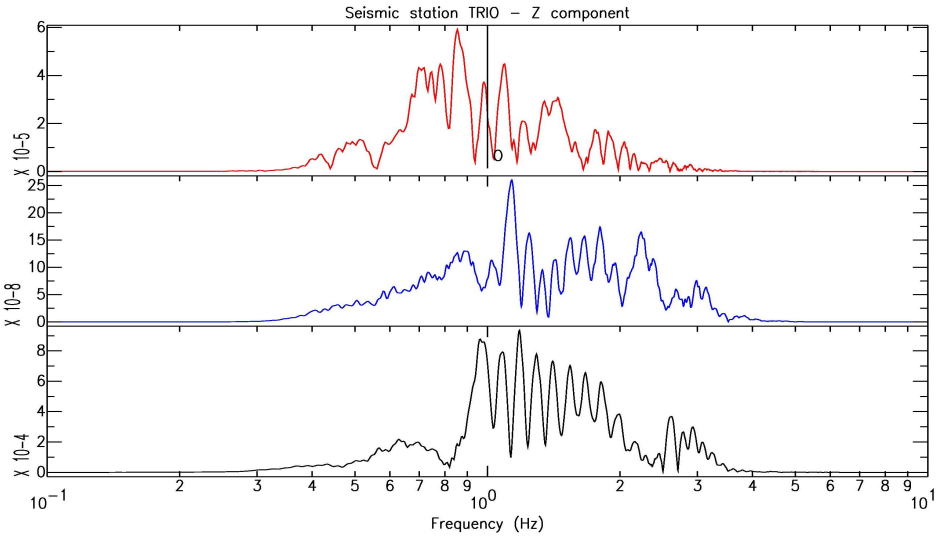

(b)

Figure 5.25: Result of spectral analysis for the signals in Figure 5.24

5.5.2 Simulations with perturbed models

I have produced another set of synthetic seismograms using the meshes described in paragraph 4.3.3. Among all the profiles I have selected the following ones to perform these simulations: the one including station HUGH and the one including station STARR. I have chose STARR because it belongs to a plain zone and HUGH because it is located in a mountain area. Simulations results are shown in figures from 5.26(a) to 5.29. In order to comprehend the effects produced in the propagation of seismic waves by variations in the definition of the models RAMPDEM and BEDMAP, I have used as benchmarks the synthetics seismograms obtained by the simulations described in paragraph 5.5.1.
Differences between these two sets of simulations are really small: this depends on the fact that I have introduced int he two models variations in height having a maximum value of $100\ m$ and I have filtered each signal between $0.4\ Hz$ and $3\ Hz$. According to equation 2.10 this kind of variations should not affect the frequencies of the signals in a hard way, so the result I have obtained is not surprising. Nevertheless changes in the shape of the signal could be greater than the ones observed.
According to what I have said in paragraph 3.4 data belonging to RAMPDEM model are the most reliable ones; thus the results reported in this paragraph show that, in order to obtain major improvements into the shape of synthetic signals, the bedrock definition should be changed in a more dramatic way: variations in height should have values major than $100\ m$. Unfortunately I have not got enough time to determine exactly the amount of this variations needed to improve the shape of the synthetics seismograms.

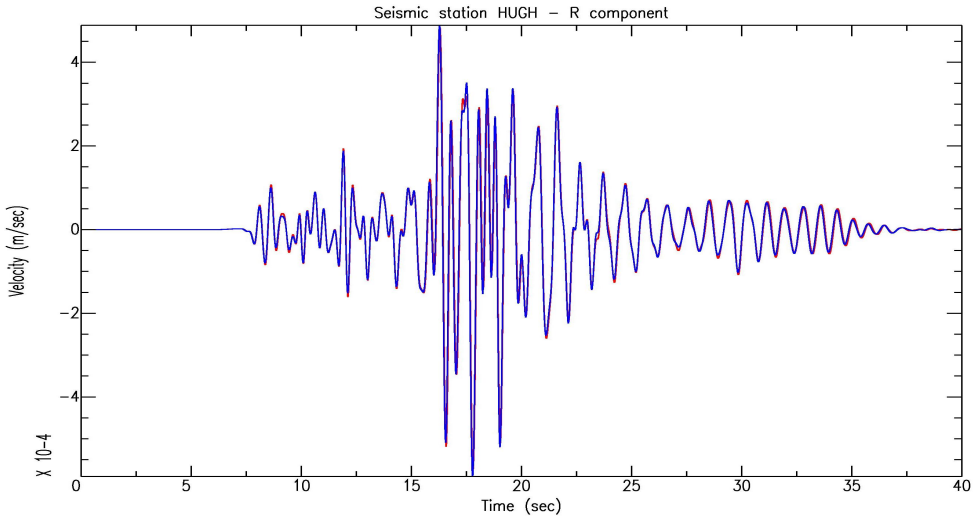

(a)

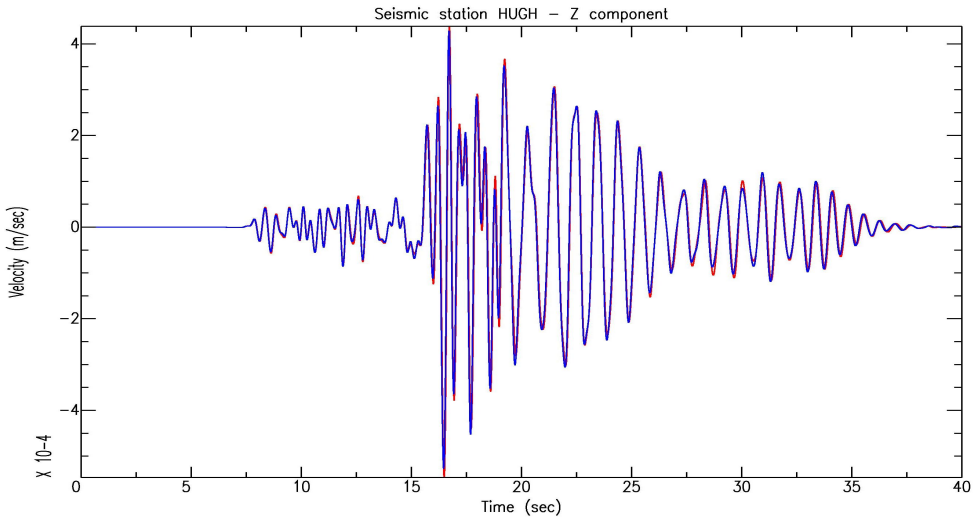

(b)

Figure 5.26: Comparison between synthetics obtained for the station HUGH using the original meshes (blue line) and the ones obtained perturbing the profile (red line). Radial components are shown in Figure 5.26(a), vertical components are shown in Figure 5.26(b)

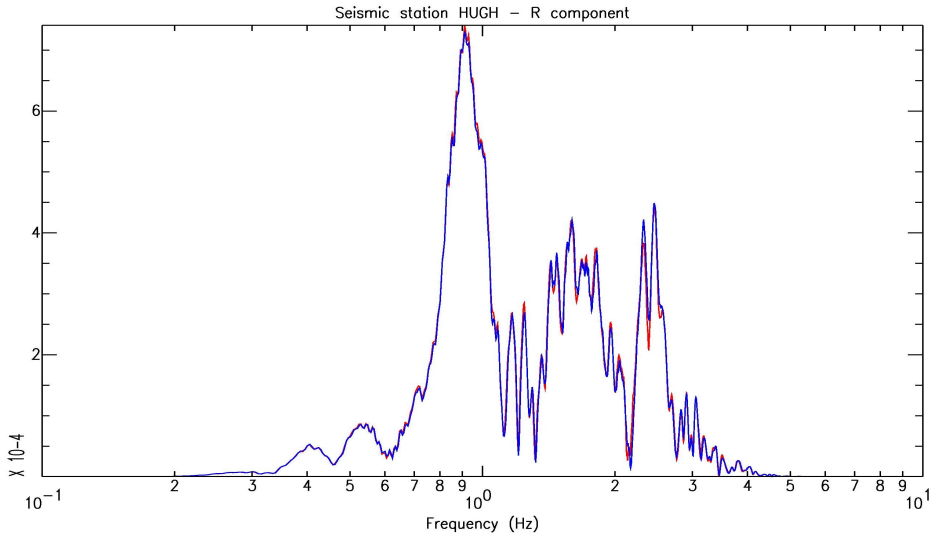

(a)

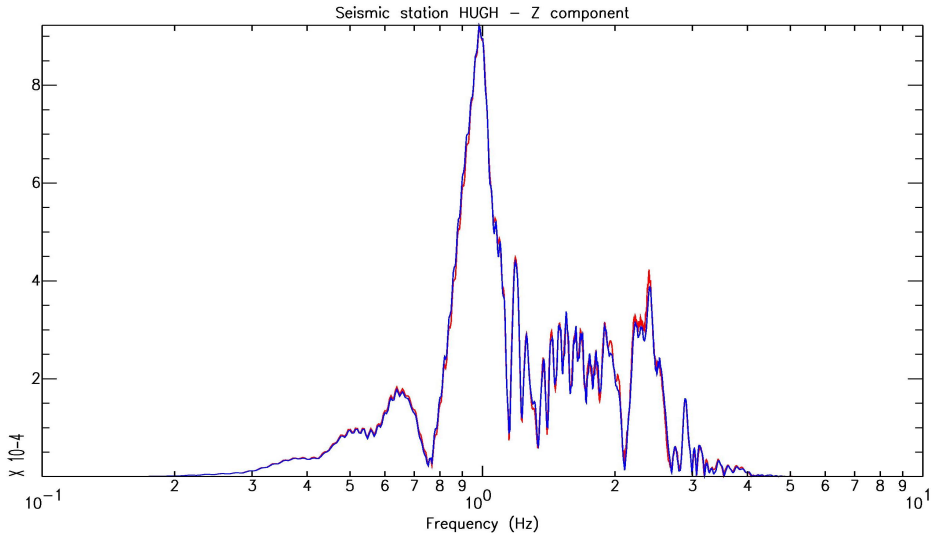

(b)

Figure 5.27: Result of spectral analysis for the signals in Figure 5.26

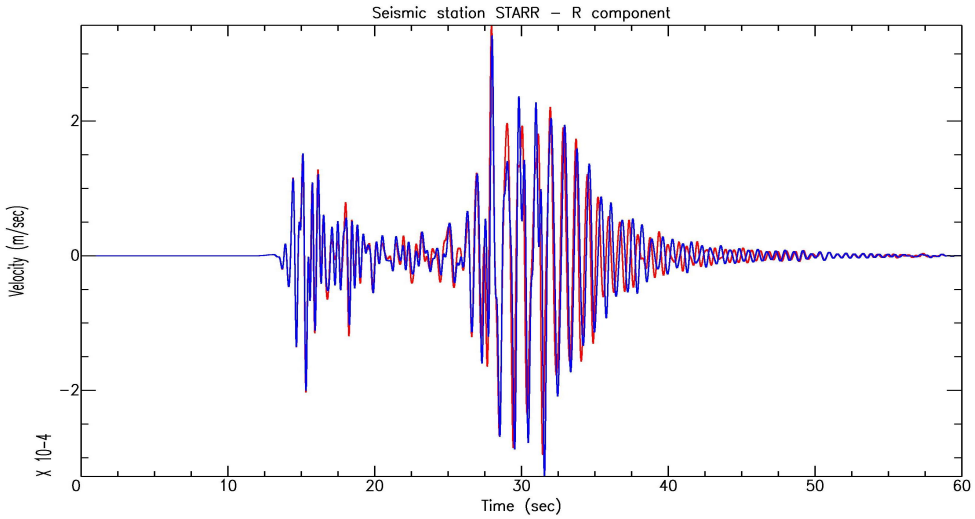

(a)

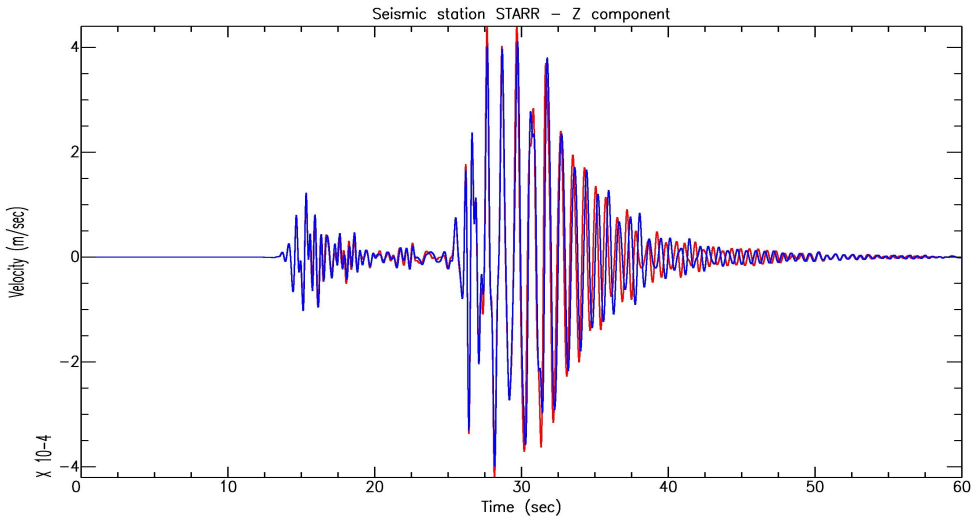

(b)

Figure 5.28: Comparison between synthetics obtained for the station STARR using the original meshes (blue line) and the ones obtained perturbing the profile (red line). Radial components are shown in Figure 5.28(a), vertical components are shown in Figure 5.28(b)

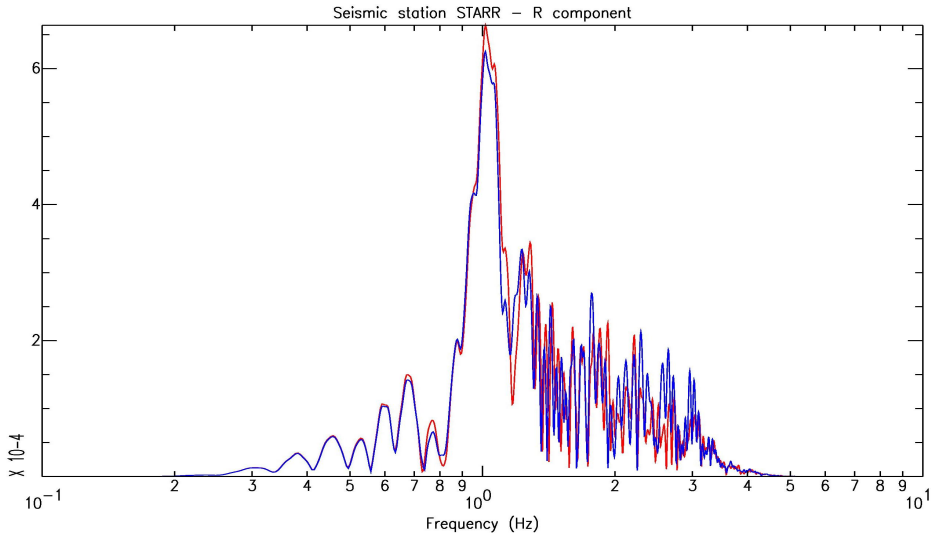

(a)

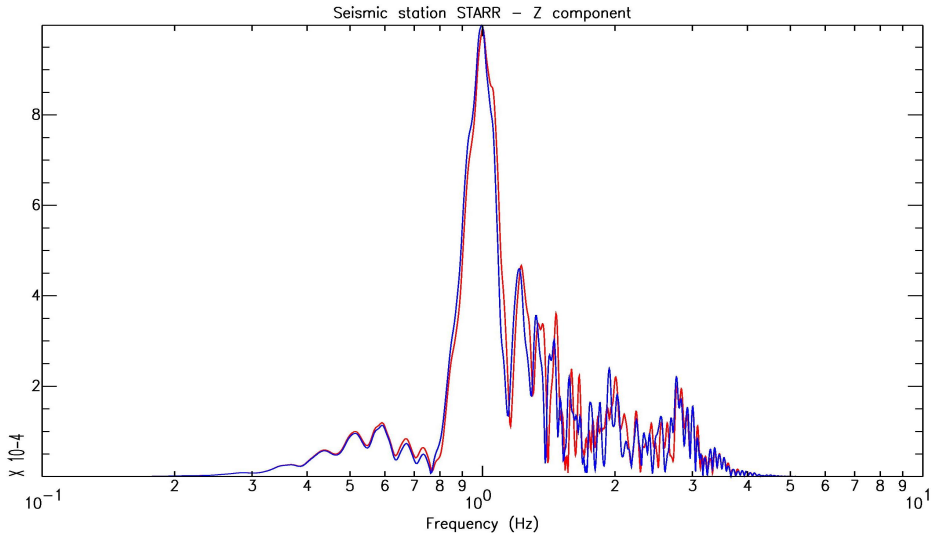

(b)

Figure 5.29: Result of spectral analysis for the signals in Figure 5.28

5.5.3 Simulations with meshes not honoring BEDMAP model

I have performed one last set of simulations in order to understand the size of the error committed when some discontinuities within the model of investigation are not honored by the mesh, but are represented storing the physical properties belonging to different materials on the GLL points of the same spectral element.
To perform these simulations I have used the meshes described in paragraph 4.3.2 and as for the simulations described in the previous paragraph I have considered just two seismic stations: HUGH and STARR. As I have explained in paragraph 5.4 if an external model is used, in the simulation the attenuation for solid medium cannot be taken into account; thus I have performed another set of synthetic seismograms using the meshes honoring the bedrock interface but without using attenuation. The results of these simulations are shown in figures from 5.30 to 5.33.
Even in this case the differences between the two sets of synthetic seismograms are small: this can be explained considering that the bedrock interface does not show dramatic height variations with high spatial frequency, and that even in the mesh not honoring this interface, I have used elements with small linear dimensions (about $50\ m$).
In conclusion the representation of discontinuities, not honored by the mesh, by means of the approximation described above, should not introduce errors in the synthetic seismograms, on condition that must be used elements with linear dimensions comparable with the grid spacing definition of the geological model.
This result is of fundamental importance because it justifies the results obtained in paragraph 5.3: because of difficulties in the meshing process I have decided to create a three-dimensional mesh of David Glacier without honoring the bedrock interface. I have then used a modified version of the *solver* which determines if the GLL points are above or below the bedrock interface and consequently assigns them the ice or rock physical properties. The dimension of spectral elements used in the 3D mesh are comparable with the horizontal definition of the data sets used to create the geological model of the David Glacier. Accordingly with the results showed in this paragraph the inaccuracies introduced in the synthetics seismograms by this approximation are small. Thus I can conclude that the poor knowledge on both the geological model and the source of events are the main causes of the incoherences between recorded data and synthetics seismograms.

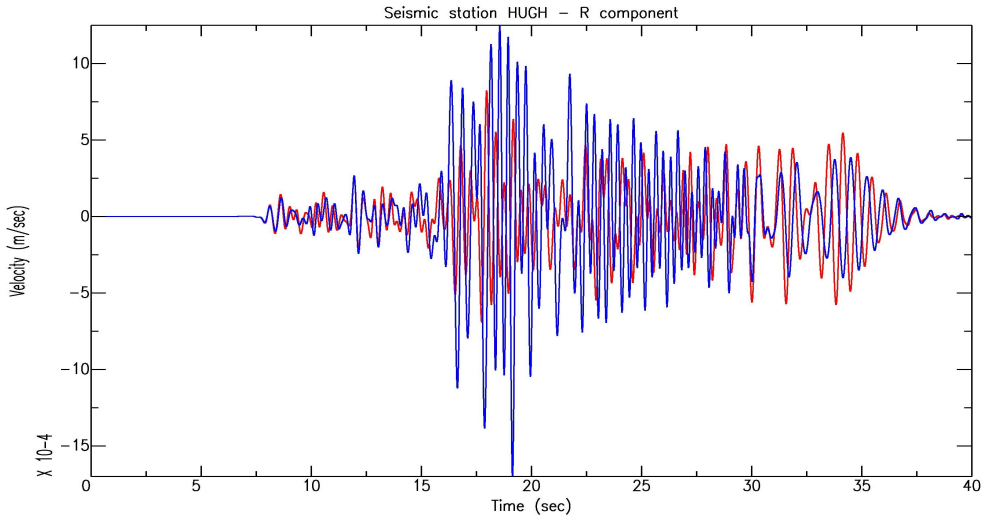

(a)

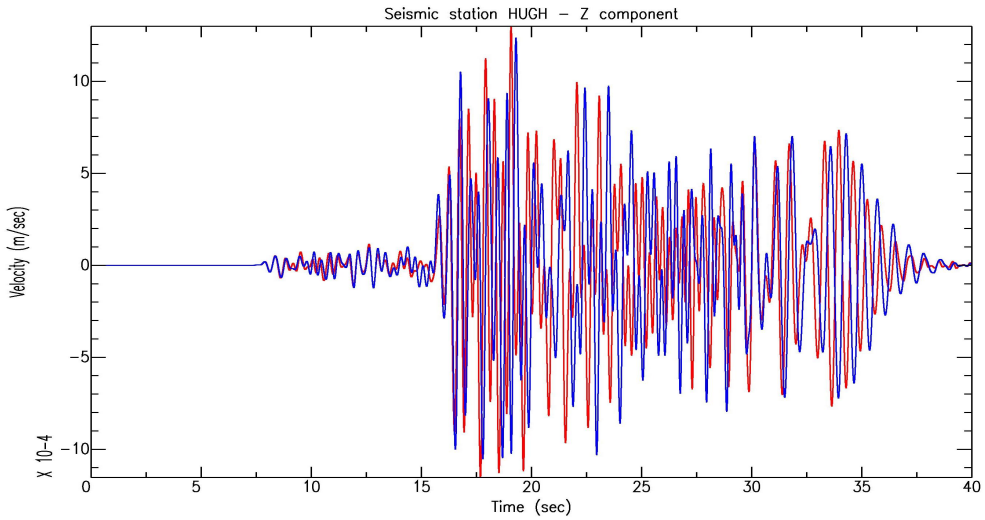

(b)

Figure 5.30: Comparison between synthetics obtained for the station HUGH using the original mesh (blue line) and the one which does not honor the bedrock interface (red line). In both cases the attenuation for solid medium was not used. Radial components are shown in Figure 5.30(a), vertical components are shown in Figure 5.30(b)

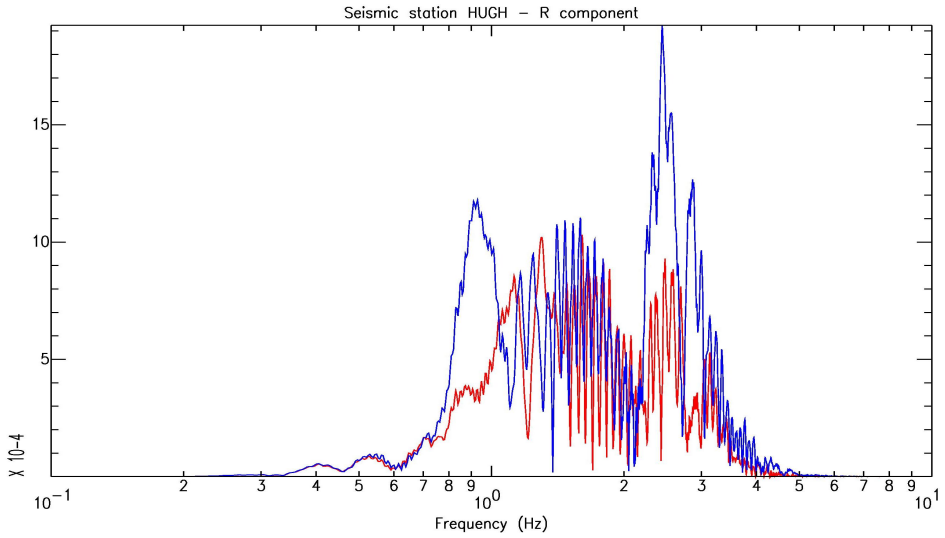

(a)

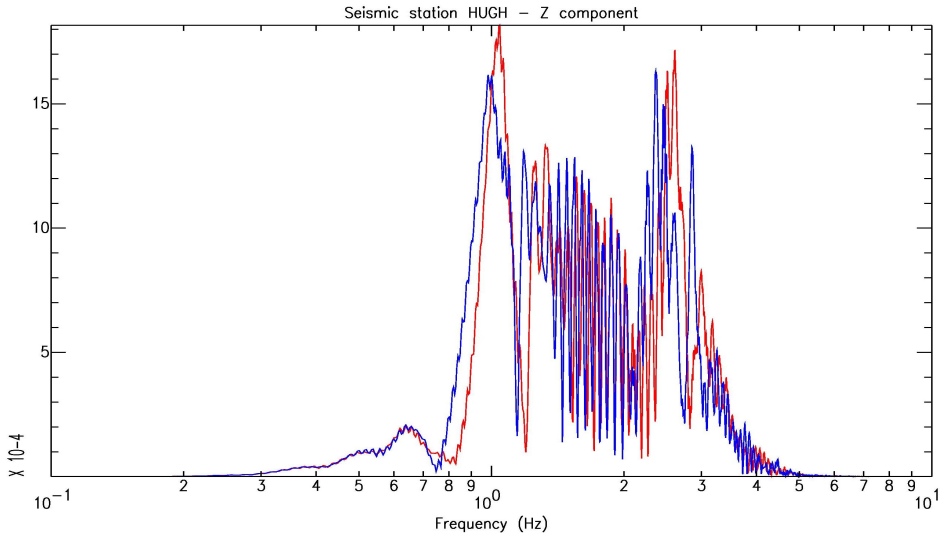

(b)

Figure 5.31: Result of spectral analysis for the signals in Figure 5.30

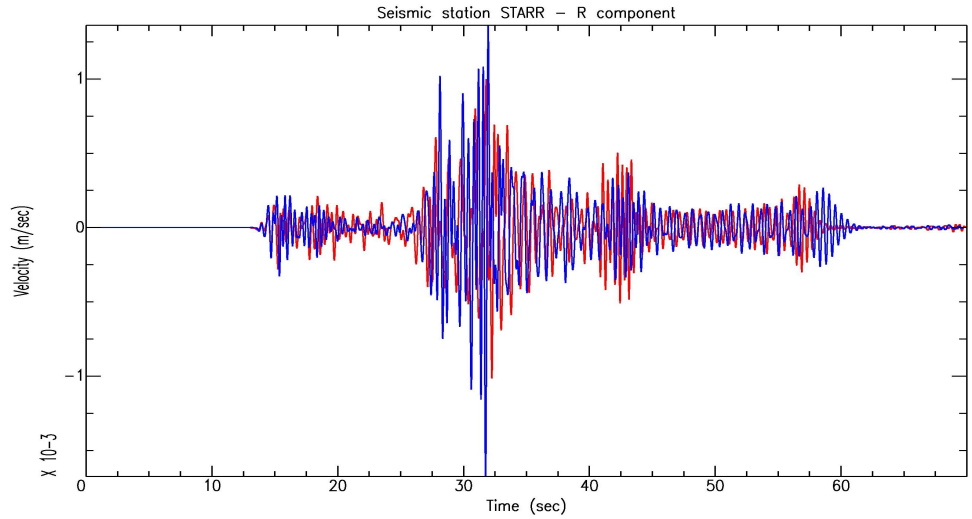

(a)

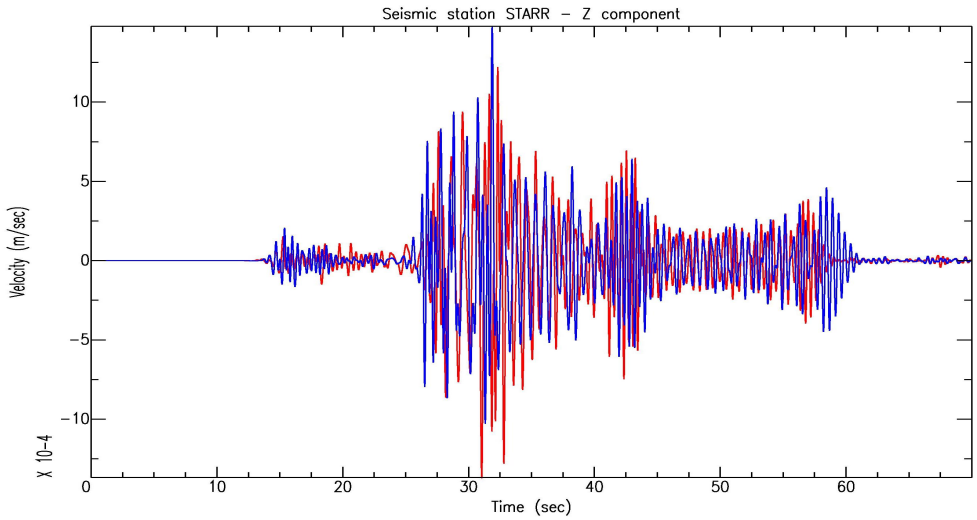

(b)

Figure 5.32: Comparison between synthetics obtained for the station STARR using the original mesh (blue line) and the one which does not honor the bedrock interface (red line). In both cases the attenuation for solid medium was not used. Radial components are shown in Figure 5.32(a), vertical components are shown in Figure 5.32(b)

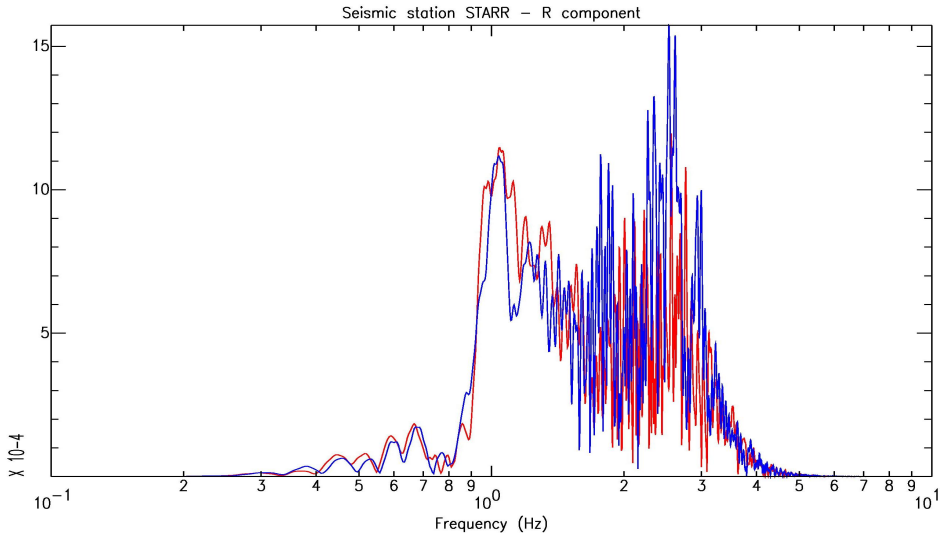

(a)

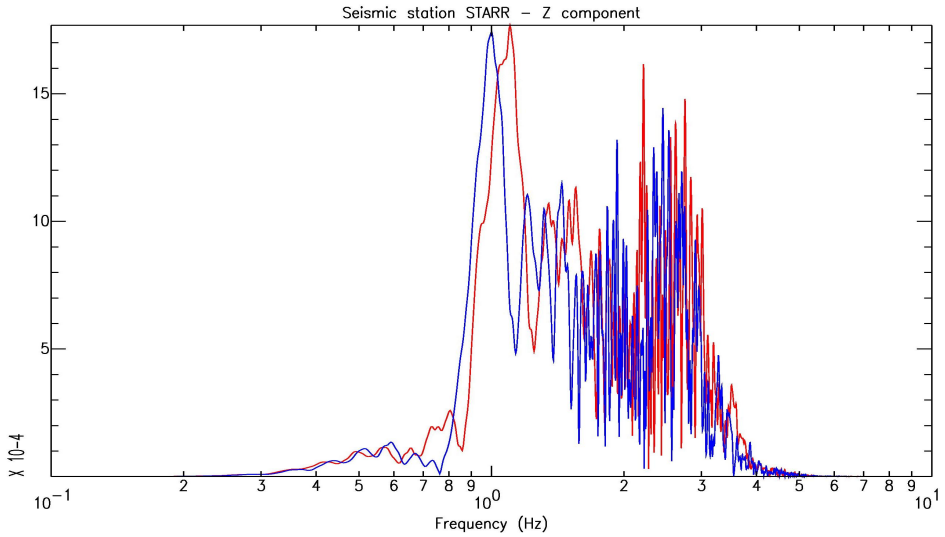

(b)

Figure 5.33: Result of spectral analysis for the signals in Figure 5.32

Conclusions

In the final part of this thesis I would like to make some general remarks about the spectral element method, about the generation of unstructured meshes using CUBIT and about the results obtained on the role of ice in seismic wave propagation.
In the study of seismic waves propagation the meshing process is of fundamental importance, as clearly explained in paragraph 2.4 and in Chapter 4, and at the same times is not an easy task. CUBIT is a powerful software thanks to the variety of meshing tools which it provides, furthermore it is really versatile because it is capable to handle Python scripts by mean of which users can implement their own meshing schemes and tools. On the other side it has to be taken into account two important factors: first of all the software presents high system requirements, thus the creation of a complex mesh with millions of elements cannot be accomplished without the use of a good graphic station. Furthermore the complexity of the software oblige the user to make a lot of practice in order to be able to obtain the desired mesh: for example the outline I have presented in paragraph 4.3.1 could be not directly applied to every two-dimensional model, but each case has to be analyzed deeply in order to find the right meshing approach.
SPECFEM package represents a very good and accurate implementation of the spectral element method described in Chapter 2: the fact that it is open source let the user to add new features to the original code by developing new subroutines, as I have done in paragraph 5.5.3. Notwithstanding even if this implementation of SEM presents lower computational cost if compared with others numerical methods, it requires the use of computer clusters thus it cannot be considered or used as an explorative approach to a problem without having a good a priori knowledge of it: the geology of the study area and in particular the source of the events that has to be reproduced must be well known in order to obtain good results.
The synthetics seismograms obtained by the 3D simulation I have performed show differences in amplitude with the original data recorded by the seismic stations at David Glacier. An explanation of these differences can be found in the fact that to represent the source of an event of the UP-S cluster, I have used the value of mean scalar moment calculated for the events belonging to the DW cluster. I have made this choice because reliable scalar moments have not been determined for the UP-S cluster events, while events belonging to DW cluster had been widely analyzed ([34]) and their characteristics are well known, thus I have preferred to use their scalar moment mean value as a first approximation.
3D synthetics present also differences in phase and larger amplitudes in the high frequency region (i.e. $\nu > 1\ Hz$) of the whole spectra. I have thought that these features could de-

pend by the approximations I have made in the definition of both the topography and the subglacial morphology, and also on the representation of the bedrock interface by mean of melting different physical properties in the same spectral element (see paragraph 4.2). Thus I have decided to further investigate these aspects using the package SPECFEM2D: in fact the creation of a mesh in two dimensions is easier and faster than in three dimensions, and also the numerical simulations have a lower computational cost because of the reduction of the number of elements.
The results of these 2D simulations show that variations in the definition of both topography and subglacial morphology do not introduce relevant effects. Thus differences in waveforms between data and synthetics seismograms are caused mainly by errors in the definition of the geological models which are bigger than the perturbations I have introduced in the two models themselves (see paragraph 5.5.2), or to errors in the definition of the source..
Furthermore results shown in paragraph 5.5.3 demonstrate that when a discontinuity within the model of investigation is not honored by the mesh, but is represented storing physical properties of different materials on the GLL points of the same spectral element, the error introduced in the synthetics seismograms is small if the dimension of the elements used in the mesh are similar to the spatial resolution of the approximated discontinuity.
The relevant amount of high frequencies in the spectra of synthetic seismograms cannot be explained considering only effects due to the definition of the geological model. I think that this feature can be related to the fact that I have considered the ice layer as an homogeneous medium with constant physical properties. This is an important approximation: in fact changes in the internal structure of ice or variations in environmental parameters such as the temperature can produce both the partial melting of some zones of the glacier and the creation of areas with high density gradient. Furthermore the presence of crevasses may obstruct the propagation of compressional high frequency waves.
SPECFEM3D_BASIN is capable to deal with these kind of features like lateral variations in compressional-wave speed, shear-wave speed and density. Nevertheless modeling these kind of properties requires a deep geological knowledge of the study area and anyway present important difficulties: the creation of a mesh which honors crevasses with small linear dimension is a quite prohibitive task.
There is another approximation I have made that has to be taken into account: in order to represent the source I have used the components of the moment tensor. Because these events are supposed to be caused by the rupture of an asperity beneath the ice layer, it should be useful to create the analytical representation of a this kind of source and to introduce it in the SPECFEM package in order to better represent the initial wave field of the events.
I was aware that a complete reproduction of recorded seismograms was not possible, mainly because of the poor knowledge on the geology of David Glacier area. Thus the aim of this work was not to produce synthetic seismograms in order to make a quantitative comparison with recorded data: my intention was to distinguish between the waveform propagation effects due to the structural model and those possibly caused by the representation of the source. Even if the spectral element method is well implemented in the SPECFEM package, the code is still under development and new features and improvements are constantly

added: this fact gave rise to some complications and delays in the evolution of this work. As a consequence more work needs to be done in order to fully understand the physics related to the *basal earthquakes* recorded at David Glacier. Nevertheless I have well explored all the main aspects of this subject and I have set up the numerical environment necessary for future analysis. The poor knowledge on the geological model is the critical factor for reconstructing the geometry and the physics of the seismic source.

References

[1] Aki, K., Richards, P.G., 1980. *Quantitative Seismology*, Freeman and Co., New York

[2] Bannister S., Kennett B.L.N. (2002). *Seismic activity in the Transantarctic Mountains - results from a broadband array deployment*. Terra Antartica, 9, 41-46.

[3] Baroni C. (ed.) (1996). *Mount Melbourne Quadrangle (Victoria Land)- Antarctic Geomorphological and Glaciological 1:250,000 Map Series*. Ministero dell'Universit e della Ricerca Scientifica e Tecnologica -Italia. Programma Nazionale di Ricerche in Antartide (P.N.R.A.).

[4] Bielak, J., Ghattas, O., and Kim, E. J. 2005. *Parallel octree-based finite element method for large-scale earthquake ground motion simulation*. Computer Modeling in Engineering and Sciences, 10(2):99112.

[5] Capponi, G., Crispini, L., Meccheri, M., Musumeci, G., Pertusati, P.C., 1999. *Relief Inlet Quadrangle (Victoria Land). Antarctic Geological 1:250 000 Map Series*. Museo Nazionale dell'Antartide.

[6] Carmignani, L., Ghezzo, C., Gozzo,G., Lombardo, B., Meccheri, M., Montrasio, A., Pertusati, P.C., and Salvini, F. *Geological Map of the Area between David and Mariner Glaciers, Victoria Land, Antarctica*. Mem.Soc.Geol.It.,33,1987.

[7] E. Casarotti, M. Stupazzini, S.-J. Lee, Dimitri Komatitsch, A. Piersanti and J. Tromp. 2007. *CUBIT and seismic wave propagation based upon the spectral-element method: An advanced unstructured mesher for complex 3D geological media*, in: Proceedings of the 16th International Meshing Roundtable, Seattle, Washington, USA, October 14-17, 2007, Springer, p. 579-597.

[8] A. Capra. *Victoria Land Network for DEFormation control*

[9] Casula G., S. Danesi, M. Dubbini and L. Vittuari 2007. *Tidal forcing on David Glacier and Drygalski Ice Tongue in the 10th ISAES X Online Proceedings, in Antarctica: A Keystone in a Changing World* Online Proceedings of the 10th ISAES X, edited by A. K. Cooper and C. R. Raymond et al., USGS Open-File Report 2007-xxx, Extended Abstract yyy, 1-4.

[10] Courant, R., Friedrichs, K. O., and Lewy, H. 1928. *Über die partiellen differenzgleichungen der mathematischen physik (on the partial difference equations of mathematical physics)*. Mathematische Annalen, 100:3274.

[11] cubit.sandia.gov

[12] Deichmann, N., J. Ansorge, F.Scherbaum, A. Aschwanden, F.Bernardi and G.H. Gudmundsson. 2000. *Evidence for deep icequakes in an Alpine glacier*. Ann. Glaciol., vol. 31, p. 85-90.

[13] Dimitri Komatitsch and Qinya Liu and Jeroen Tromp and Peter Süss and Christiane Stidham and John H. Shaw. 2004. *Simulations of Ground Motion in the Los Angeles Basin based upon the Spectral-Element Method*. Bulletin of the Seismological Society of America, vol. 94, p. 187-206.

[14] Komatitsch, D., Tsuboi, S., and Tromp, J., 2005. *The spectral-element method in seismology*. In: Levander A. and Nolet G., (eds), *Seismic Earth: ArrayAnalysis of Broadband Seismograms*, volume 157 of Geophysical Monograph, pages 205228 American Geophysical Union, Washington DC, USA.

[15] Dimitri Komatitsch and Jeroen Tromp. 1999. *Introduction to the spectral-element method for 3-D seismic wave propagation*. Geophysical Journal International, vol. 139, p. 806-822.

[16] Dimitri Komatitsch and Jean-Pierre Vilotte. 1998. *The Spectral Element method: an efficient tool to simulate the seismic response of 2D and 3D geological structures*. Bulletin of the Seismological Society of America, vol. 88, p. 368-392.

[17] G. Ekström, M. Nettles, G. A. Abers. 2003. *Glacial Earthquakes*. Science 302, 622.

[18] F. Borfecchia e M. Frezzotti, *Satellite image mosaic of the Terra Nova Bay area (Victoria Land, Antarctica)*. Memorie della Societa Geologica Italiana, 46, 1989, p. 521-523.

[19] F. Pellegrini. *Scotch 5.1 Users Guide*. Technical report, LaBRI, Universite Bordeaux I, August 2008. Available from http://www.labri.fr/ pelegrin/scotch/.

[20] Paolo Gasperini, Gianfranco Vannucci, *FPSPACK: a package of FORTRAN subroutines to manage earthquake focal mechanism data*, Computers & Geosciences, Volume 29, Issue 7, August 2003, Pages 893-901, ISSN 0098-3004, DOI: 10.1016/S0098-3004(03)00096-7.

[21] geodynamics.org/

[22] Goldstein, P., D. Dodge, M. Firpo, Lee Minner. 2003. *SAC2000: Signal processing and analysis tools for seismologists and engineers*. Invited contribution to The IASPEI International Handbook of Earthquake and Engineering Seismology, Edited by WHK Lee, H. Kanamori, P.C. Jennings, and C. Kisslinger, Academic Press, London.

[23] Intergovernmental Panel on Climate Change (2007). M.L. Parry, O.F. Canziani, J.P. Palutikof, P.J. van der Linden and C.E.Hanson. *Summary for Policymakers. Climate Change 2007: Impacts, Adaptation and Vulnerability. Contribution of Working Group II to the*

Fourth Assessment Report of the Intergovernmental Panel on Climate Change Cambridge University Press, Cambridge, UK. p. 722.

[24] Liu, H., K. Jezek, B. Li, and Z. Zhao. 2001. *Radarsat Antarctic Mapping Project digital elevation model version 2*. Boulder, Colorado USA: National Snow and Ice Data Center. Digital media.

[25] Lythe, M.B., Vaughan, D.G. and the BEDMAP Consortium. 2000. *BEDMAP - bed topography of the Antarctic. 1:10,000,000 scale map. BAS (Misc) 9*. Cambridge, British Antarctic Survey.

[26] J. Virieux. *P-SV wave propagation in heterogeneous media: velocity-stress finite-difference method*, in: Geophysics, 1986, vol. 51, p. 889-901.

[27] M.R. Bennett. *Ice streams as the arteries of an ice sheet: their mechanics, stability and significance*. Earth Sci. Rev. 61 (2002), p. 309339.

[28] Neave, K.G. and J.C. Savage. 1970. *Icequakes on the Athabasca Glacier*. J. Gepjys. Res., vol. 75(8), 1351-1362.

[29] A. T. Patera. 1984. *A spectral element method for fluid dynamics: laminar flow in a channel expansion*. J. Comput. Phys., vol. 54, p. 468-488.

[30] Pilant, W. L., 1979. *Elastic waves in the earth*. Elsevier Science Publ. Co., Inc.

[31] R.C.Y. Chin, G. Hedstrom and L. Thigpen. *Numerical methods in seismology* J. Comp. Phys. 54 (1984), pp. 1856.

[32] Sridhar Anandakrishnan and Charles R. Bentley. 1993. *Microearthquakes beneath ice streams B & C, West Antarctica: Observations and implication*. J. Glaciol., 39:455-462.

[33] Sridhar Anandakrishnan and Richard B. Alley. 1994. *Ice stream C, Antarctica, sticky-spots detected by microearthquake monitoring*. Ann. Glaciol., 20:183-186.

[34] S. Danesi, A. Morelli, S. Bannister. *Repeating earthquakes from reiterated rupture of an asperit under an Antarctic outlet glacier*. Earth and Planetary Science Letters Volume 253, Issues 1-2, 15 January 2007, Pages 151-158.

[35] S. Bannister, and B.L.N. Kennett. *Seismic activity in the central Transantarctic Mountains: results from a broadband array deployment*. Terra Antartica, 9, 41-46, 2002.

[36] EPICA community members. *Eight glacial cycles from an Antarctic ice core*. Nature 429, 623-628(10 June 2004).

[37] M. Frezzotti, A. Capra, L. Vittuari. 1998. *Comparison between glacier ice velocities inferred from GPS and sequential satellite images*. Ann. Glaciol. 27, p. 5460.

[38] M. Frezzotti, I.E. Tabacco, A. Zirizzotti. 2000. *Ice discharge of eastern dome C drainage area, Antarctica, determined from airborne radar survey and satellite image* Analysis, J. Glaciol. 46, p. 253264.

[39] V. Damm. 1996. *Subice morphology deduced by Radio Echo Soundings (RES) in the area between David and Mawson Glaciers, Victoria Land*. Geol. Jahrb. B89, p. 321331.

[40] Swithinbank, C.W.M., 1954. *Ice streams*. Polar Record 7, 185186

[41] E. Tabacco, C. Bianchi, M. Chiappini, A. Zirizzotti, E. Zuccheretti. 2000. *Analysis of bottom morphology of the David GlacierDrygalski Ice Tongue, East Antarctica*. Ann. Glaciol. 30, p. 4751.

[42] top500.org/